REPORT DOCUMENTATION PAGE

Form Approved
OMB No. 0704-0188

1. AGENCY USE ONLY (*Leave Blank*)	2. REPORT DATE	3. REPORT TYPE AND DATES COVERED
	13 Feb. 1998	**Final, 2 Jun. to 2 Dec. 1997**

4. TITLE AND SUBTITLE
New Intense Light Source: Use of Dielectric Solids to Power Thermophotovoltaic Electric Generators and to Pump Lasers.

5. FUNDING NUMBERS
C
NAS3-97154

6. AUTHOR(S)
L.G. DeShazer, A.S. Kushch and K.C. Chen

7. PERFORMING ORGANIZATION NAME(S) AND ADDRESS(ES)
Quantum Group, Inc.
11211 Sorrento Valley Rd.
San Diego, CA 92121

8. PERFORMING ORGANIZATION REPORT NUMBER
None

9. SPONSORING/MONITORING AGENCY NAM(S) AND ADDRESS(ES)
NASA Lewis Research Center
21000 Brookpark Rd.
Cleveland, OH 44135
BMDO, Attn: TOI/SBIR, 7100 Defense, Pentagon
Washington, DC 20301-7100

10. SPONSORING/MONITORING REPORT NUMBER

11. SUPPLEMENTARY NOTES

12a. DISTRIBUTION/AVAILABILITY STATEMENT
Approved for public release; distribution unlimited

12b. DISTRIBUTION CODE

13. ABSTRACT (*Maximum 200 words*)

Report developed under SBIR contract

A new light source using dielectric solids has been developed to power thermophotovoltaics (TPV) and to pump lasers. The light source is a refractory solid emitter heated to relatively high temperature by combustion. The dielectric solid was chosen to have selective thermal emission with nearly narrowband emission peaked at various visible and IR wavelengths. The combination of the selective emitter with an optical waveguide is called a "superemissive light pipe" (SELP) and greatly increases its effectiveness. TPV was demonstrated by using an ytterbium garnet crystal SELP emitter powering a silicon photocell, and an erbium garnet crystal SELP emitter powering a GaSb photocell. Thulium emitters were chosen to pump neodymium lasers, but no irrevocable cw laser action was observed, yet some enhanced 1064 nm emission was recorded.

14. SUBJECT TERMS
Electric Generator, Laser, SBIR Report, Superemissive Solid, Thermophotovoltaics

15. NUMBER OF PAGES 69

16. PRICE CODE

17. SECURITY CLASSIFICATION OF REPORT	18. SECURITY CLASSIFICATION OF THIS PAGE	19. SECURITY CLASSIFICATION OF ABSTRACT	20. LIMITATION OF ABSTRACT
Uncl.	**Uncl.**	**Uncl.**	**UL**

NSN 7540-01-280-5500

Standard Form 298 (Rev. 2-89)
Prescribed by ANSI Std. Z39-18
298-102

New Intense Light Source based on Dielectric Solids to Power Thermophotovoltaic Electrical Generators and to Pump Lasers

Section I. Project Objectives

The objectives were the construction and testing of an improved superemissive light pipe (SELP) and the subsequent testing of this SELP for pumping a neodymium laser and generating electricity with an existing thermophotovoltaic (TPV) unit. The specific objectives were the choice of a crystal for the SELP that will match neodymium absorption properties, design and fabrication of an optical waveguide for the SELP, test neodymium laser using SELP as pump, and measurement of electrical power generated by TPV using SELP.

Section II. Work Accomplished

The work performed was mostly experimental, broken down into six tasks for this project. The first four tasks involved the design, fabrication and testing of the SELP using ytterbia, erbia and thulia emission. The last two tasks were concerned with the testing of the SELP operation for laser pumping and TPV.

A. Choice of Dielectric Superemitter Material

Superemitter crystals were investigated to spectrally match the absorption of neodymium (Nd^{3+}) in the 790-890 nm range for the laser task, and to match the photovoltaic response for silicon (Si) and gallium antimonide (GaSb) for the TPV task.

1. Spectroradiometer Setup

Emission spectra of three selective emitters using ytterbia, erbia and thulia were measured with a remote-sensing spectroradiometer (model SR5000, CI Systems, Westlake Village, CA). The detector used was a Si/PbS sandwich, thermoelectrically cooled to -30°C, with circular variable filter wheel, both covering 0.4 to 2.5 μm, with an internal blackbody reference. The selective emitter spectra were measured with a field of view (FOV) 1.5 mR, scan time 16 seconds, at a distance of 6 meters. The instrument was first calibrated with an external blackbody at 1100°C supplied by CI Systems (model SR-2-33-SA-1"). The mantles were run with premixed propane at fuel input rate of 2,990 Watts (10,200 Btu/hr for propane 4.1 SCFH (standard cubic foot hour), corrected for pressure) and a compressed air flow rate at 75 SCFH. Spectra were recorded using a10-scan average.

Because of much smaller dimensions of the three laser crystals (0.7% Nd:YVO_4, 1% Nd:YVO_4, and 1.1% Nd:YAG) and weaker total radiant output signals due to absorption by the crystals, the instrument conditions had to be changed for laser crystal throughput measurements in

order to enhance the signal-to-noise ratio. The sample-to-detector distance was decreased to 3.1 meters and the FOV was increased to 2.4 mR. The scans were run with 8 seconds per scan and the results were reported on 20 scan average. Also it was found necessary to increase the external blackbody temperature to 1200°C to obtain a better calibrated response function for the Si detector in 0.4-1.2μm region. In some cases, a 10x neutral density filter was added to prevent saturation of the detector. The ytterbia and thulia emitters were heated to high temperature with a micro-torch at a propane fuel input of 400 Btu/hr. After adjusting the air proportion to obtain the optimal flame length, the transmission spectra of ytterbia and thulia selective emitters through the indium-tin-oxide (ITO) IR-cutoff filter and the three laser crystals were measured.

The measurement procedure was as follows. First, the transmission spectra through the crystals (in appropriate holders) were taken. The spectra were again taken after the crystals were removed from the holder (leaving the holder in place). Finally, the ITO filter was removed from the line-of-sight, and spectra were obtained with only emitter itself.

2. Spectra of Ytterbia, Erbia and Thulia Emitters

The spectral matching of ytterbia, erbia and thulia selective emitters to the TPV and laser applications was assessed by using mantles made by the relic process using the rare-earth sesquioxides (R_2O_3). There will be no substantial spectral differences between the mantles and crystalline emitters, except for the possible presence of impurities in the mantles.

Figure 1 shows the measured ytterbia spectrum. The spectrum shows a narrow emission band centered at 980 nm. Ytterbia has an emission band at E_g= 1.29 eV coincident with its single observed absorbing energy level above the ground state. Visible emission of the ytterbia emitter is due to the high-energy (blue-shifted) tail of this infrared absorption ($<10^{-4}$ of the peak emission) and impurities in the Yb emitter.

The erbia emitter appears pink in color at room temperature and has a yellowish green color when ignited. The erbia spectrum (Figure 2) shows five narrow bands below 2.5 μm, with emission bands at 540 nm, 652 nm, 804 nm, a doublet at 984 and 1012 nm and a major emission band at 1544 nm with E_g = 0.827 eV. The erbia emitter would only weakly pump neodymium lasers but is ideal for GaSb TPV usage.

Thulia emitters are white at room temperature. Measurements were made only on mantles since Tm crystals were not available due their long delivery time (> 6 months). Thulia has three narrow bands at 699 nm, 818 nm, 1170 nm and a major broad band at 1780 nm as shown in Figure 3. The color of the Tm selective emitter changes from rosy-red color at low temperatures

(low fuel input rate) to white at high fuel input rate (Figure 4). The near IR emission band at 818 nm appears to be ideal for pumping neodymium lasers, having more energy content in the Nd pump band than Yb emitters. Thulia was chosen as the selective emitter to pump neodymium lasers. The strategy in our experiments was to reflect the strong IR emission at 1.7 mm back to the selective emitter in order to recuperate its energy.

3. Comparison of SELP with Superemissive Felt and Mantle

The selective emissive mantle, felt and SELP are quite different in terms of their physical dimensions and surface area per unit weight. This greatly affects the thermal gradient and heat transfer rate in the emitter structure during ignition and cooling. Both the mantle and felt emitter types consist of fine fibers. The difference is that the mantle consists of continuous fiber, while the felt consists of discontinuous short fibers. Because of the small dimension (5-10 μm) of the fiber, there is very little thermal gradient in the fiber itself which allows rapid thermal equilibrium with flame. As a result, both emitter types have good thermal shock resistance. The felt is thicker than the mantle and has a temperature gradient in the thickness direction, giving greater graybody background (Figure 5). The SELP emitter structure has the largest dimension, highest thermal gradient and the worst thermal shock resistance among three emitter forms. The emitter fibers in the felt and mantle are polycrystalline, which possess grain boundaries, porosity and lattice defects whereas the SELP type emitter is a single crystal with very few lattice defect.

The combustion setup was different in heating up the mantle and felt to obtain spectra. The mantle was heated by introducing a pre-mixed propane and air, which ignited inside the inner mantle surface. The mantle has a thin wall thickness (255 μm) and is quite open allowing exhaust gases to escape. Because of its thin thickness, there is almost no temperature gradient between the inner and outer mantle surfaces. The openness of the mantle allows the emission from the inner surface to escape through the outer surface. The mantle has a "cleaner" spectrum, *i.e.* narrower and more define emission bands than felt.

The felt was heated by a torch that mixed the propane and air before entering the torch tip. The heated area was concentrated in a much smaller area. The surface temperature of the felt depends much on the torch flame stoichiometry and can be higher than the mantle The felt under torch appears white, and shows a relatively smaller emission bands in the visible range when compare with the spectrum of the mantle. A single layer felt is 1-2 mm thick. Multi-layered felt emitter is a good thermal insulator and a good heat retainer so there is a greater thermal gradient in the felt The spectrum of the felt has broader emission peaks.

B. SELP Design and Fabrication

1 SELP Rods

The principal idea of SELP is to generate selective emission within a solid state emitter which can be made from rare earth oxide crystals and deliver this energy to the target by a waveguide which is optically coupled to the emitter. The principal design concepts are covered by U.S. Patents 5,500,054 "Superemissive Light Pipes and Thermophotovoltaic Systems Including Same" and 5,503,685 "Thermally Stimulated Focused Photon Sources," assigned to Quantum Group Inc. Another patent is pending for the SELP laser.

Major advantages of such a design for TPV and laser applications are: 1) SELP approach allows for physical separation of the high temperature heat sources from the targets which is very important for providing an effective and simple photovoltaic (PV) and laser cooling systems, 2) SELP is capable of generating and delivering to the PV cells an extremely high light intensity that permits concentrator type PV cell utilization, so makes the overall system more cost effective, 3) emission spectrum can be controlled by the solid-state emitter chemistry, so it can be tuned for different type PV cells and heat source temperatures in order to achieve maximum system efficiency, 4) a variety of heat sources can be used, including fossil fuel combustion, nuclear, radioisotope, solar, and chemical to generate a narrow band emission, 5) high efficiency photon collection and recuperation system can be employed by using an optical waveguides, and 6) robust emitter/combustion system can be fabricated from SELP components.

Crystal emitters for this project were made by the Scientific Material Corporation, Bozeman, MT of ytterbium aluminum garnet (YbAG), $Yb_3Al_5O_{12}$, holmium aluminum garnet (HAG), $Ho_3Al_5O_{12}$, and two erbium aluminum garnet (ErAG), $Er_3Al_5O_{12}$. Cylindrical emitter crystals of YbAG, HAG and ErAG were 25 mm long and 5 mm in diameter, and were bonded to yttrium aluminum garnet (YAG) rods, 20 cm lomg. Another ErAG SELP crystal was 5 mm in diameter and 2 mm long. For preliminary tests a low cost SiO_2 based SELP were fabricated by coating quartz rods with rare earth oxides. Figure 6 displays the SiO_2 SELP under testing, and Figure 7 illustrates the ErAG/YAG SELP where the colored section is ErAG and the colorless section is YAG rod.

Single crystals were chosen for this experiment because they can be made with the high purity (<10 ppm) necessary for achieving low intensity for the graybody background emission. The melting point of YAG is 1940°C, which is lower than the near 2400°C melting points of rare-earth sesquioxides R_2O_3, but is still more than adequate for thermal emitter operation.

The light pipe was made from a transparent undoped single-crystal YAG, with a polished circumference as well as ends. The IR absorption edge of YAG is at 6 μm (where

the absorption coefficient a is 5 cm^{-1}), and the ultraviolet edge is at 190 nm (again, where a is 5 cm^{-1}) (3). YAG is ideal for a light pipe in SELP by having Knoop hardness of 1380 kg/mm^2 and room-temperature thermal conductivity of 10.3 W/m-K. The rare-earth aluminum garnet emitter crystals were attached to the YAG light pipes using diffusion bonding by Scientific Materials Inc.

2. Heat Sources

Three heat sources were used during the experiments. The first was comprised of the MAPP gas torches (Figures 8, 10 and 11), and the second was oxygen/acetylene torches as presented in Figures 9 and 12. The third heat source was an electric 1700 °C furnace (Figures 13 to 19). MAPP gas is stabilized methylacetyene propadiene. This fuel, patented by Dow Chemical Co., is considered as a safe substitute for acetylene. The characteristics of these two gaseous fuels are presented in the Table 1 (North American Combustion Handbook).

Table 1. Characteristics of the fuel

Characteristics	FUEL	
	Acetylene	MAPP gas
Calculated flame temperature, °C in air/oxygen	2632/3110 -	-/2927
Flammability limits, % fuel gas by volume in air	2.5 - 81	3.4 - 10.8
Gas gravity	0.92	1.48
Calorific value at stp, Gross kcal/m^3/Btu/ ft^3	13,280/1,492	21,052/2,366
Calorific value at stp, Net kcal/m^3/Btu/ ft^3	12,850/1,444	19,950/2,242
Wobbe index	1,559	1,947
Volume air/volume fuel	12.14	21.25
Stoichiometric products of combustion, % · CO_2, dry · H_2O wet · N_2, wet · total volume/fuel volume	 17.4 8.3 75.8 12.66	 15.6 11.9 74.4 22.59

The experimental test setup for combustion heat sources is schematically presented in Figure 20. The SELP rod was fixed in the insulated holder, and torches were directed toward the

superemissive crystals providing for uniform flame distribution over the crystal surface. The distal end of the SELP was pointed towards the optical power meter (Molectron PM30) as illustrated in Figures 8 and 21, or alternatively towards a PV cell (Figures 10-12). When the photon power output was investigated, a radiation shield was used in order to prevent laser power meter from observing the flame radiation.

The electric oven (Blue M56) was used as a blackbody heat source for SELP evaluation. This oven is capable of heating the SELP up to 1700 °C. It was expected that the spectra from the SELP which is heated by the electric furnace will have higher blackbody background that flame heated SELP because of IR radiation being scattered into the transparent light pipe from the oven walls. YAG exhibits high transmittance from UV region to 6 μm, so the blackbody radiation from the furnace was observed at the output end of the SELP.

3. Thermal Shock Damage

The experiments with the combustion heat sources were conducted very carefully in order to provide for uniform heating of the SELP crystals and to heat up and cool them down slowly. Thermal shock was shown to be a serious concern with respect to the crystalline garnet emitters. During start up, the flame from the torches was directed toward the crystals at some distance (usually 15 - 20 cm) then gradually moved closer until maximum power was measured. After completion of the experiments, the flame was cautiously moved away from the crystals to avoid rapid cooling. In spite of that careful procedures several SELP were damaged and fractured. Figure 22 presents the ErAG crystal damaged by thermal shock when a thermocouple touched the SELP crystal. However, there was no fracture damage to the SELP during an electric oven test. It was much easy to control temperature ramps by using electronic power controller.

C. SELP Tests

1. Temperature of Superemitter

a. Thermocouple Method

Temperature measurements are very important for SELP performance evaluation, but temperature of thermal emitters have been difficult to measure. Unfortunately, there is no single opinion about how to measure the temperature of the selective emitter. Optical pyrometry methods could not provide for adequate estimation because the correlation between emissivity of these materials and temperature is unknown. Thermocouples also can not provide for high accuracy because they radiate energy in the broad band and cool themselves more efficiently than selective emitters.

Nevertheless, we attempted to measure the temperature by using fine gage 0.0201 inch diameter wire Pt/13% Rh-Pt thermocouples manufactured by Omega (P13P - 020). There were

two approaches; the first just to take measurement at very close proximity to the selective emitter as shown in the Figure 20 (TC4). This temperature can be considered as high reference temperature (HRT). The second approach is presented in the Figure 23. The thermocouple was embedded inside a tube similar to the SELP structure (5 mm diameter, 20 cm long) made of alumina. This SELP model was heated with the combustion heat sources and the temperature measured by thermocouple was judged as a low reference temperature (LRT).

It is expected that the real selective emitter temperature is higher than that was measured by thermocouples. In addition, there is the temperature gradient across the crystal but some general tendency regarding SELP power potentials can be determined based on the reference temperature approach. Having stabilized the combustible mixture flow rate and by changing the distance between the flame and the selective emitter, it is possible to control the reference temperature and associated SELP photon output as shown in Figure 24. It was estimated that with the combustion heat sources, SELP temperature can be effectively managed up to 1600 °C.

b. Mid-IR Radiation Measurement of Temperature

The temperature of the thermal emitters was also estimated by comparing the mid-IR distribution in the 9-12 μm spectral region to the Planck blackbody distribution. Figure 25 compares the mid-IR emission from the "cold" (distal) end of the YAG light pipe to Planck distributions at 160 and 200°C, where e ~ 1. This determination is approximate but it certainly gives the correct order of magnitude of the temperature. It was checked by attaching a thermocouple to the side of the distal end of a YbAG/YAG SELP rod where the YbAG emitter is heated inside an electric furnace. The thermocouple measured 40°C at 1100°C furnace temperature, and 76°C at 1500°C furnace temperature.

The temperature of the garnet emitters is estimated by measuring the spectral distribution in the 9-12 μm region of the "hot" (proximal) end with the spectroradiometer and comparing it to Planck distributions from 1500 to 3000°C. For undoped YAG, the temperature is near 2000°C (see Fig. 26) and for ErAG, 1800°C. Again, these temperatures are approximate. Accuracy of this technique in determining temperatures of selective emitters should be further investigated.

2. SELP Spectral Investigations

a. SELP Spectra

Several experiments with combustion heat sources and an electric furnace were conducted in order to investigate the spectra of the SELP. Spectroradiometer SR 5000 (Figure 27 illustrates data processing) capable of measuring photons energy from UV to 14 μm was used for this task.

Figure 28 displays the YbAG/YAG emission spectrum taken at about 1300 °C reference temperature with four MAPP gas torches as a heat source. The flame in this case torched the selective emitter and detector was pointed to the "cold" end of the SELP. This spectral data clearly show SELP selective emission which is centered at 1 μm.

Another experiment was performed under same heat source arrangement and emitter temperature but flame was guided to the YAG (a non-selective emitter) section of the SELP. Spectra data were obtained from the YAG side of the SELP and presented in Figure 29. This data exhibit broad band emission which is typical for a gray body light source.

Figure 30 illustrates the emission coming out from the selective emitter section of the SELP when the other end of the SELP was heated with the same heat source.. The "valley" in this diagram corresponds with the 1-μm light absorption in the YbAG crystal. The selective emitter absorption phenomena will be discussed in detail in Section 2c.

Emission spectra data from the same YbAG/YAG SELP at 1320 °C electric furnace temperature (Figure 31) presented in comparison with Planck distribution for the same temperature and different emissivities. This data show very close to blackbody emitter photon energy distribution with the emissivity of about 0.25. It was expected that under furnace experiment substantial black body emission will be observed. In this case SELP is acting mostly as a waveguide for broad band radiation due to high YAG transmittance from UV to 6 μm light.

Figures 32 and 33 present the YbAG/YAG SELP spectra at 1500 °C and 1700 °C electric furnace temperature respectively. It was found that at higher furnace temperature the one micron emission increases but the black body background is still substantial.

The difference between SELP emission spectra with combustion and electric heat sources can be explained via energy transfer mechanism. Combustion heat source (low flame emissivity) heats up selective emitter by combination of convective heat transfer (from the turbulent flame jet) and conduction (inside the crystal). Electric furnace (graybody heat source) provides for high radiant heat transfer. Because of the nature of selective emitter (absorb and emit energy in a few narrow bands) it is practically "transparent" for the rest of the wavelengths outside the SELP's emission/absorption bands. This makes it difficult to transform the thermal energy effectively from the electric oven heat source to the selective emitter.

b. Comparison of Room Temperature and High Temperature Spectra

The peaks of the thermal emission of the SELPs match their room-temperature absorption peaks fairly well, with some wavelength shifting. For example, the peak of the room-temperature absorption for Yb:YAG is at 940 nm whereas the peak at high temperature is near 980 nm. The peak absorption coefficient of YbAG is determined to be 120 cm^{-1} from the Yb^{3+} peak absorption cross-section of $8x10^{-20}$ cm^2 measured at room

temperature [L.D. DeLoach *et al.*, IEEE J. Quan. Elect. 29, 1179-1190 (1993)]. The magnitude of this absorption coefficient indicates that 95% (= $1-e^{-3}$) of the thermal emission originates within a 250-μm depth (3/120 cm) of the YbAG crystal. The fine line structure of the Yb absorption group at room temperature is smoothed out at high temperatures due to the thermal line broadening. No rare-earth fluorescence is observed at high temperatures >1500°C as it is quenched by crystal phonon interactions producing fluorescence lifetimes less than 1 psc. The peak absorption coefficient of ErAG at 1.6 μm is estimated to be 40 cm^{-1} from absorption spectra taken with a 40% Er:YAG crystal.

c. Self-Absorption of Selective Emission

Splitting or bifurcation of the strong thermal emission peaks is observed for the erbium and holmium emitters. This bifurcation is particularly evident for the holmium peak at 2 μm (Fig. 34). The spectral shape of the emission is modified by absorption within the light source itself by the same species (*i.e.*, rare-earth ions) causing the emission. This phenomenon is called self-absorption and has been readily observed and analyzed in spectroscopy [R.D. Cowan and G.H. Dieke, Rev. Mod. Phys.20, 418-455 (1948)]. The absorption at the peak of the emission is stronger than at the wings of the emission, and so can produce a relative suppression of the emission at the peak to the wings, splitting the emission into two lobes. This bifurcation (see Figure 35) is called self-reversal and occurs when the peak absorption coefficient α_0 follows the condition $\alpha_0 L > 1$.

Three stages of self absorption for erbium thermal emitters are shown in Figure 36. The left-hand and center spectra in the figure show the 1.5-μm Er thermal emission from 2-mm and 25.4-mm long ErAG crystals, respectively, both in the SELP configuration. It is observed that the 25.4-mm thick crystal exhibits a near self reversal situation, while the 2-mm crystal does not appear to be self reversed. Because the Er 1.5-mm emission is a group of many (fifty-six) lines of varying peak absorptions, and not a single line, it is difficult to give a simple interpretation of the self-absorption modification here. The right-hand spectrum illustrates the emission from an erbia (Er_2O_3) mantle which has effectively a very thin thickness, demonstrating a sharply peaked emission indicative of weak self absorption.

The self-absorption effect is very important because, in fact, it determines the rare-earth doping level and emitter length through the function of the optical path length (αL).where α is the absorption coefficient (cm^{-1}) at the peak of the selective emission. For the initial experiment reported here, we used emitters that were too long or, alternately, crystals that were too highly doped. With the 100% doping levels, the crystals should have been less than a 1 mm in length. However, with that length, the crystals would not remain bonded to the YAG light pipe because differential thermal expansion would break the bond

between the rare earth garnet and the undoped YAG garnet. By calculations using Cowan and Dieke's formulas [*loc. cit.*], it was found that a single-crystal Tm:YAG emitter at approximately a 10% doping level should be used with a 5-mm length. A Tm:YAG/YAG SELP could not be obtained in time for this six-month Phase I study in order to verify this determination. Thulium was the selective emitter chosen to pump neodymium lasers.

d. Graybody Background

The weak, broadband, background emission up to 4 μm is due to graybody emission from impurity and color-center absorption in the light source. The reduction of this graybody emission is of primary concern in making an efficient selective thermal emitter. Single crystal garnets can be grown with high purity and low density of crystalline structural defects, primarily as a result of the well-developed laser technology which has grown high optical quality garnet crystals in large sizes for over thirty years. Therefore, garnets are chosen as selective emitters in this investigation to reduce the graybody background. The dominate impurities in garnets giving potential graybody emission are trivalent chromium (Cr^{3+}), divalent rare earths (such as Yb^{2+}), and other unwanted trivalent rare earths (such as Sm^{3+}). For example, for the YbAG/YAG SELP, we observed a bluish color due to Yb^{2+} content in what should have been a water-white YbAG crystal. By temperature cycling, the blue color was annealed out of the YbAG, and no divalent absorption was subsequently identified.

Color-center absorption due to as-grown structural defects give rise to a broadband absorption. The crystal defects trap electrons which produce broadband absorption both in the visible and infrared regions. Ion mobility occurs for O^{-2} in garnets at temperatures above 1300°C [K.B. Schwartz and A.G. Duba, J. Phys. Chem. Solids 46, 957-962 (1985)], which also leads to broadband absorption. Finally, color centers can be formed by phase changes, both solid-solid and solid-liquid, near the garnet's melting point. However, it is believed that the garnet emitter temperatures are too low in the current experiment to observe such phase-change absorption. Figure 37 compares the graybody background emission for heated YAG (undoped) and YbAG. Both garnet crystals have nearly identical graybody backgrounds, both in magnitude and shape. The YAG spectrum on the left-hand side shows emission possibly arising from chromium impurities in the visible region and broadband emission from as-grown color-center defects which peak near 1.6 μm.

3. SELP Photon Power Investigation

The major objective of this investigation was to evaluate the potential photon energy density that can be obtained from the SELP and delivered to a target such as a PV cell or laser crystal. It was expected that outcoming light divergence will depend on the SELP crystal

material. In order to collect all the energy from the SELP at the detector (PM 30) and define a distance between the SELP and face of the detector, we measured photon energy form the Er_2O_3 coated SiO_2 SELP as a function of the distance form SELP to detector. These data presented in Figure 38, showing that the gap of about 2 mm is adequate for total energy collection. During these experiments, we tried to be more conservative setting the gap within 0.7-1.5 mm.

The photon power measurement setup for combustion heat sources schematically presented in the Figure 20, 21 and 39. Figure 39 illustrates general arrangement for test setup with an electric furnace as a heat source and the Figures 15, 16, 18 and 19 display the hardware under test conditions. The first set of experiments was conducted with YbAG/YAG and YbAG/YAG SELPs using MAPP gas torches as shown in Figure 8. The results of the test with the ErAG/YAG SELP is presented in the following Table 2.

Table 2. Photon Power Output from ErAG/YAG SELP
ErAG crystal is 25 mm long and 5 mm in diameter; YAG section 20 cm long and 5 mm in diameter. Heat source was C_2H_2/O_2 torch.

Emitter Reference Temperature, °C	**Photon Power Output, W**	**Photon Power Density, W/cm^2**
1000	0.19	0.97
1100	0.33	1.68
1122	0.38	1.94
1200	0.50	2.55
1500 - 1600	3.39	17.30

This experiment demonstrated capability of the SELP to provide for a high level of radiant flux density to be delivered to the target. Note that majority of TPV systems are designed to operate with the radiant flux density at the PV face in the range of 6 - 9 W/ cm^2, assuming high photon collection efficiency. At the same time, typical TPV generator design usually considers placing the emitter at the center of the device and PV arrays around the emitter. This is the simplest solution that allows constructing an uncomplicated burner/emitter system and providing for effective PV cooling scheme. Such configuration features have very high (over 50%) photon losses due to large end area and PV-face illumination usually less than 4-5 W/cm^2. We consider the SELP approach as an extremely powerful tool to minimize photon losses and increase the efficiency of TPV/laser systems

From the other point of view, the radiant flux density that was achieved during this experiment is not a maximum obtainable for SELP technology. It is obvious that the photon power which is generated and delivered via SELP strongly depends the temperature of the selective emitter. By boosting temperature up we expect to increase significantly radiant flux

density and the way to reach higher emitter temperature is to fabricate SELP of smaller substrate diameter that will intensify turbulence and associated heat transfer in the combustion zone.

There are two major advantages of having extremely high radiant flux with the small area of illumination. For TPV application it is possible to benefit by using high concentrator type PV cell, for example the PV cell manufactured by SunPower and Amonix are rated up to 250 suns or 25 W/ cm^2 of incident illumination. It minimizes the area of the PV arrays and cost of the TPV device. The second advantage of this approach is flexibility to design the PV arrays with PV cell which are located at some distance away from each other to provide for superior heat rejection capability. For the laser application it is obvious that high radiant flux from the SELP will allow to design a higher capacity lasers.

Combustion test of YbAG/YAG SELP showed similar results in a compatible temperature range. These results presented in Figure 40. The photon power output was continuously raising starting from 60 mW at 800 °C up to 600 mW at 1300 °C. There are no data which reflect the performance at higher temperature with combustion heat source because the SELP was damaged by thermal shock.

Much higher photon emissive power was recorded when the same YbAG/YAG SELP was tested in the electric furnace (Figure 41 and 42). This test was conducted with better capability to manage the heat source temperature by electronic power controller. The temperature was gradually increased from 1000 to 1700 °C and photon energy was measured at stable temperature conditions. This test was repeated and the results were consistent as shown on the diagram (Figure 41). Maximum power density of about 27 W/cm^2 (Figure 42) was achieved at 1700 °C which is comparable with the highest radiant flux measured from the advanced emissive matrix (AEM) combustion devices which have been developed at Quantum in last three years.

It was mentioned above that we expected to observe a substantial difference in spectra and photon power output from the SELP with a combustion and electric heat sources due to different heat transfer mechanism. The comparison of the photon energy production at the same temperature range is presented in Table 3.

As shown in Table 3, within the 1000 - 1200 °C temperature interval, the SELP - electric furnace setup produced approximately three times more photon energy than SELP - combustion arrangement. In other words, blackbody radiation "leaks" throughout the SELP when the electric furnace is used. If the same tendency extends over elevated temperatures (1700 - 1900 °C), we expect from SELP - combustion devices about 10 W/cm^2 at 1700 °C and approximately 18 W/cm^2 at 1900 °C of selective photon output which could be effectively converted to electricity by silicon PV cells.

Table 3. Photon emissive energy generated by YbAG/YAG SELP with combustion and electric heat sources

Parameters	Temperature, °C		
	1000	1100	1200
Photon Power Output, W Combustion Heat Source (CHS)	0.28	0.42	0.57
Photon Power Output, W Electric Furnace (EF)	0.9	1.2	1.67
Ratio EF/CHS	3.21	2.86	2.93

D. Spectral Filters for SELP

The main purpose of spectral filters is to recuperate the optical energy that is outside the absorption bands of the neodymium laser crystals. Return of radiation to the selective emitter by reflection from the filter will improve the energy efficiency of the emitter. The energy from the radiation having undesired wavelengths will be recycled in the emitter, reducing its radiative heat loss. Figure 43 shows a photograph of the test of the recuperative ability of an ITO filter, and Figure 44 shows the spectral responses of two different ITO filters. The difference between the two ITO filters is the relative content of tin (Sn) to indium (In) oxides. The ratio of tin to indium of 8:92 gives the best response for our application to pump neodymium lasers in the 790-890 nm bandwidth. The 8:92 ITO reflects light at wavelengths longer than 1 mm, and an added dielectric coating will extend the cutoff down to 890 nm

E. SELP Pumping Test of Neodymium Laser

SELP pumping of Nd:YAG and Nd:YVO_4 laser slabs (3x5x10 mm) was conducted, investigating the optical coupling efficiency from the SELP into the laser gain medium. The schematic of the laser pumping experiment is given in Figure 45, and a photograph of the setup is shown in Figure 46. The thulia emitter was heated by a torch giving light in the neodymium pump bands 790-890 nm. Since a thulium garnet crystal was not available, a thulia felt was prepared as substitute at Quantum Group. The ITO filter position is labelled as "IR Bandpass Filter" which reflected the 1.7 μm emission of Tm back onto the emitter, recuperating the otherwise lost emission energy. Various methods were used to coupled the Tm emission into the laser crystals: juxtaposition of laser crystal to the SELP rod, reflectors collecting emission into crystal, and lenses focusing light into crystal. For the present selective emitter design, a condenser lens

(labelled *L* in Figure 45) was found to be the most effective. The laser crystals were mounted vertically in a holder than also acted as a light/heat shield for other optical components.

The Nd:YAG laser slab had its entrance pump face (5x10 mm) antireflection (AR) coated centered at 808 nm and the back pump face, high reflectance (HR) coated in the wavelength band centered at 808 nm. These coatings maximized the use of the selective emission in pumping the YAG crystal. The Nd:YVO_4 laser slabs did not have coatings on the pump faces.

The emitter optical power transmitted by the laser crystals was monitored by a power meter.(*PM2*). The expected laser gain was probed by a cw 1.064-mm Nd:YAG laser (*L1*) pumped by a semiconductor laser diode. This probe wavelength also overlapped the gain bandwidth of Nd:YVO_4, making it effective in detecting any laser gain for Nd:YVO_4. The alignment of the optical setup was determined by a cw He-Ne gas laser (*L2*) at 632.8 nm. The laser slabs were mounted vertical in order to allow space for the use of torches at the end of the light pipe and the SR5000 spectroradiometer.

The laser active crystals were in the shape of slabs (3x5x10 mm) with the pump face being the largest 5x10 mm face. The laser emission would exit from the 3x5 mm faces, transverse to the pump faces. Figure 47 shows the Nd:YAG fluorescence at 980 and 1064 nm exiting from those faces as detected by the SR5000 spectroradiometer at the "Probe Power Meter" position. Since the spectroradiometer does not have high resolution (30 nm at 1 mm), the usual spectral fine structure of the Nd fluorescence is not observed. The Nd:YAG had too low a laser gain (< 2%) to be detected by the laser probe beam in our setup.

In addition, the SR5000 spectroradiometer was used in the location of the "Emitter Power Meter" to examine the spectrum of the pump light transmitted by the laser crystal slabs, and in the position of the "Probe Power Meter".to measure the slab emission spectra . Figure 47 shows the lack of transmitted pump light spectrum through the Nd:YAG, due to the high reflectance (HR) coating on the back pump face..

The transmission through three laser crystal slabs were measured to understand the absorption and fluorescence bands in the crystal. The signal-to-noise ratio for these measurements were lower than the pure mantle spectra due to crystals' small dimensions and the 3.1 meter minimum distance required for focusing the spectroradiometer. The spectra of the ytterbia felt selective emission through the 0.7% Nd:YVO_4 and Nd:YAG crystals are given in Figures 48-49. The spectra of thulia through the same crystals are given in Figures 50-51.

The thulia felt through the ITO filter has relatively smaller emission bands at 699 and 816 nm than those in the thulia mantle spectrum. The band at 1.17 μm was seemingly lacking, however it may have been masked by a sharp spike due to the detector change and low sensitivity of the silicon detector in this wavelength. The peak of the broad band at 1.78 μm shifted to 1.68

μm. For the 0.7% Nd:YVO_4 crystal, both the thulia and ytterbia emitter spectra show similar absorption peaks at 750, 805, 880 nm and strong absorption at 1000-1150 nm.

It is believed that for Nd:YVO_4 under the thulia excitation, the crystal was near laser threshold, if not slightly above it. Dielectric mirrors were placed parallel to the 3x5 mm crystal faces of the Nd:YVO_4 slab to form a laser resonator with 5% output coupling and 100% back reflector. Figure 52 shows the enhanced Nd:YVO_4 fluorescence spectra with this setup, but under circumstances of poor detection having low resolution (~30 nm). Also, IR background from the selective emitter overlapping this spectral region made it difficult to detect the cw laser action. We attempted to reduce the IR background by using various filters in the pump beam, but it was not successful as these filters also reduced the pump power. An improved ITO filter with a dielectric overcoat should be the solution. Pulsing the pump beam by a mechanical chopper would provide the relaxation-oscillation signature needed to verify laser action.

F. TPV Measurement using SELP

Two types of photovoltaic cells were utilized during the TPV experiments. The first was Si concentrator type (250 suns) purchased from SunPower, Sunnyvale, CA. It has rectangular shape, 1.5 cm x 1.5 cm with active area 1.56 cm^2. This cell was mounted on a metal plate 5 cm x 5 cm. Maximum conversion efficiency occurs at about 1.0 μm, with spectral cutoff at 1.15 μm.

The second PV cell was manufactured by Edtek, Kent, WA. This cell is a concentrator type GaSb cell, circular in shape with 5-mm diameter. This cell shape perfectly fits the size of our SELPs. Maximum conversion efficiency is at 1.55 micron, with cutoff at 1.73 micron. The GaSb cell was mounted on a copper water-cooled heat sink.

In order to avoid energy losses, the distance between the PV cell and the "cold" end of the SELP was maintained from 0.2 to 1.0 mm during all the tests. The TPV measurement setup is presented in the Figures 10-12 (SELP with combustion systems) and 13, 14, 17 (SELP with electric furnace).

The results of the YbAG/YAG SELP - combustion test is presented in Figure 53. The temperature was in the range from 800 to 1300 °C. Si PV cell was used without any cooling system. No substantial PV temperature rise observed during the test. Maximum PV power was about 45 mW which corresponds to 230 mW/cm^2 of PV power density. Because this SELP was damaged by thermal shock, we were unable to test this SELP at elevated temperatures. Nevertheless, it is a good power density taking into account the relatively low emitter temperature.

Much more impressive results were obtained for the ErAG/YAG - combustion test with the GaSb PV cell (setup presented in Figures 10-12). Maximum SELP photon power output

during this experiment was measured to be 1.05 W. Emitter temperature at this point was estimated of about 1350 °C. PV power production was 306 mW or 1.56 W/ cm^2. Photon to electron conversion efficiency was calculated to be 29% indicating that selective emission was delivered to the PV cell. Note that the maximum photon emission from the same Er SELP was measured later on to be 3.39 W, which is three times more than was that discussed above. Assuming the same PV conversion efficiency, we can expect to obtain the PV power density of about 5 W/ cm^2 at a 1500 - 1600 °C emitter temperature.

The SELP PV electric furnace test was conducted with YbAG/YAG SELP because at this time ErAG crystals were damaged by thermal shock. We measured PV power output versus electric furnace temperature for both Si and GaSb cells. The results of this test are displayed in Figures 54 and 55. It was found that the GaSb PV cell produces more power than Si cell at the same reference temperature conditions. Again, it is not a surprise because the SELP output spectra with electric furnace heating contains a large blackbody background as we mentioned above.

Data presented in Figure 55 display the consistency of the test results which were obtained from YbAG/YAG SELP - electric furnace system coupled to the Si PV cell. The first set of measurements was conducted when the electric furnace temperature was ramping up to 1700 °C, the second set was done in the furnace cooling regime. Both curves are very close, confirming consistence of the tests results.

The most exciting phenomena was observed that the distant end of the SELP was less than 100 °C on the side and less than 160 °C on the cross section surface at the maximum furnace temperature. Figure 19 illustrates the SELP setup during the experiment, showing a SELP temperature of 59 °C at the furnace temperature of 1300 °C. PV thermal loading in this case is much lower compared with the typical TPV combustion device when emitter is separated from the PV array with the quartz shield. In such systems, PV cells are usually located a few inches away from emitter, collecting limited useful energy from emitter as well as strong long wavelength parasitic IR radiation from the hot quartz shield. The SELP effectively reduces PV thermal loading and thus allows the PV cell to be placed in close contact (ideally optically coupled) with the SELP output end, essentially increasing the photon collection efficiency.

Section III. Technical Merit of Project

A new light source using dielectric solids has been developed to power TPV and to pump lasers. The light source is a refractory solid emitter heated to a relatively high temperature (over 2000°C adiabatic flame temperature) by combustion. The solids studied were the rare-earth oxides of ytterbium, erbium, holmium and thulium in the form of single crystals, felts and mantles

as thermal selective emitters. The combination of the selective emitter with an optical waveguide is called a "superemissive light pipe" (SELP) and greatly increases its effectiveness. High potential for TPV was demonstrated by using an ytterbium garnet crystal SELP emitter powering a silicon photocell, and an erbium garnet crystal SELP emitter powering a GaSb photocell.

Thulium emitters were chosen to pump neodymium lasers, over the ytterbium and erbium emitters, through a spectroscopic investigation. This study uncovered that the self-absorption effect is very important consideration to determine the rare-earth doping level and emitter length through the function of the optical path length (αL).where α is the absorption coefficient (cm^{-1}) at the peak of the selective emission determines the optical path length. For the initial experiment reported here, we used emitters that were too long or, alternately, crystals that were too highly doped. With the 100% doping levels used here, the crystals should have been less than a 1 mm in length. However, with that short length, the crystals would not remain bonded to the YAG light pipe because differential thermal expansion would break the bond between the rare earth garnet and the undoped YAG garnet. It was predicted that a single-crystal Tm:YAG emitter at approximately a 10% doping level should be used with a 5-mm length.

No irrevocable evidence of cw laser action was observed, yet some enhanced 1064 nm emission was recorded for the Nd:YVO_4 crystals.. It is believed that the laser performance was near its threshold, but the overlapping IR background from the selective emitter and the low spectrometer resolution made it difficult to detect the laser action. A Tm SELP needs to be fabricated to reach laser performance.

High temperature spectroscopy of rare-earth compounds was begun during this project, and appears to be a very fruitful study for the future. Also, a noninvasive temperature measurement of selective emitters was begun to be developed using the blackbody emission in the lattice absorption region (9-12 μm) of the crystals.

Section IV. Potential Applications

The use of SELP as an optical source would reach applications in both the defense and commercial markets. The self-powered self-contained aspects of SELP powered systems give its usefulness immediately to TPV electrical generators, lasers, and even as direct light sources. Table 4 lists some of the applications for these SELP-powered systems. Self-powered lasers pumped by SELP give self-contained mobile systems needed for applications in isolated environments as satellites, submarines, battlefields and third-world countries, where traditional electrical power is restricted or intermittent. SELP increased efficiency of TPV electrical

generators would give rapid deployment power supplies and auxiliary power units for emergencies and disasters.

Using the SELP as a light source directly would provide a low-cost, long-life, efficient light for applications where very high brightness (power per area per solid angle) is not required. A red-orange light source using SELP, which is possible, would provide a light activator for photodynamic therapy (PDT). Since this source can be tuned over the red-orange spectrum, the selection of PDT drugs is not limited by the light source, which it currently is.

Table 4. Applications of SELP-Powered Systems

SELP Powered System	Defense	Civilian
TPV Electrical Generator	Power Supply for Satellites & Submarines Rapid Deployment Power Supplies	Self-Powered Appliances Auxiliary Power Unit for Emergencies & Disasters
	Battery Charging	Electrical Generators for Off-line Homes, RVs, Boats
	Field Kitchens	Sensors and actuators
Lasers	Battlefield Surgery	Third-World Laser Medicine Field Medicine (Veternary)
	Submarine Detection and Communication	Underwater Obstacle Avoidance
	ASW Laser Sound Sensing	Bathymetry Underwater Rescue
	Biological and Chemical Warfare Defense Laser Weapons (IRCM, LASS) New IR and Tunable Laser LIDAR Security Systems	Environmental Monitors Material Processing Wind Shear Detection Security Systems
Direct Light Source	Water Purification for Deployed Troops	Water Purification IR Security Systems Photodynamic Therapy

Section V. Justification of Phase II Continuation

The work conducted during the Phase I project demonstrated the usefulness of the SELP design in producing thermal selective emission to power both TPV and lasers. The experimental verification of ErAG SELP application to TPV was highly successful. It produced a photovoltaic electrical power density of 1.56 W/cm^2 (0.306 W) with a GaSb cell, 5 mm in diameter. This work should continue into a Phase II project to construct an operating engineering model of a SELP TPV unit involving Er SELP emitters and GaSb photovoltaiccells.

The use of SELP for pumping lasers showed promise but the SELP laser was a harder experiment to carry out. Thulium was the selective emitter chosen to pump neodymium lasers. Thulium garnets were not available for Phase I since they could not be delivered within the six month time period so no Tm SELPs were available. It was determined that a single-crystal Tm:YAG emitter with a 10% doping level should be in with a 5-mm length bonded to YAG to make a Tm:YAG/YAG SELP. However, thulia mantles were made and investigated in pumping both Nd:YAG and Nd:YVO_4 laser slabs. Some enhanced 1064-nm emission was recorded from the Nd:YVO_4 slab but no irrevocable evidence of laser action was obtained. Most of the problem is the current status of our lab equipment gives only low spectral and slow time resolution. This laser experiment should to be repeated with a Tm SELP under higher resolution. A much improved SELP can be constructed to produce higher emission powers and much reduced thermal fracture damage due to differential thermal expansion. Lower rare-earth concentrations, as determined by the self-absorption effect, and near 5-mm thin selective emitter lengths would lead to an improved SELP. We believe these improvements would lead to a clear demonstration of laser action pumped by SELP.

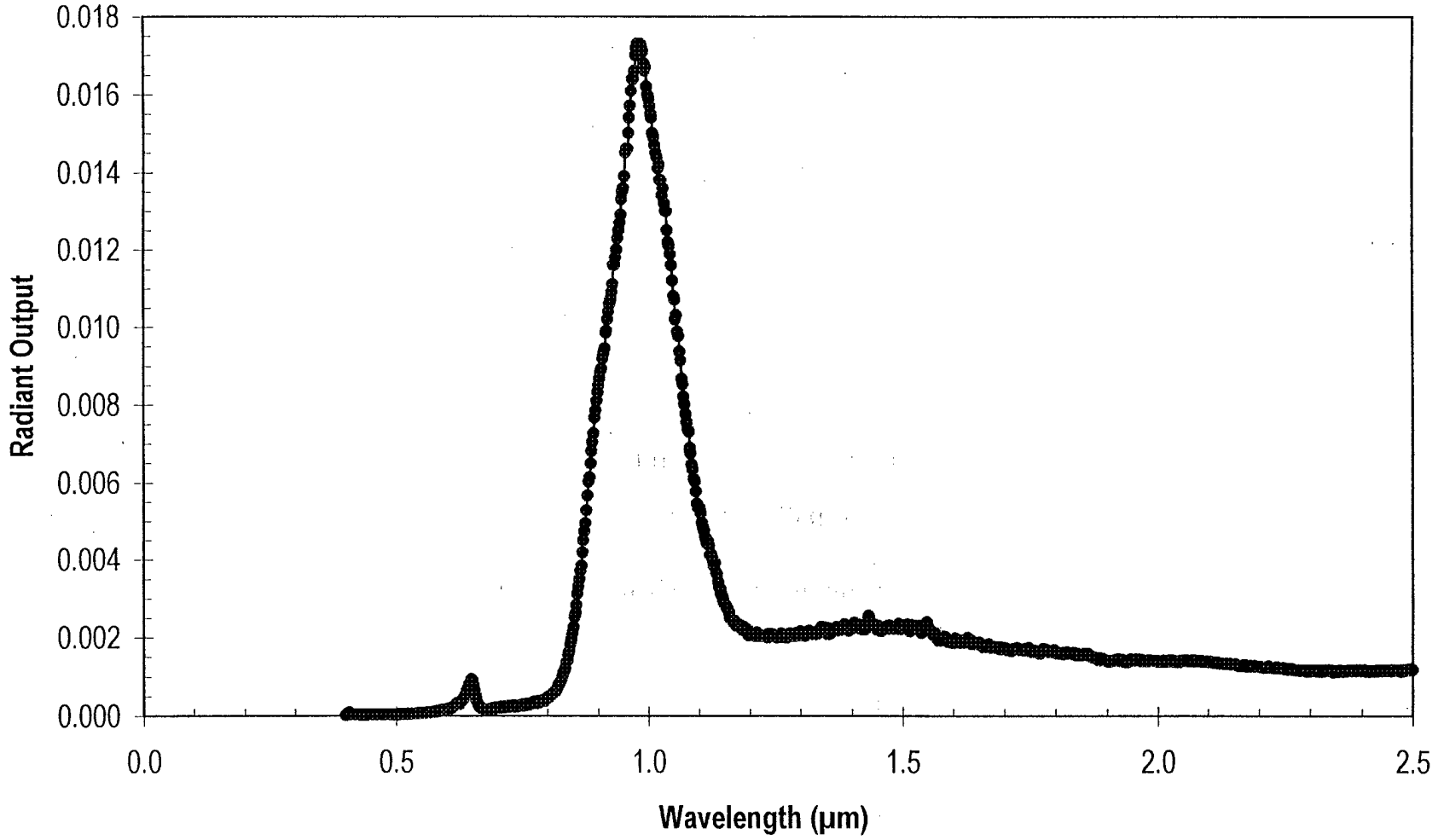

Figure 1. Ytterbia Mantle Spectrum.

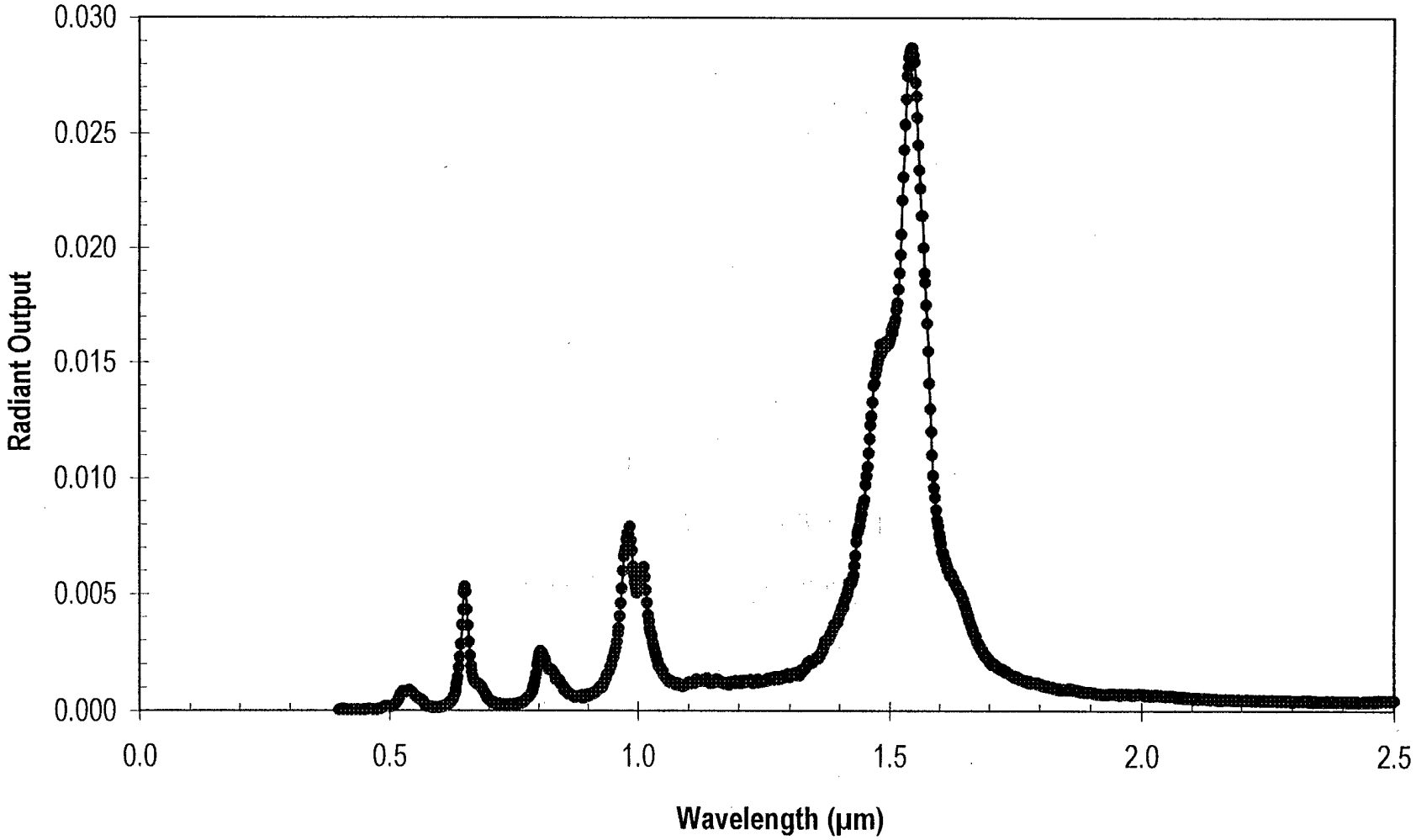

Figure 2. Erbia mantle spectrum

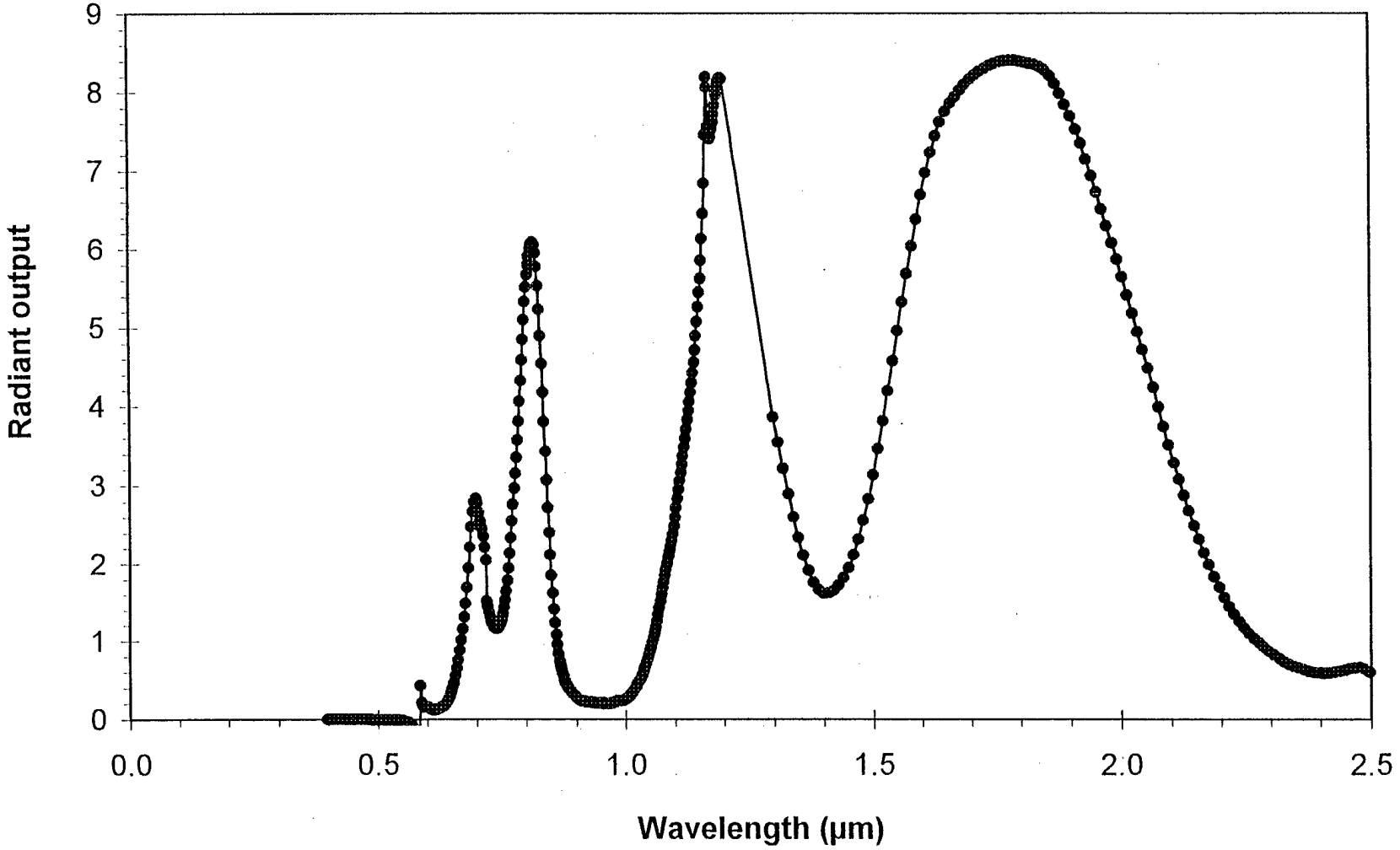

Figure 3. Thulia mantle spectrum.

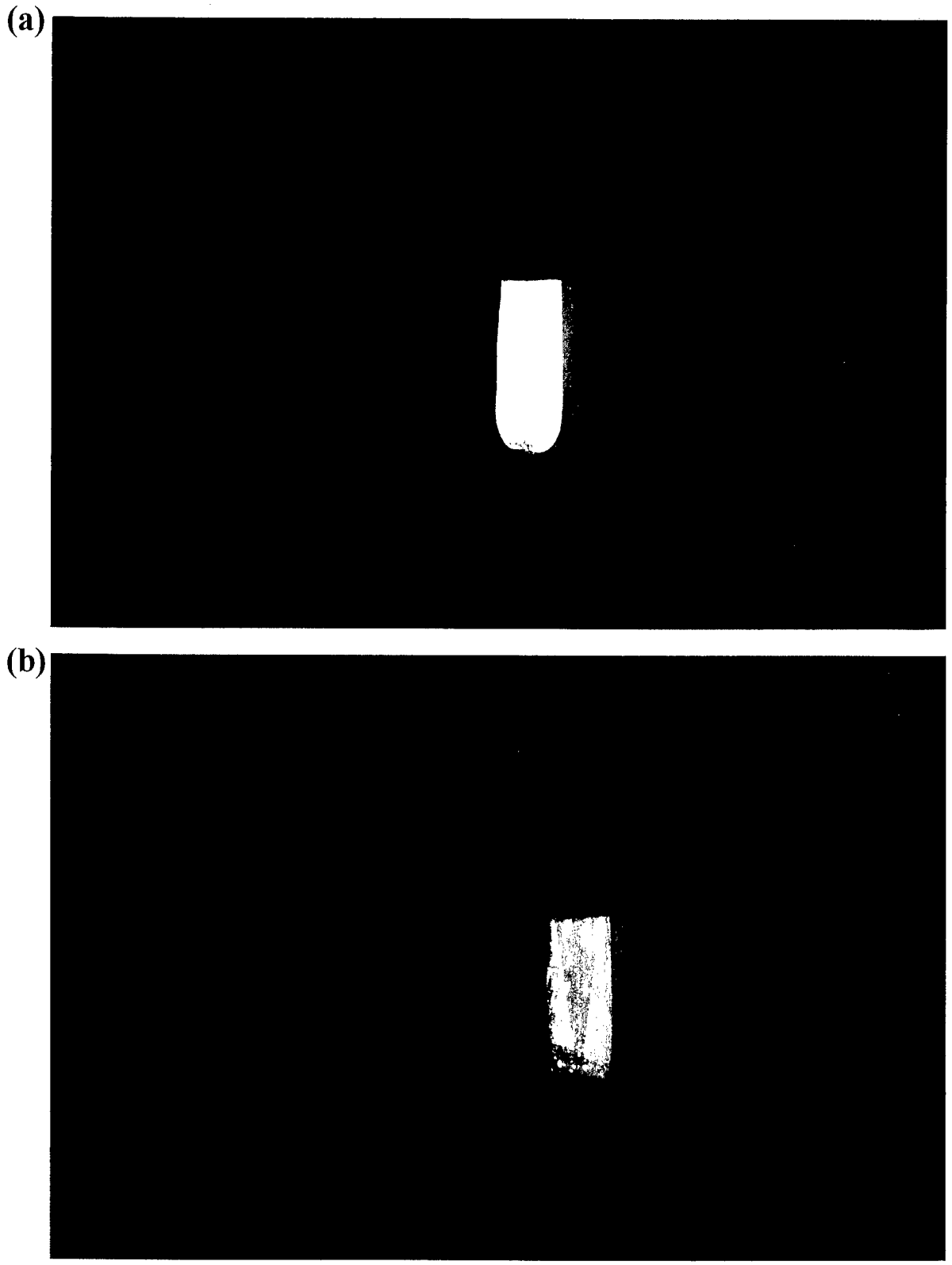

Figure 4. The thulia mantle shows white color at high fuel input rate (a) and rosy-red color at low fuel input rate (b).

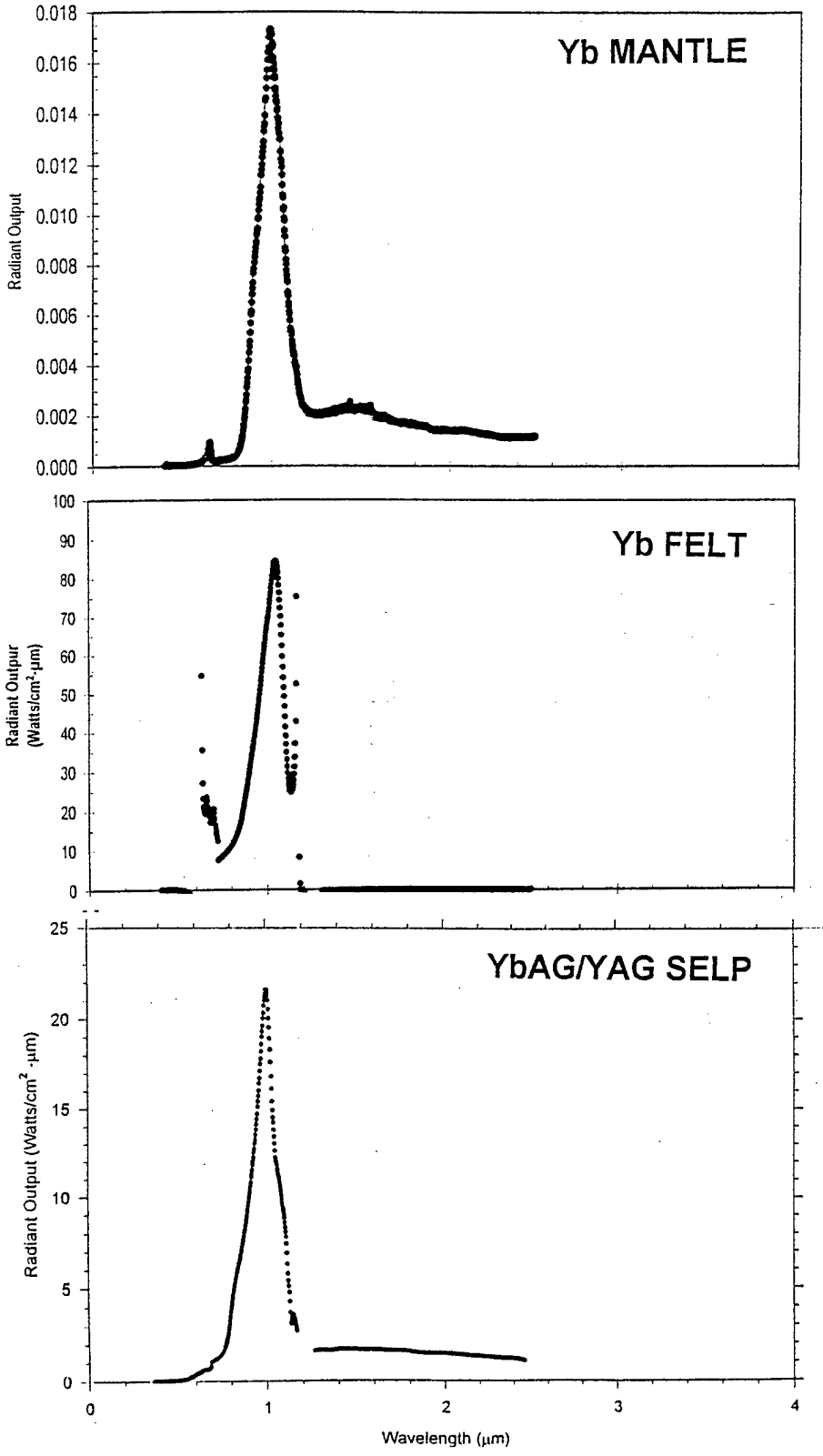

Figure 5. Spectra of ytterbia mantle, felt and light pipe.

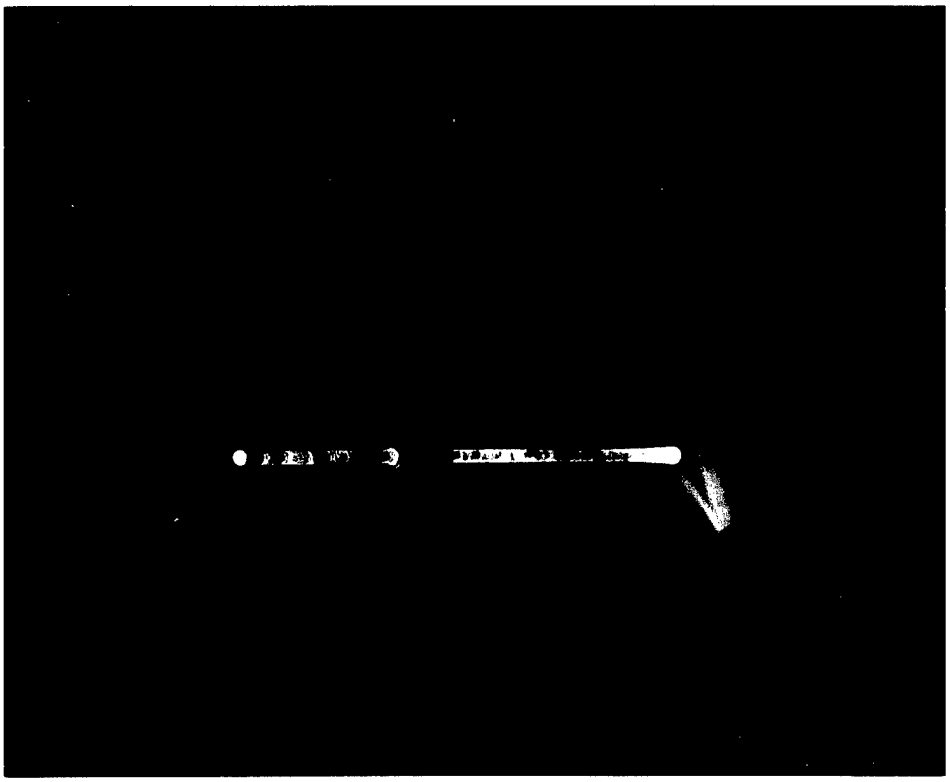

Figure 6. Er_2O_3 coated SiO_2 SELP of 20 cm in length and 3 mm in diameter heated by torch.

Figure 7. ErAG/YAG SELP rod of total length 22.5 cm long and 5 mm in diameter with ErAG crystal of 2.5 cm fused to one end of the 20 cm long YAG.

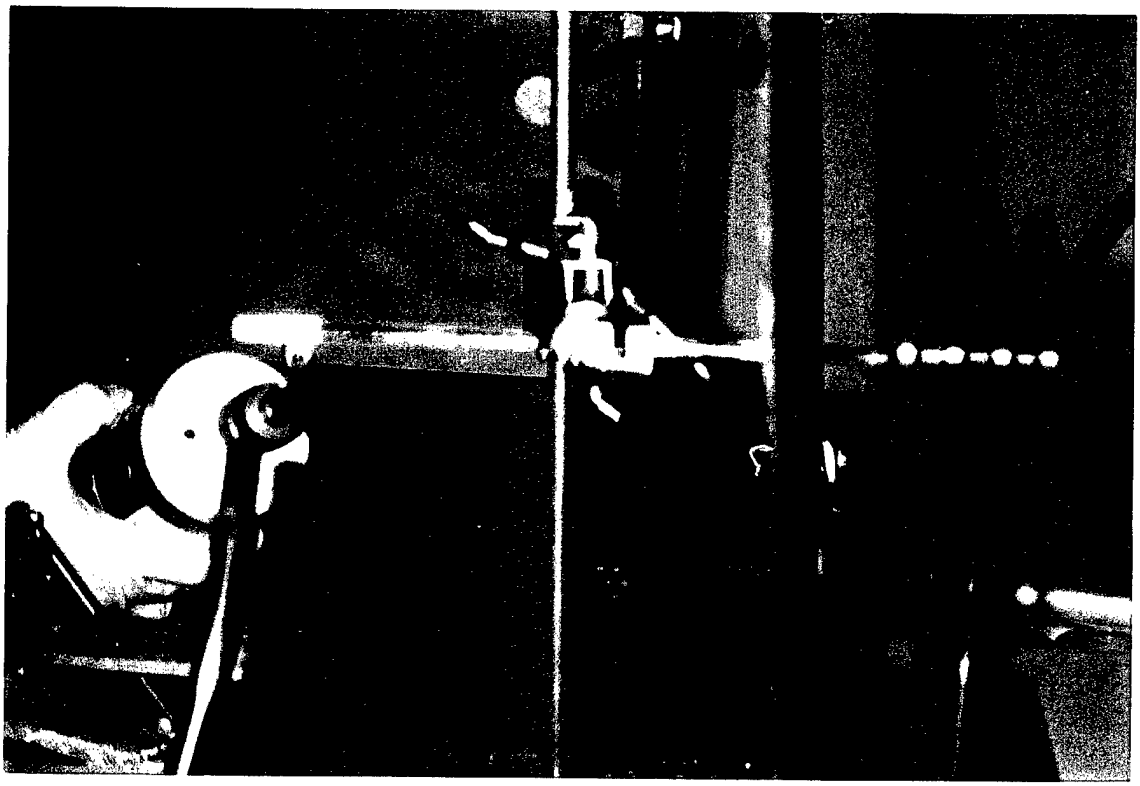

Figure 8. Photon Power measurement of ErAG/YAG SELP.

Figure 9. Close-up of SELP oxygen/acetylene torch assembly.

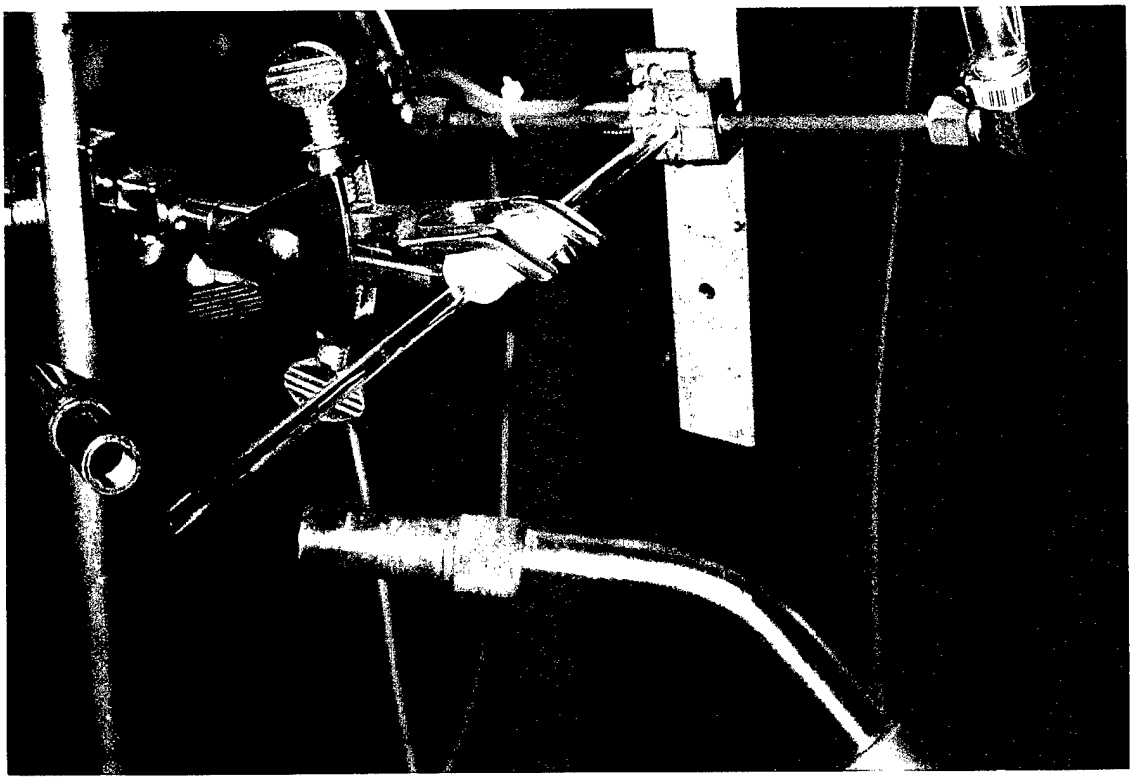

Figure 10. PV cell power measurement setup for ErAG/YAG rod.

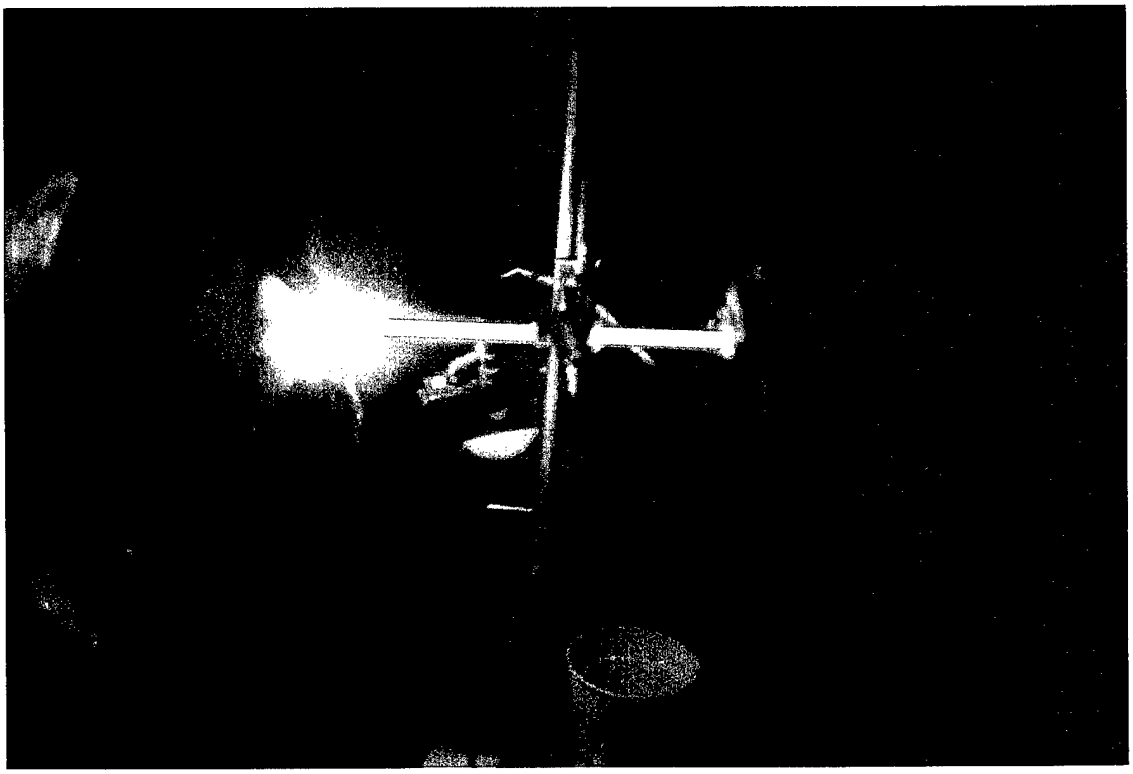

Figure 11. Photo of PV power measurement of ErAG/YAG with torch running.

Figure 12. Another view of PV cell power measurement of ErAG/YAG SELP during torching.

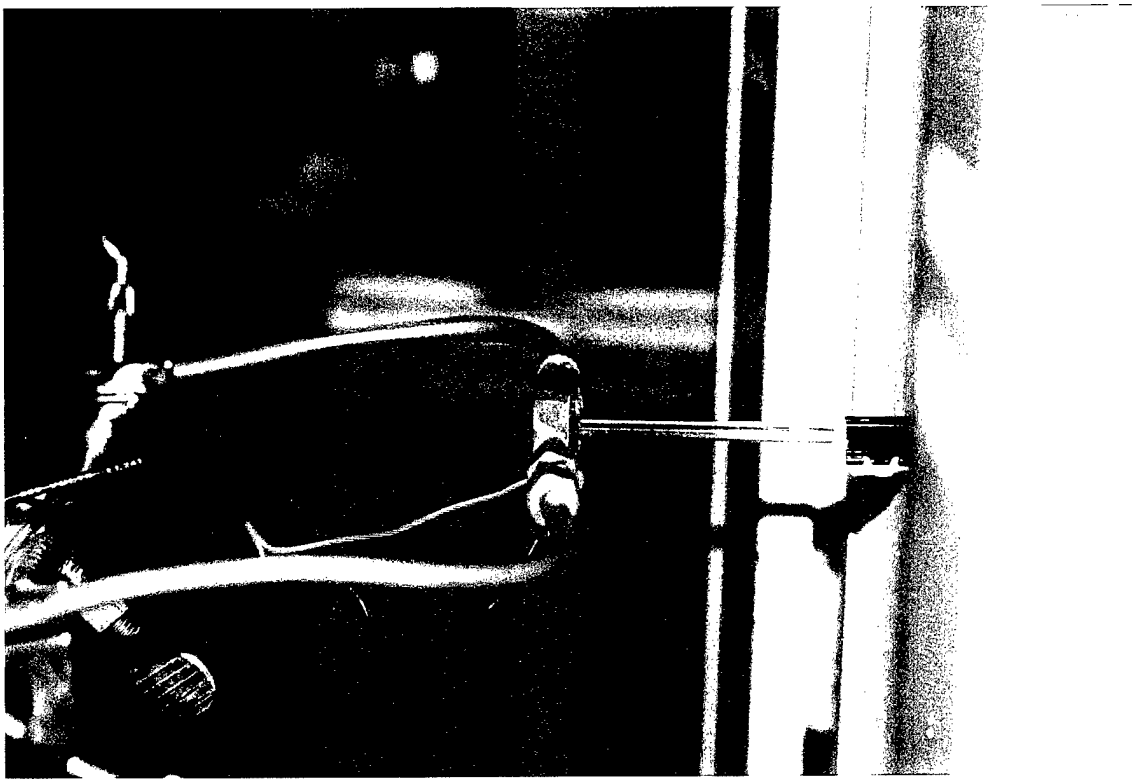

Figure 13. Close-up of YbAG/YAG SELP power measurement setup using high temperature furnace as heat source.

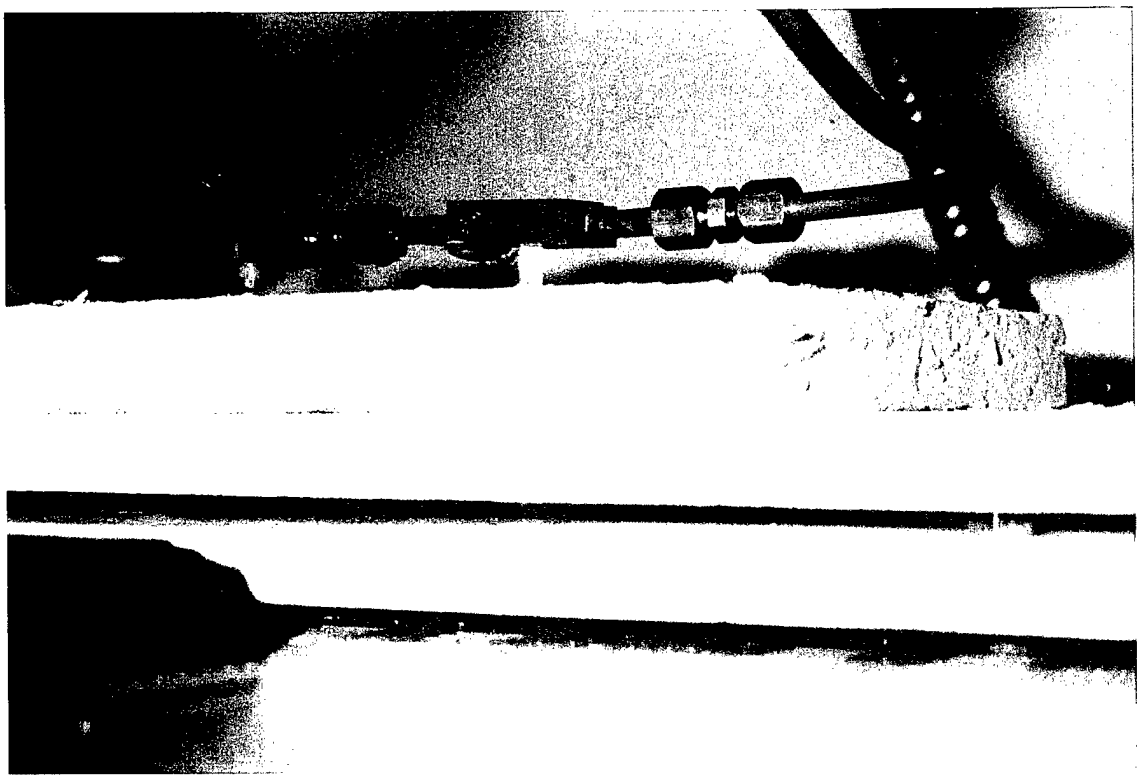

Figure 14. PV cell power measurement of YbAG/YAG SELP with the electric furnace temperature at 1700°C.

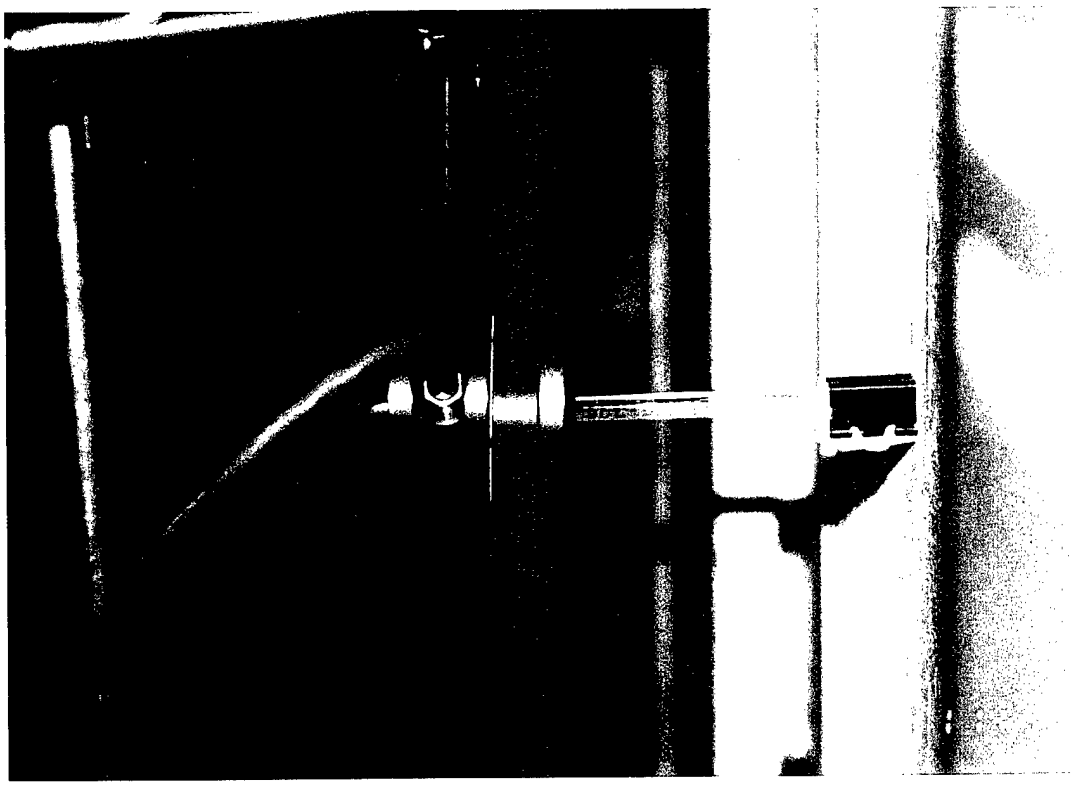

Figure 15. Photon output measurement of YbAG/YAG SELP with high temperature furnace as heat source.

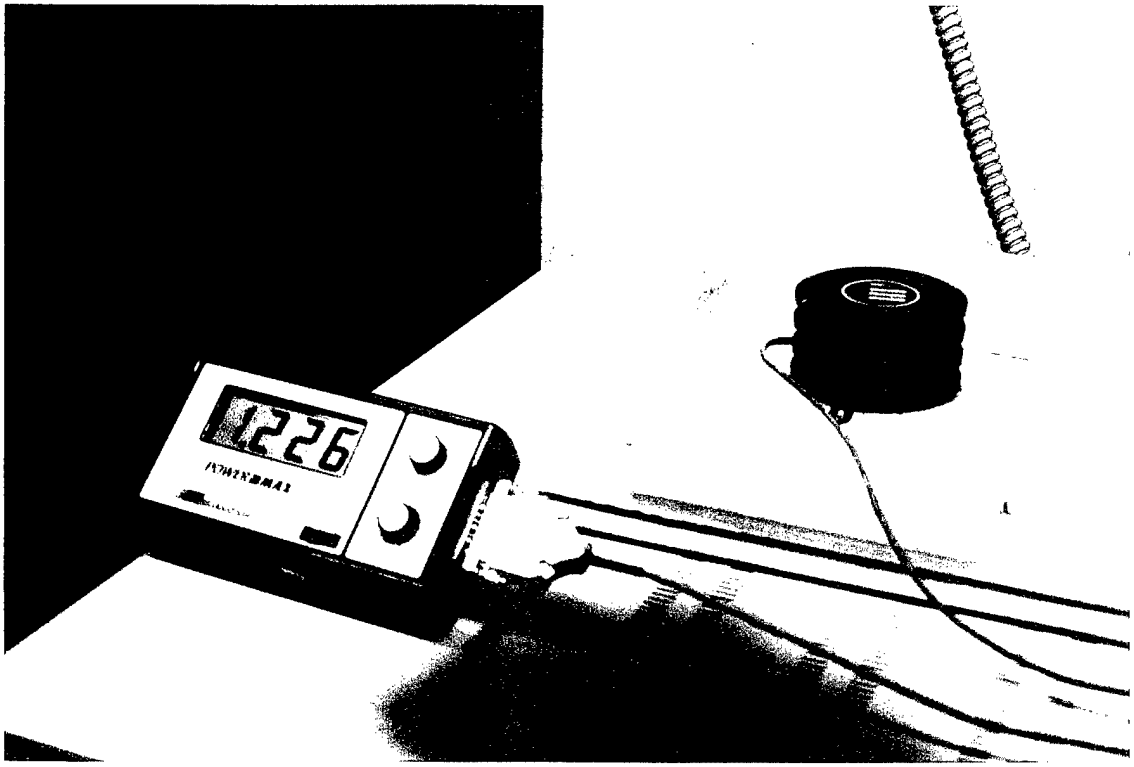

Figure 16. Photon output characterization of YbAG/YAG SELP in the electrical furnace test showing power meter portion.

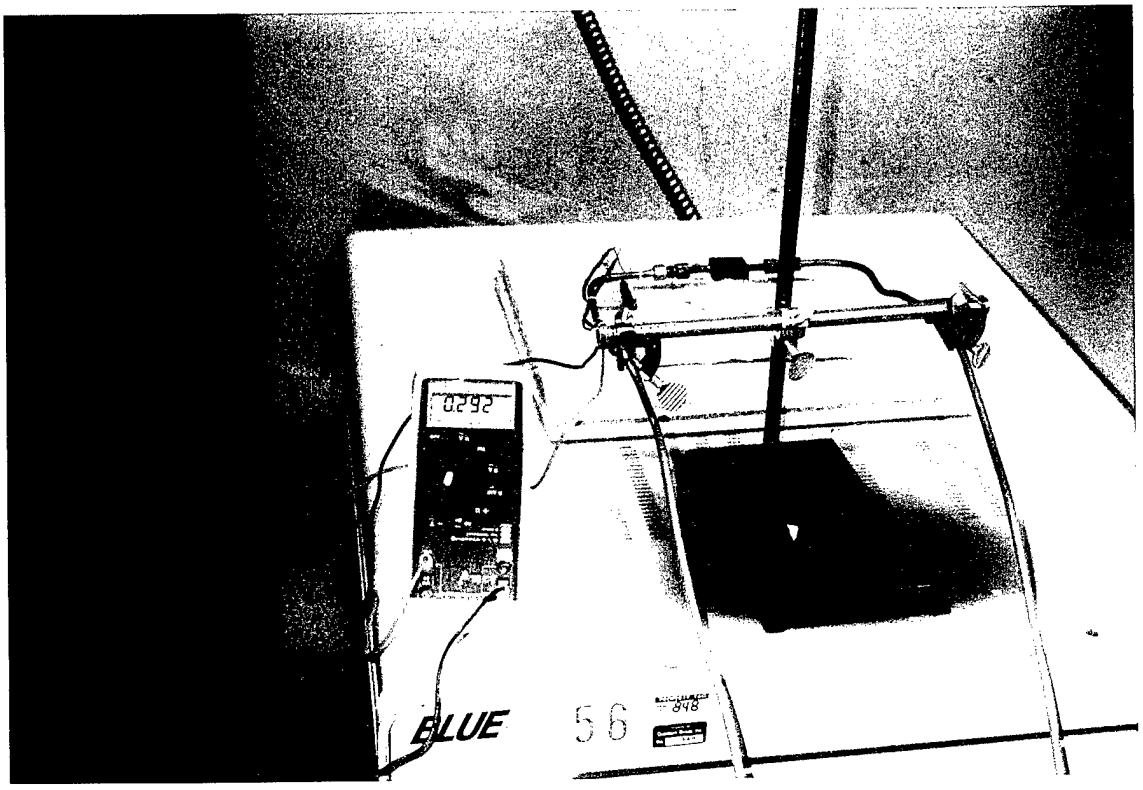

Figure 17. GaSb PV cell power evaluation of YbAG/YAG SELP PV using high temperature electric furnace as the heat source.

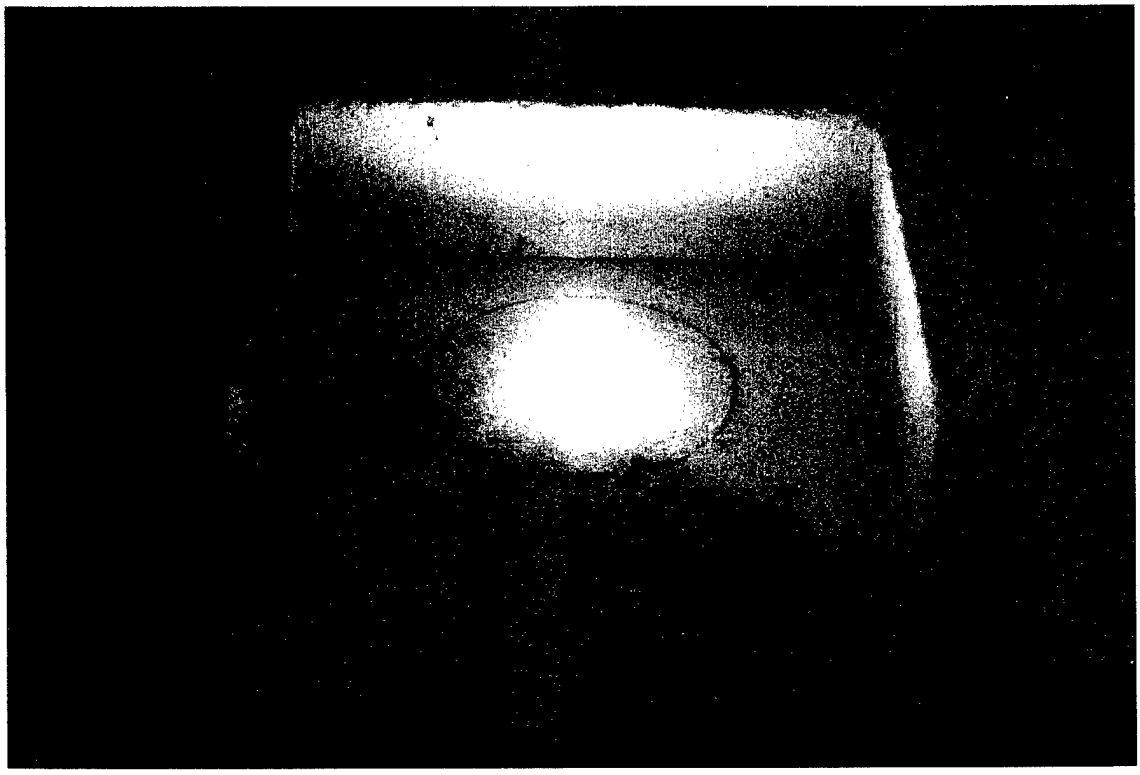

Figure 18. YbAG/YAG SELP under electric furnace test.

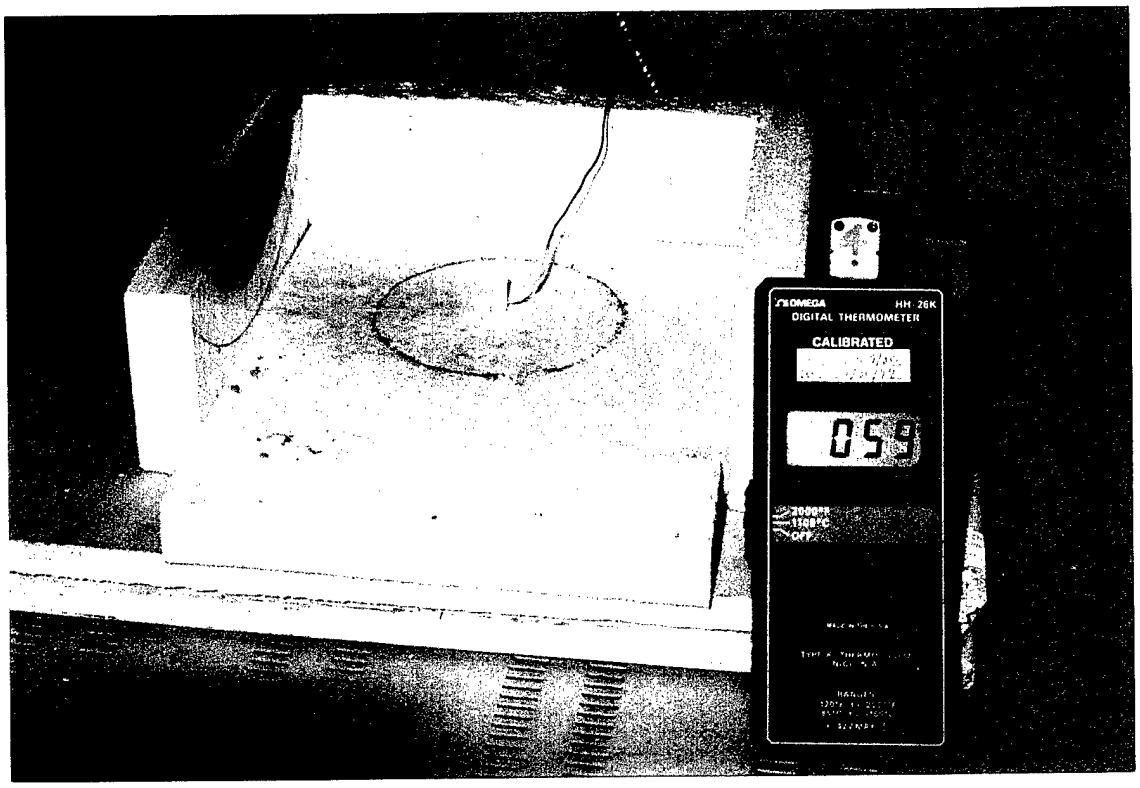

Figure 19. Temperature measurement of distal end of YbAG/YAG SELP in the electric furnace test .

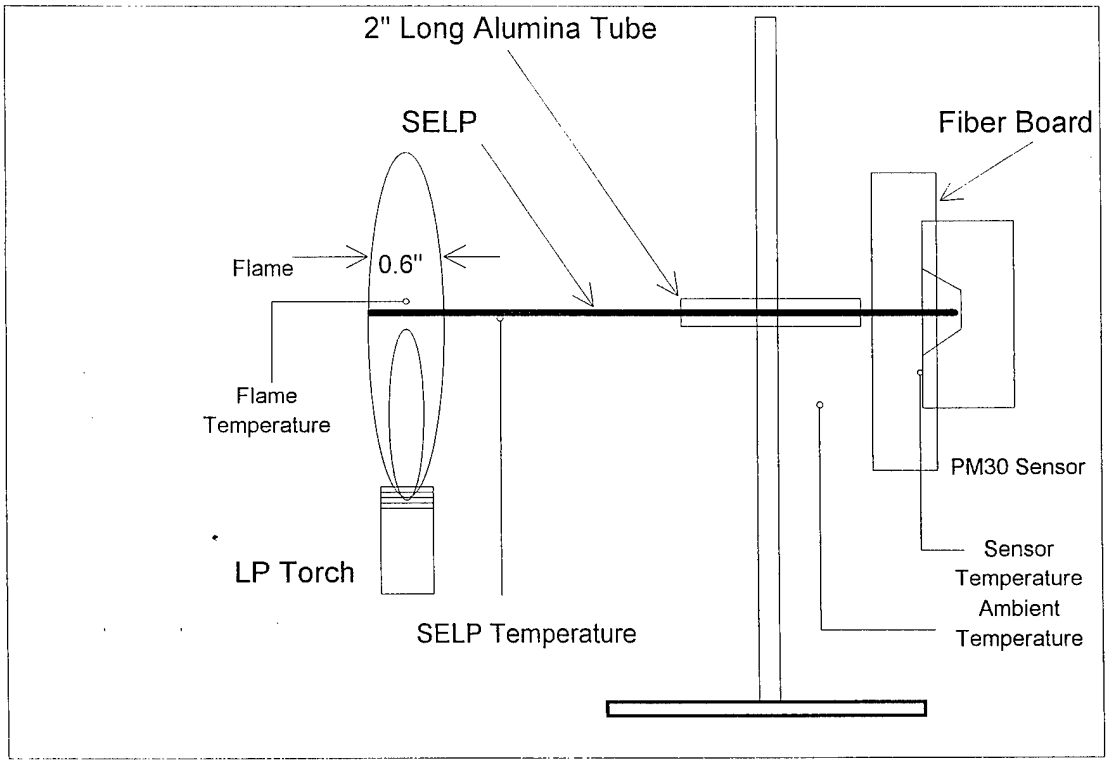

Figure 20. Schematic of SELP photon power measurement setup.

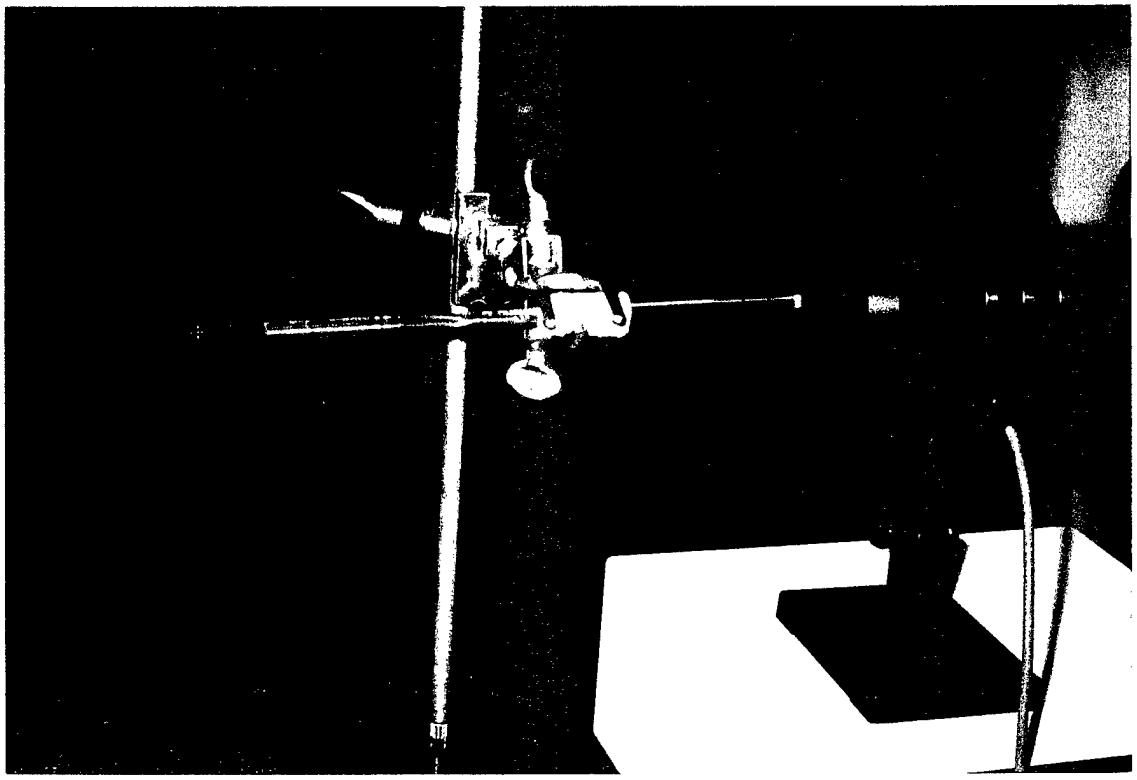

Figure 21. ErAG/YAG SELP and laser power meter Molectron PM30.

Figure 22. ErAG/YAG crystal fractured by thermal shock during rapid cooling.

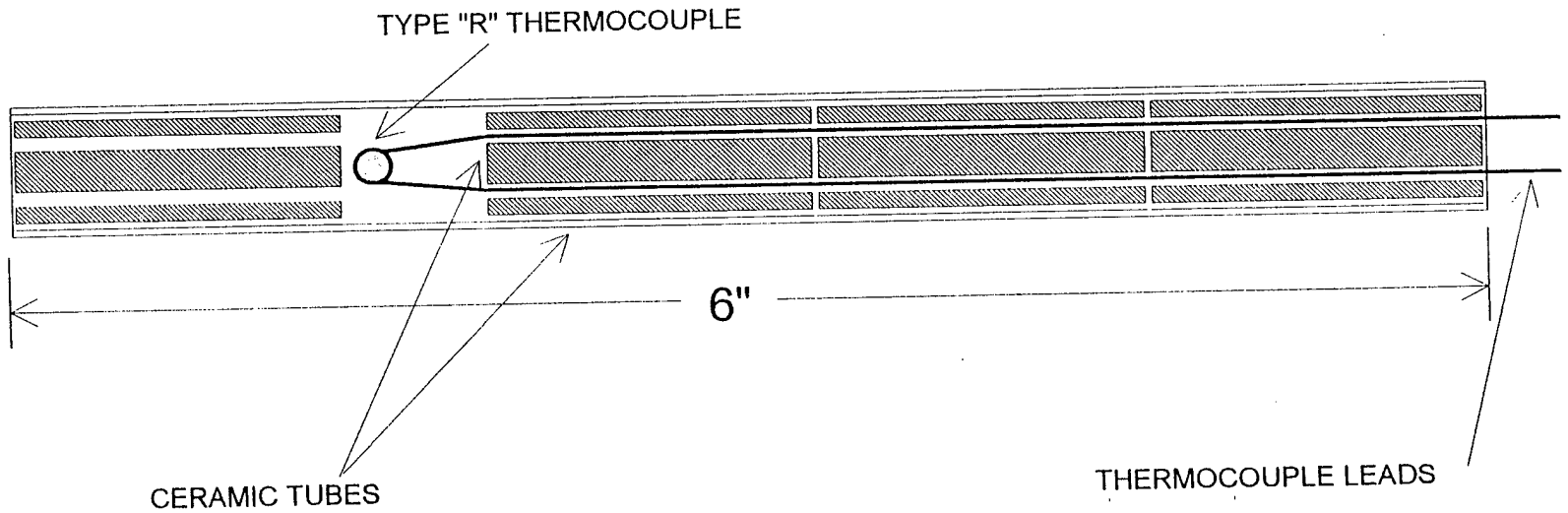

Figure 23. SELP temperature estimation assembly.

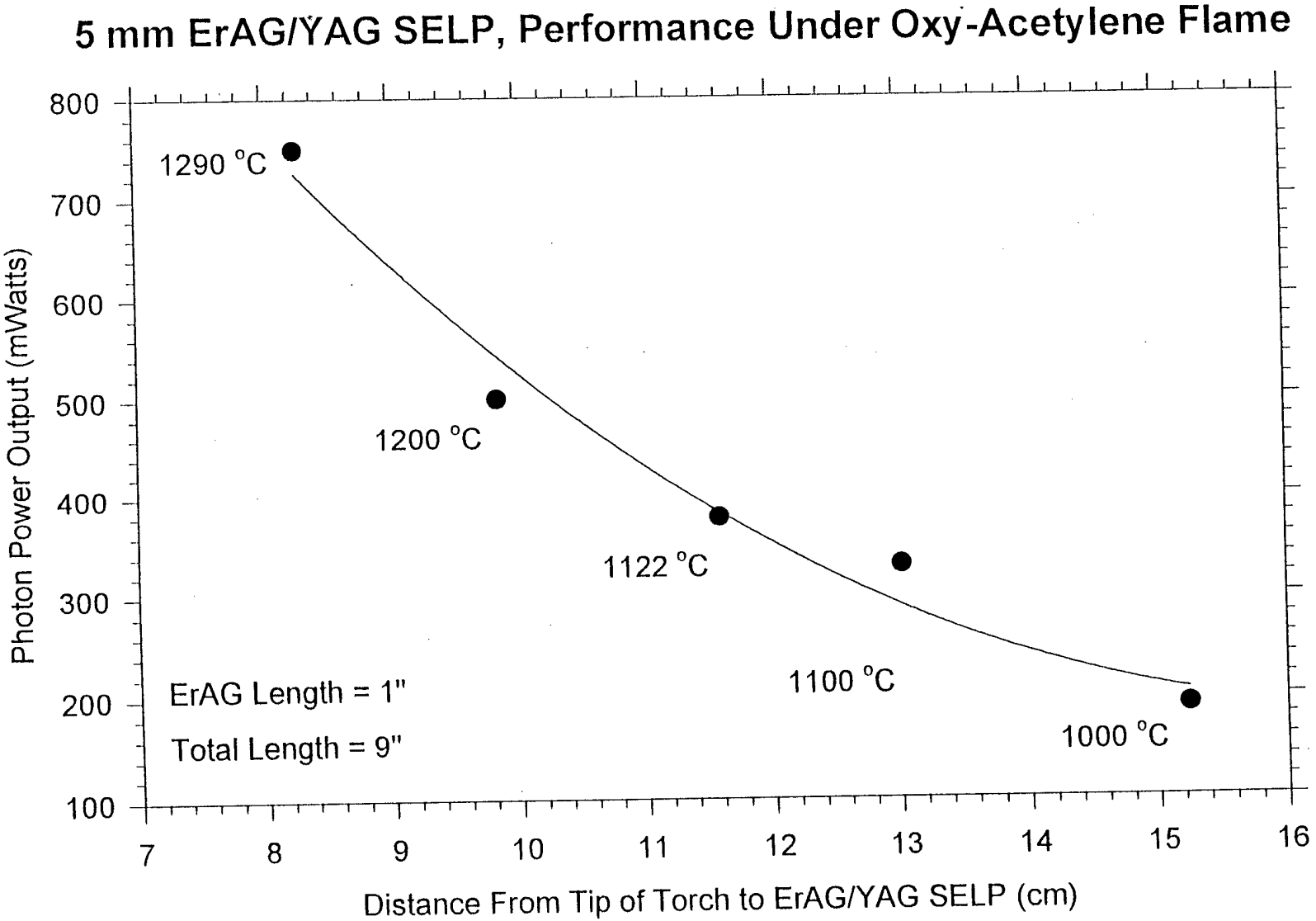

Figure 24. SELP temperature profile versus flame position.

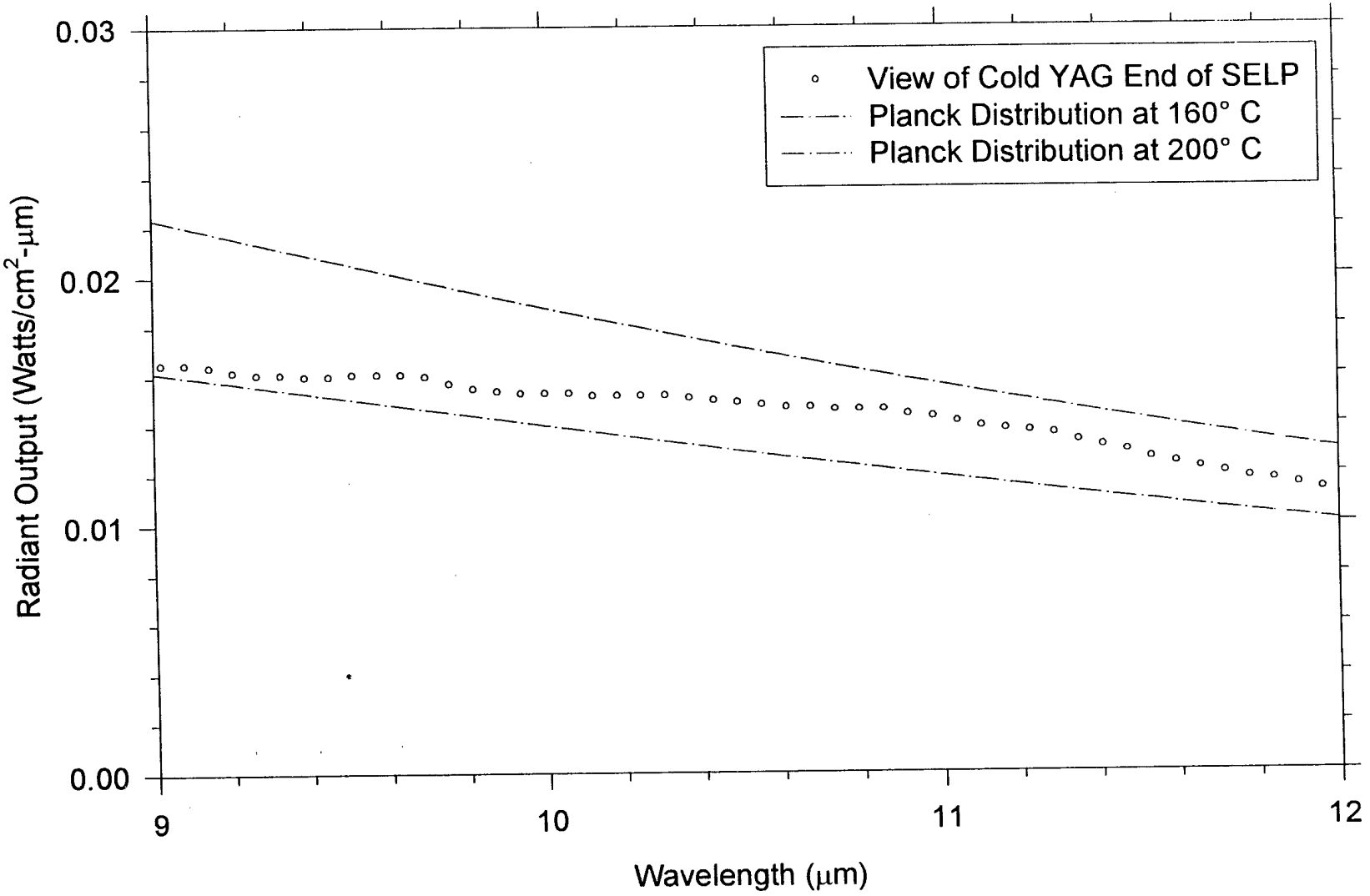

Figure 25. SELP temperature estimation of SELP from the distal ("cold") end.

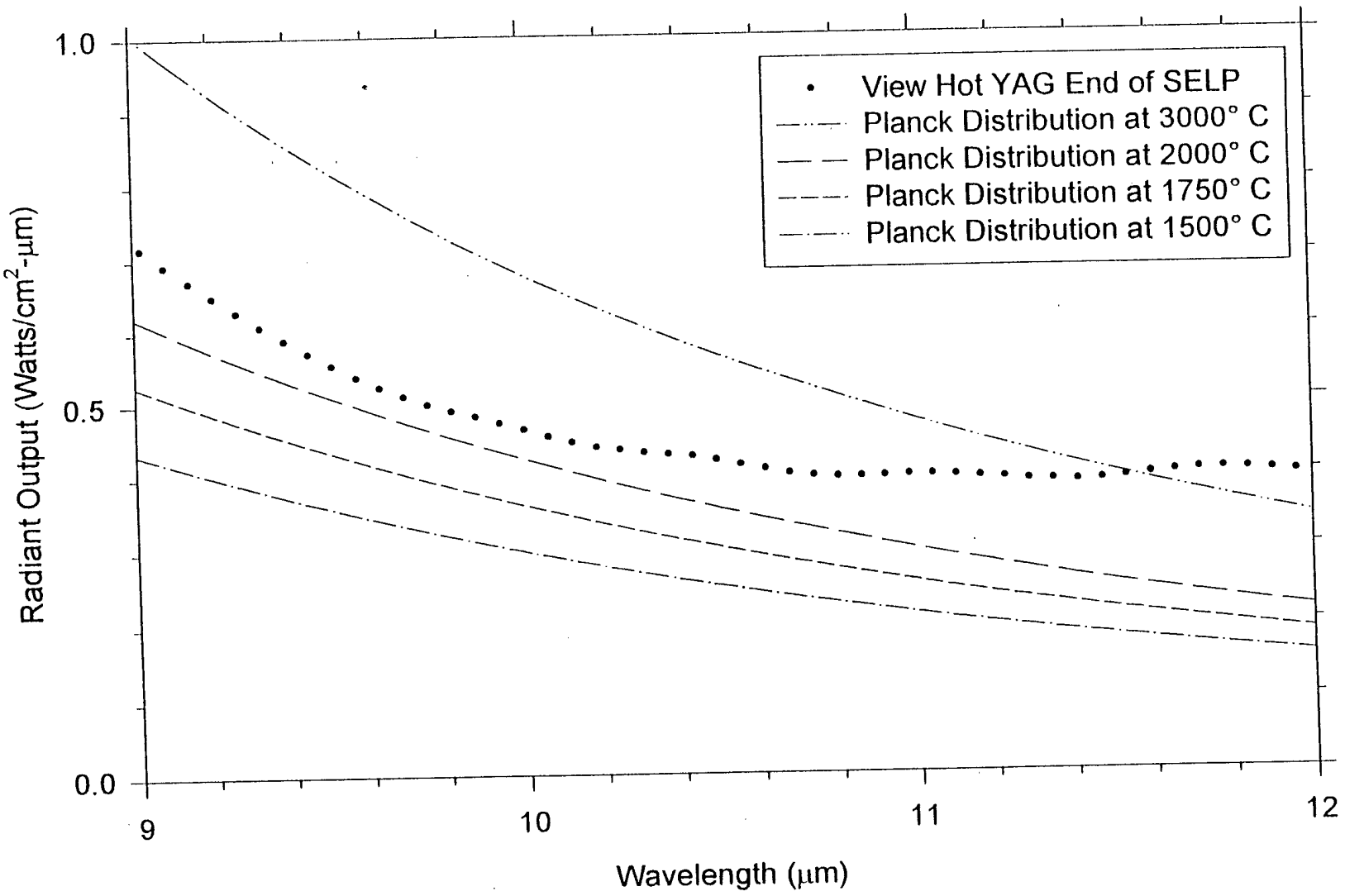

Figure 26. SELP temperature estimation of SELP from the proximal ("hot") end.

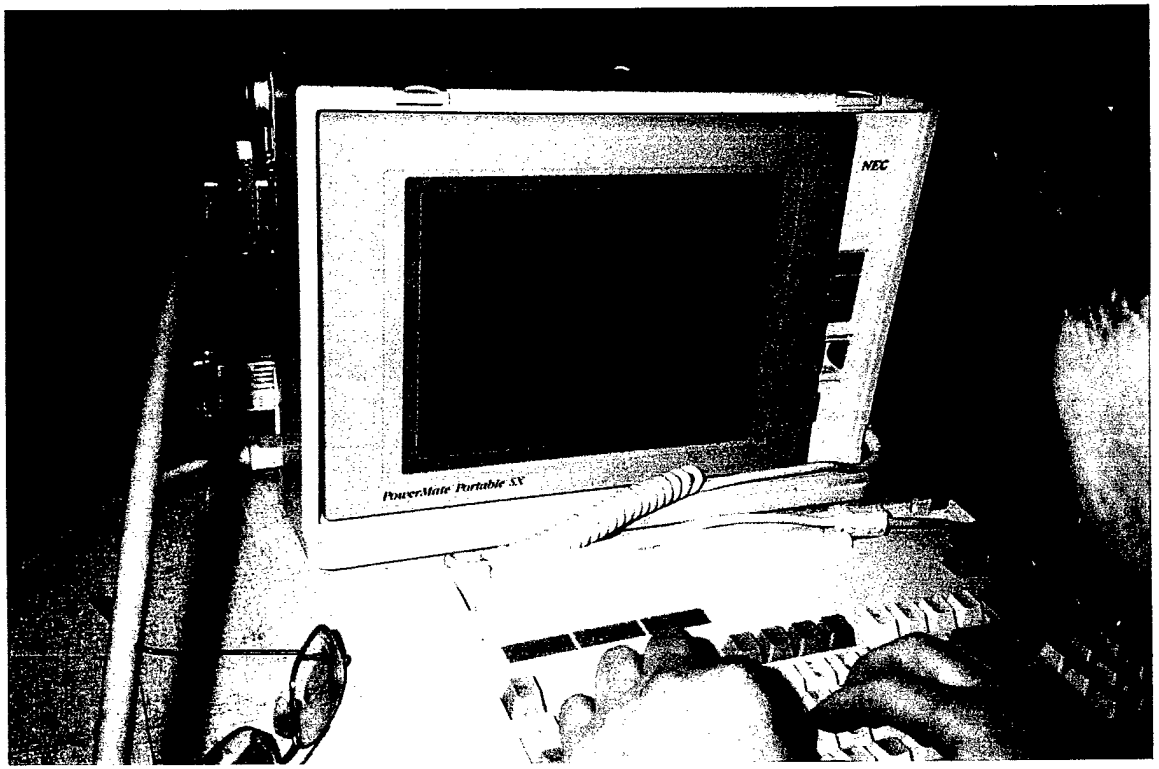

Figure 27. SR5000 data processing.

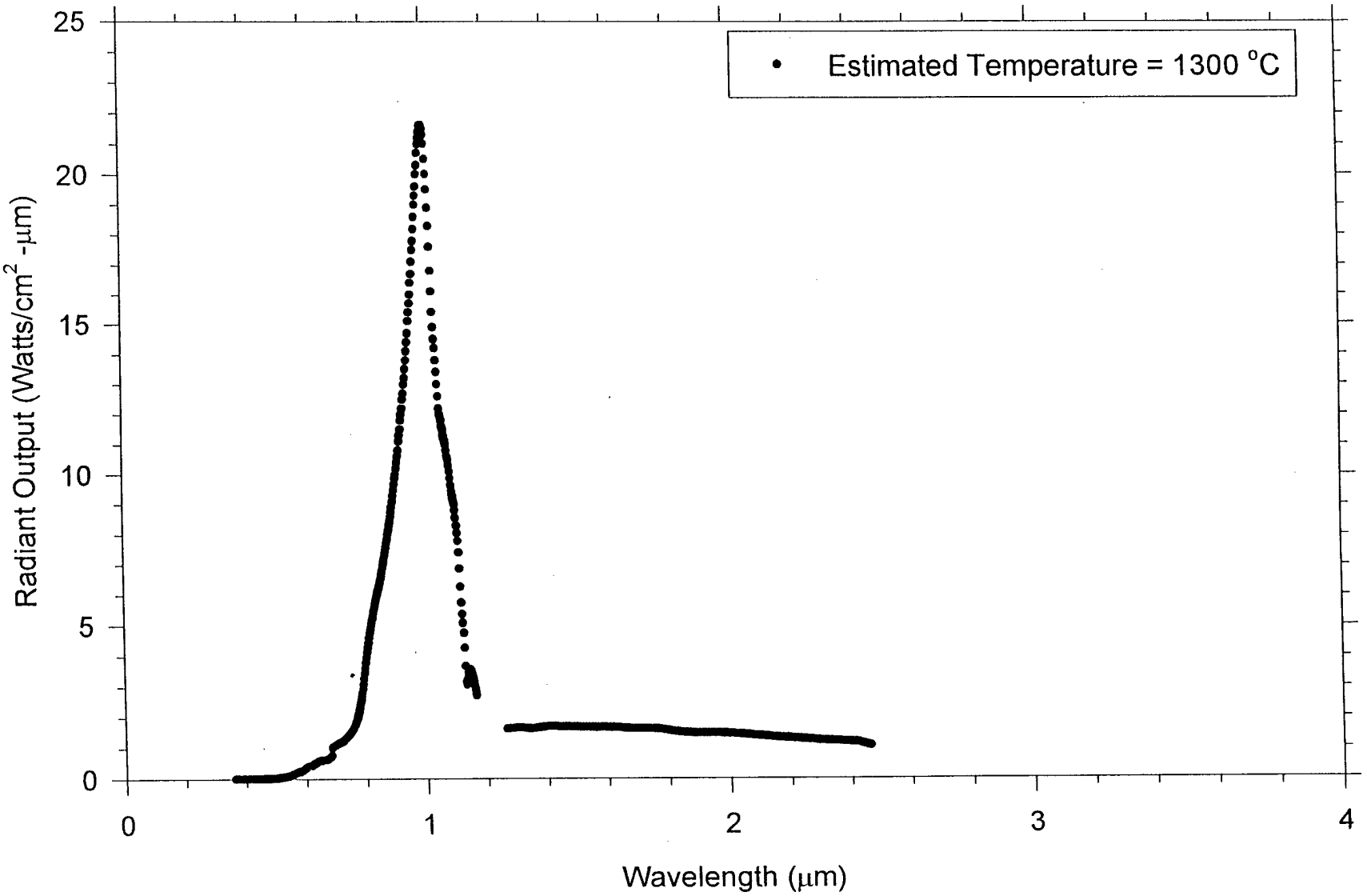

Figure 28. YbAG/YAG SELP spectrum using torch as the combustion heat source. Spectrum measured from YAG end with reference temperature at 1300°C.

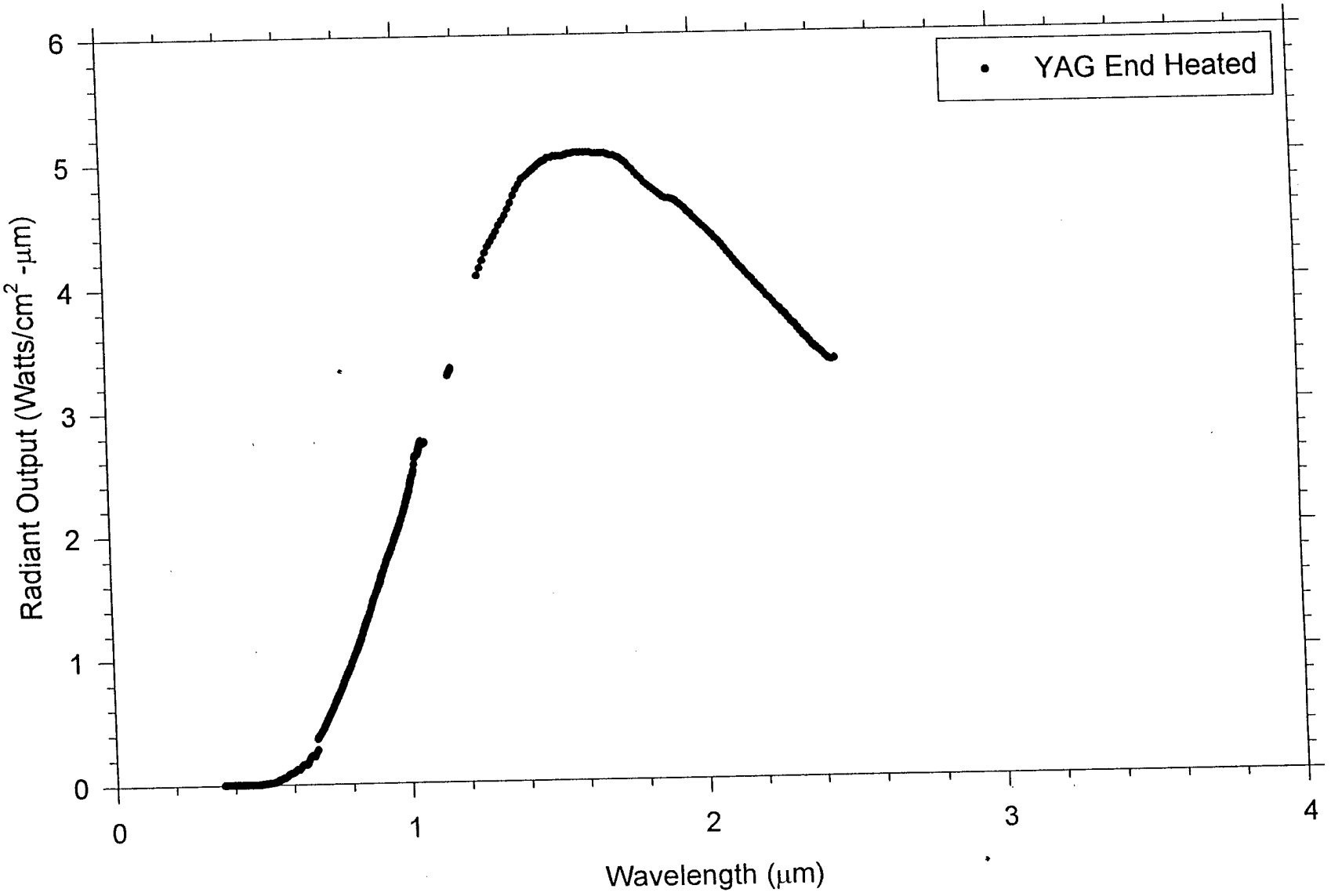

Figure 29. YAG spectrum at 1300°C reference temperature.

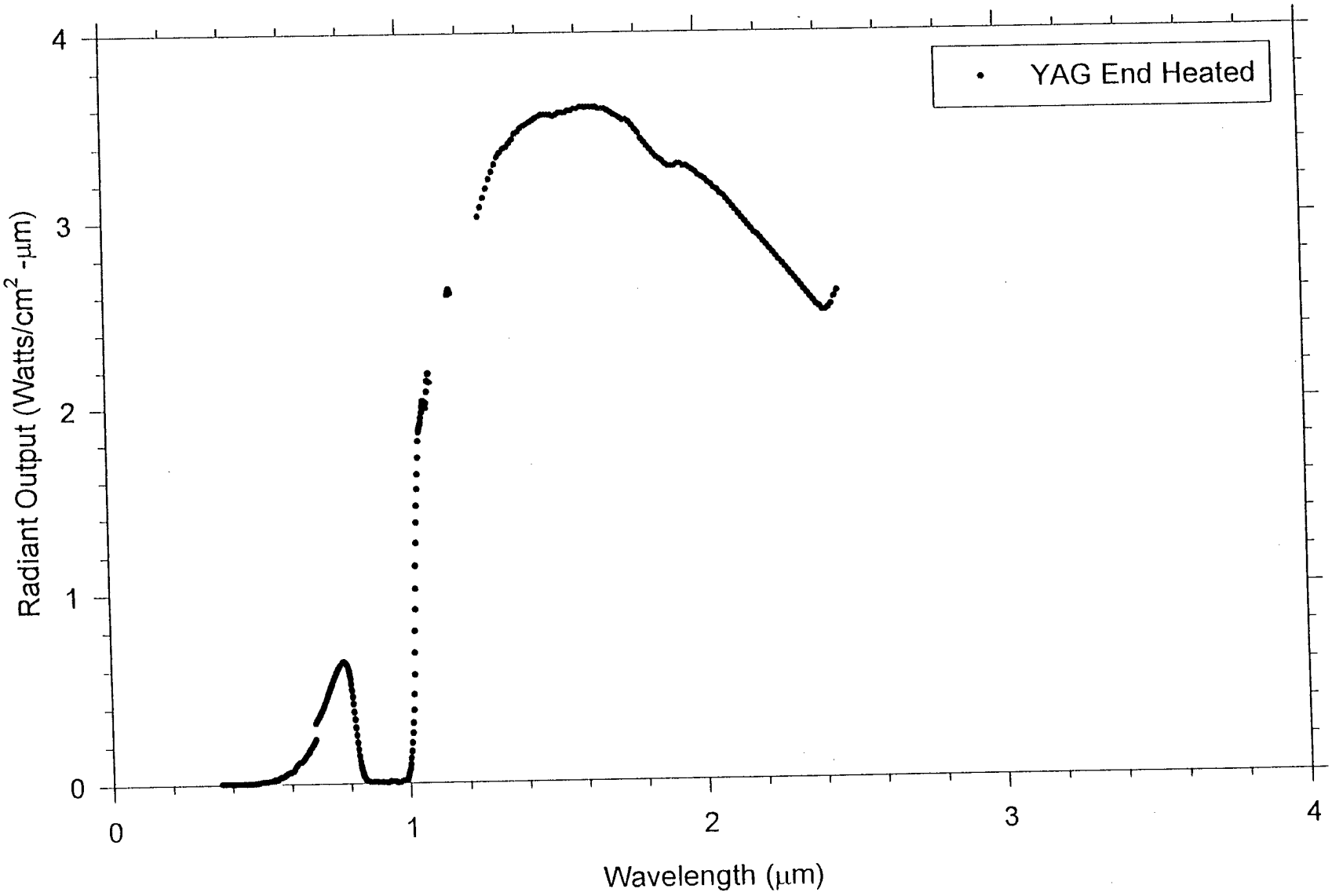

Figure 30. YAG spectrum at 1300°C viewed and measured from the YbAG crystal end.

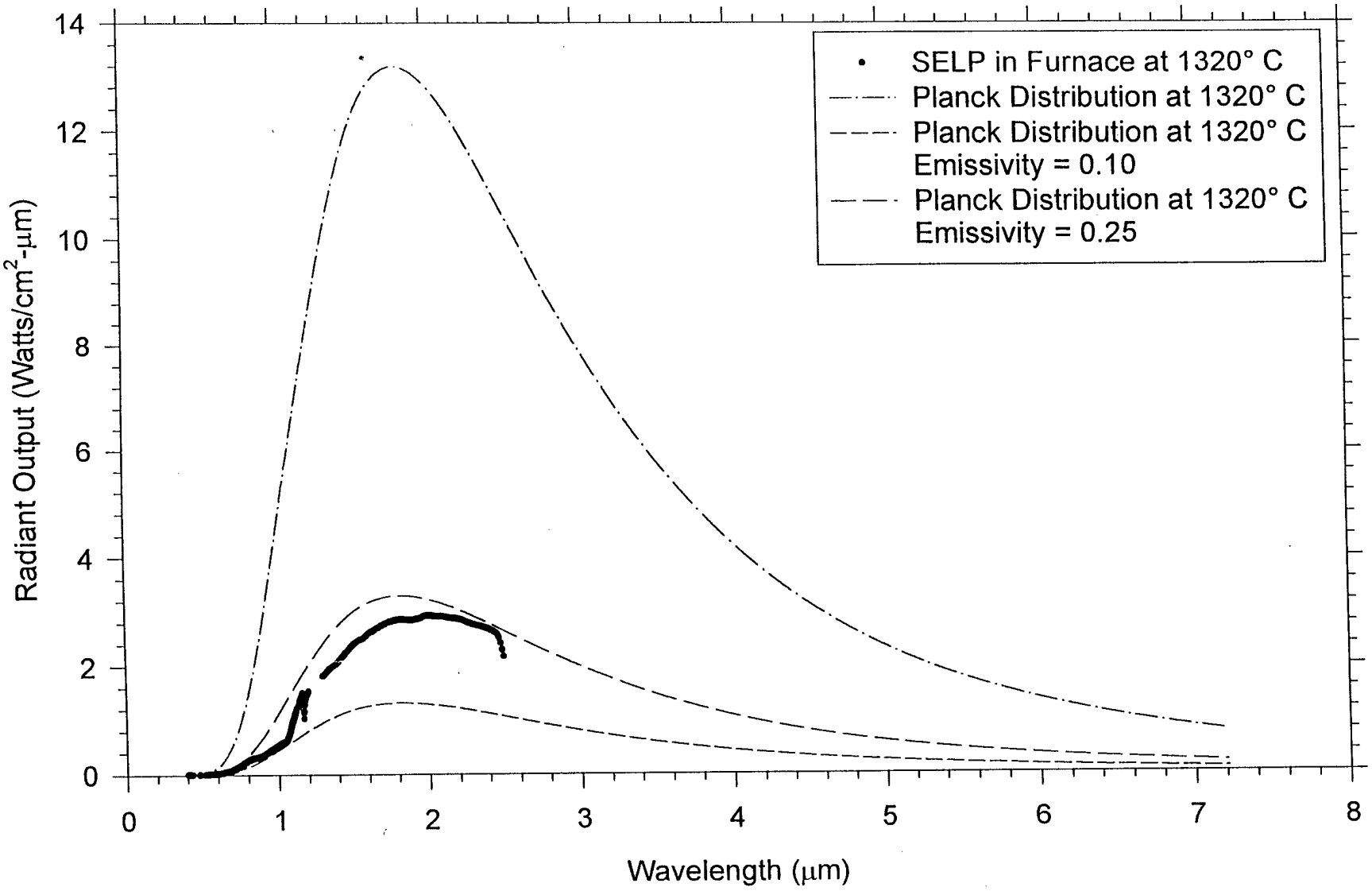

Figure 31. YbYAG/ YAG SELP Spectrum in Comparison with Planck Distribution Electric Furnace

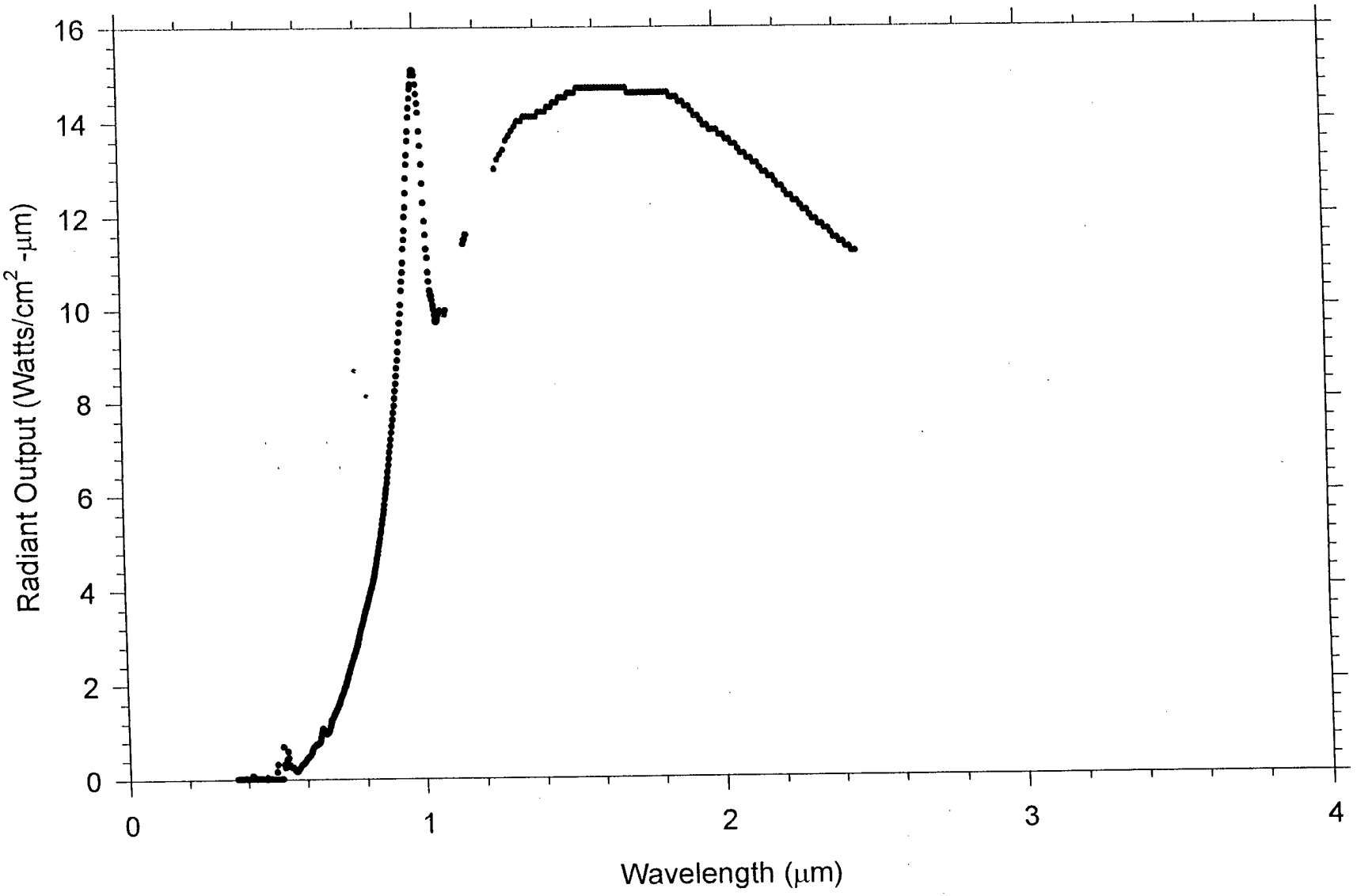

Figure 32. YbAG/YAG SELP Spectrum Electric Furnace Temperature 1500°C

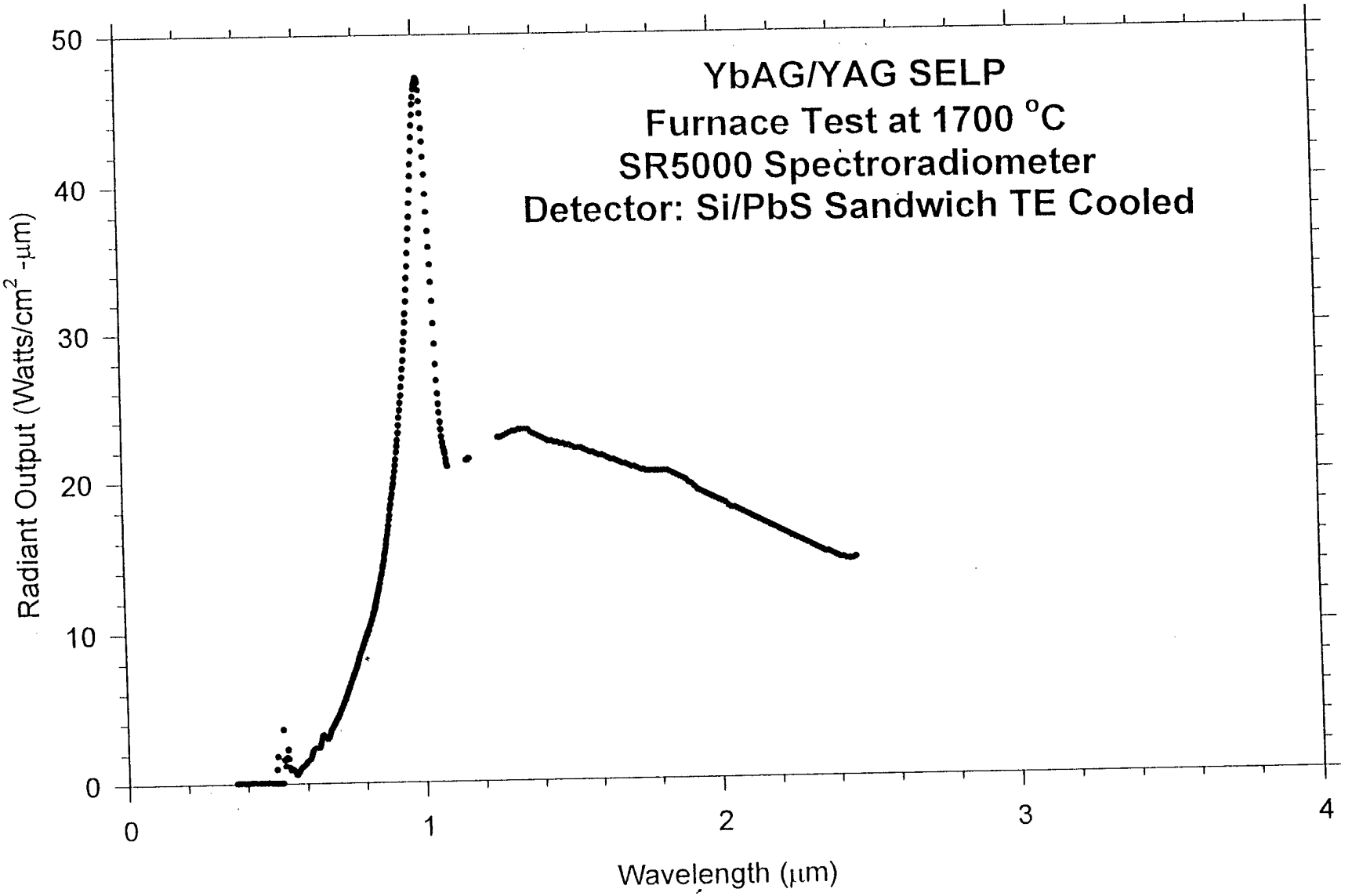

Figure 33. YbAG/YAG SELP Spectrum Electric Furnace Temperature 1700°C

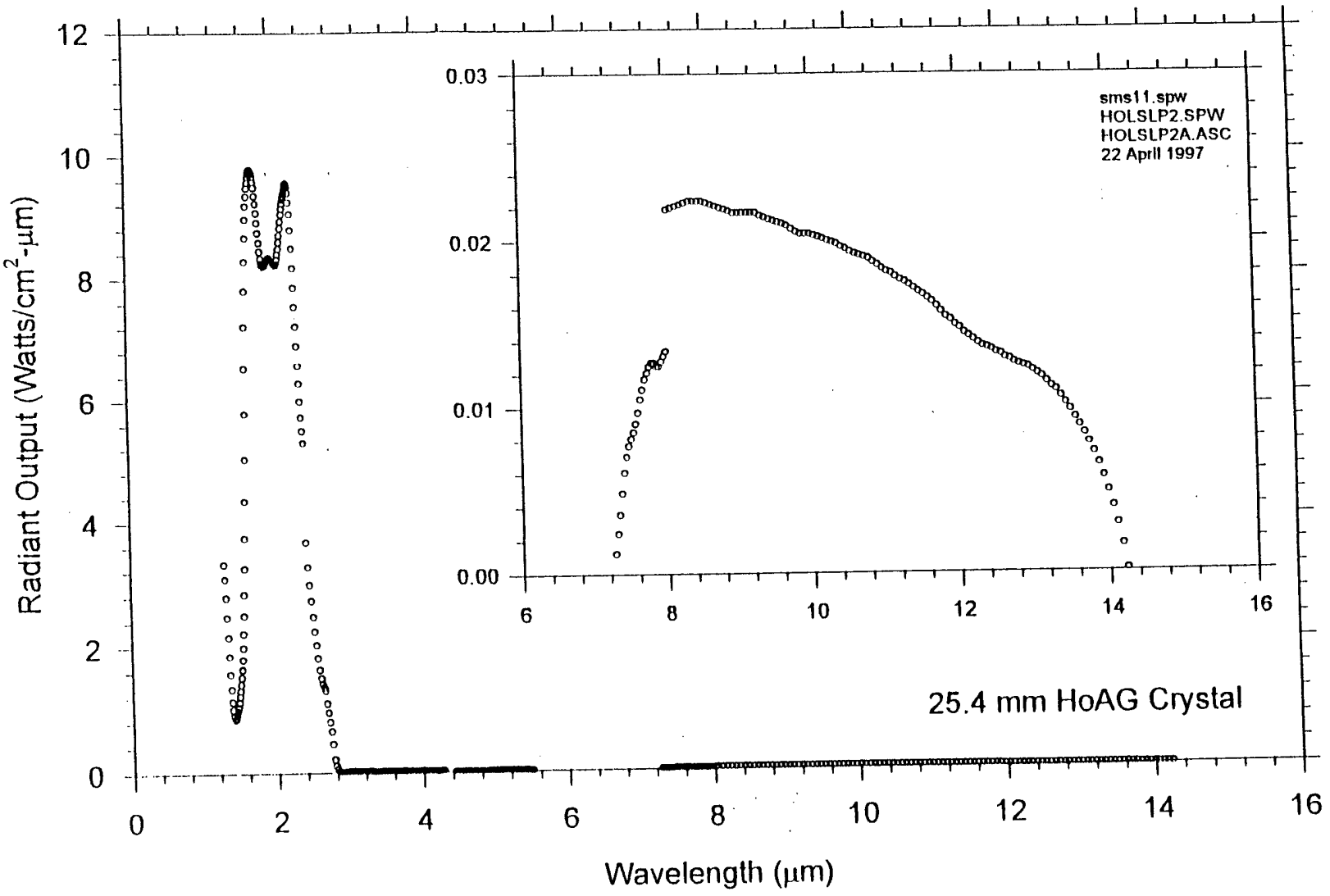

Figure 34. Spectrum of Holmium SELP Thermal Emission

Ref: R.D. Cowan and G.H. Dicke, Rev. Mod. Phys. 20, 418 (1948)

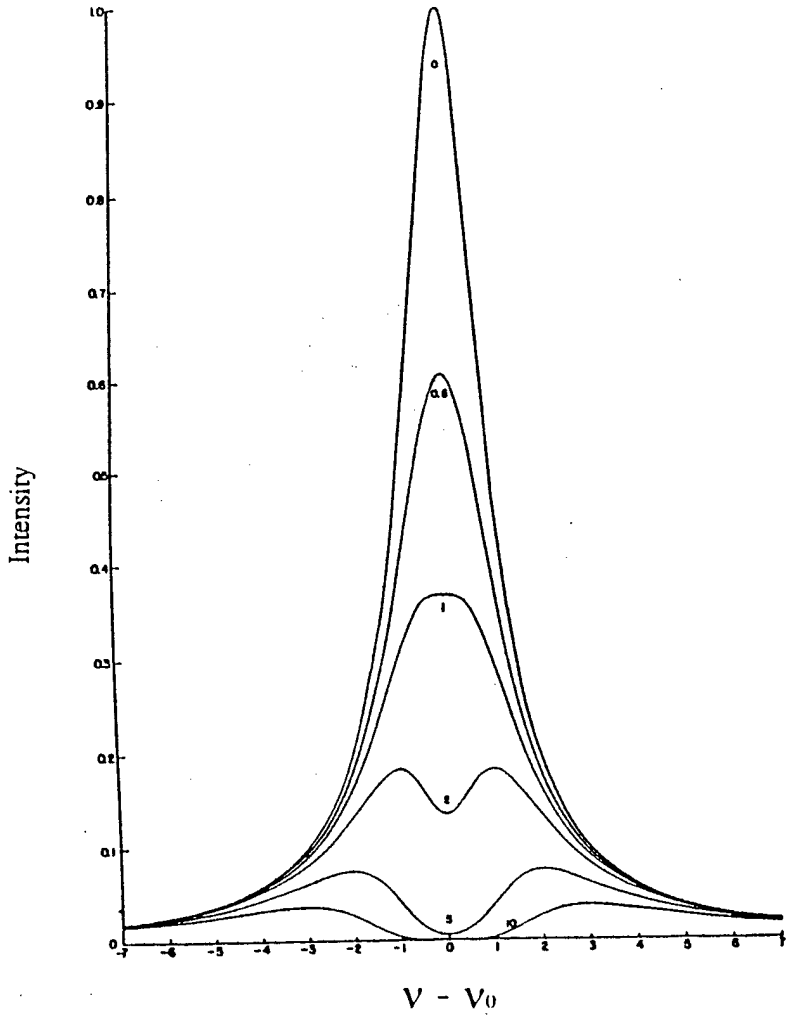

Figure 35. Self-Absorption of Thermal Emission

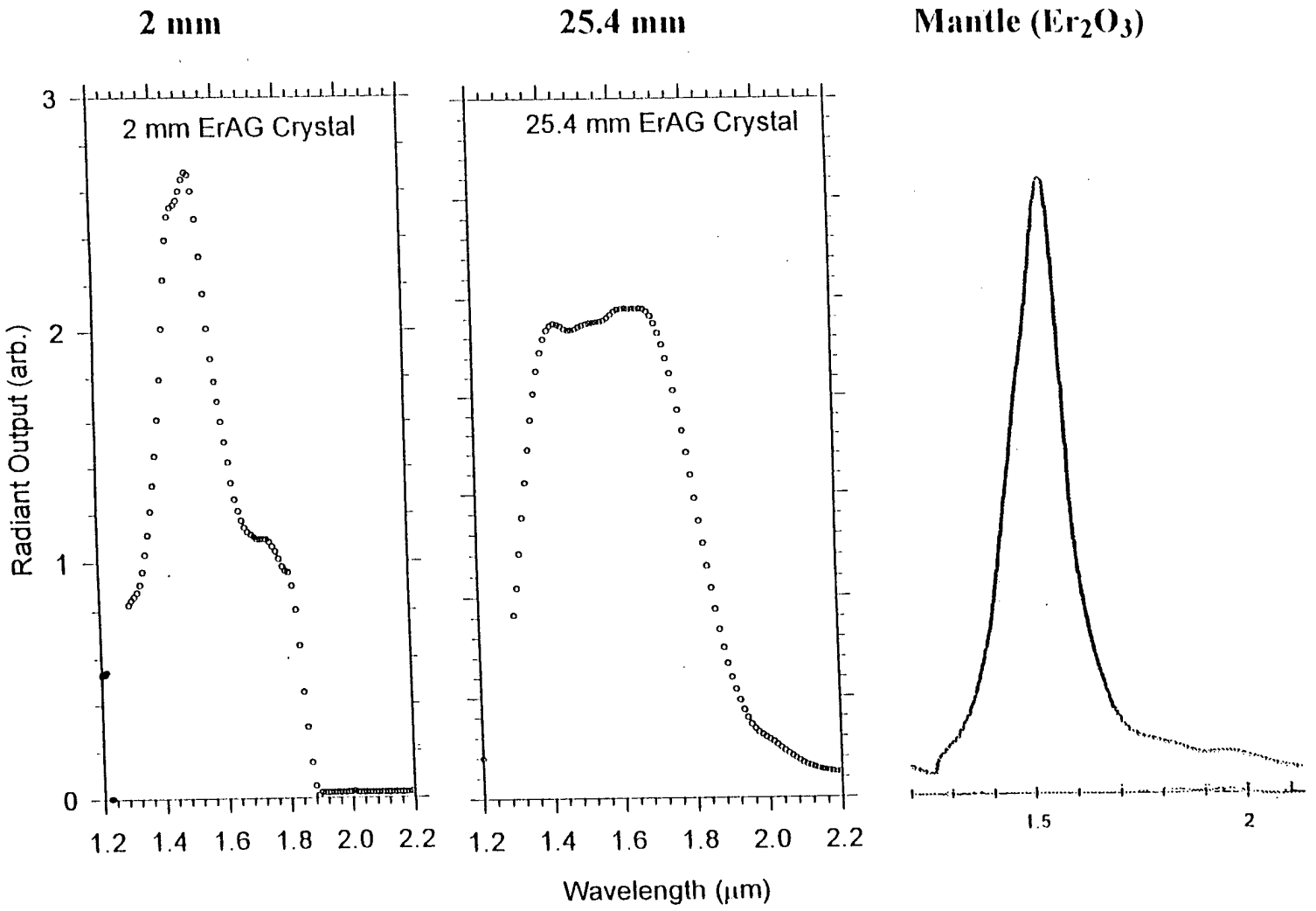

Figure 36. Effect of Emitter Thickness

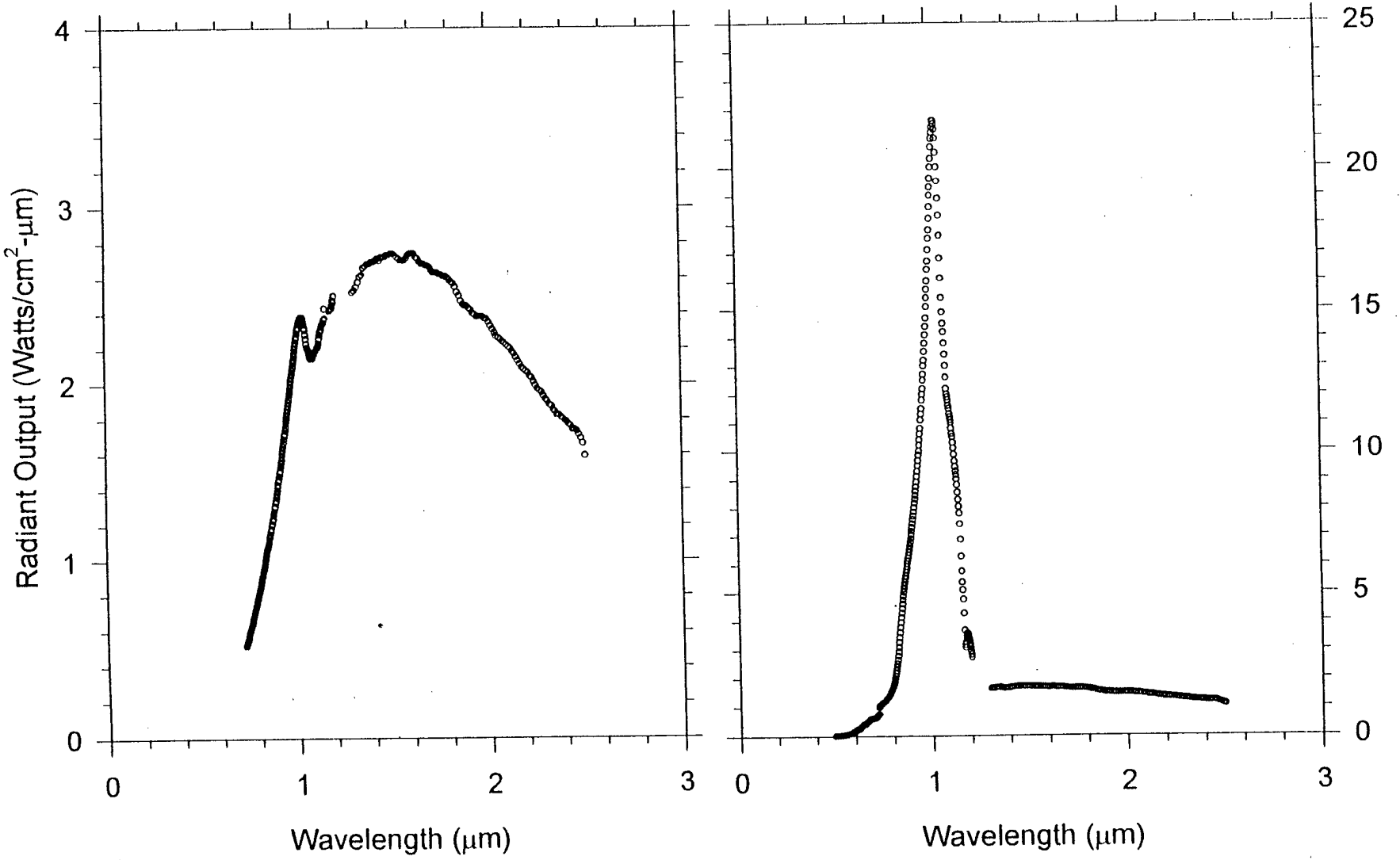

Figure 37. Graybody Background Emission

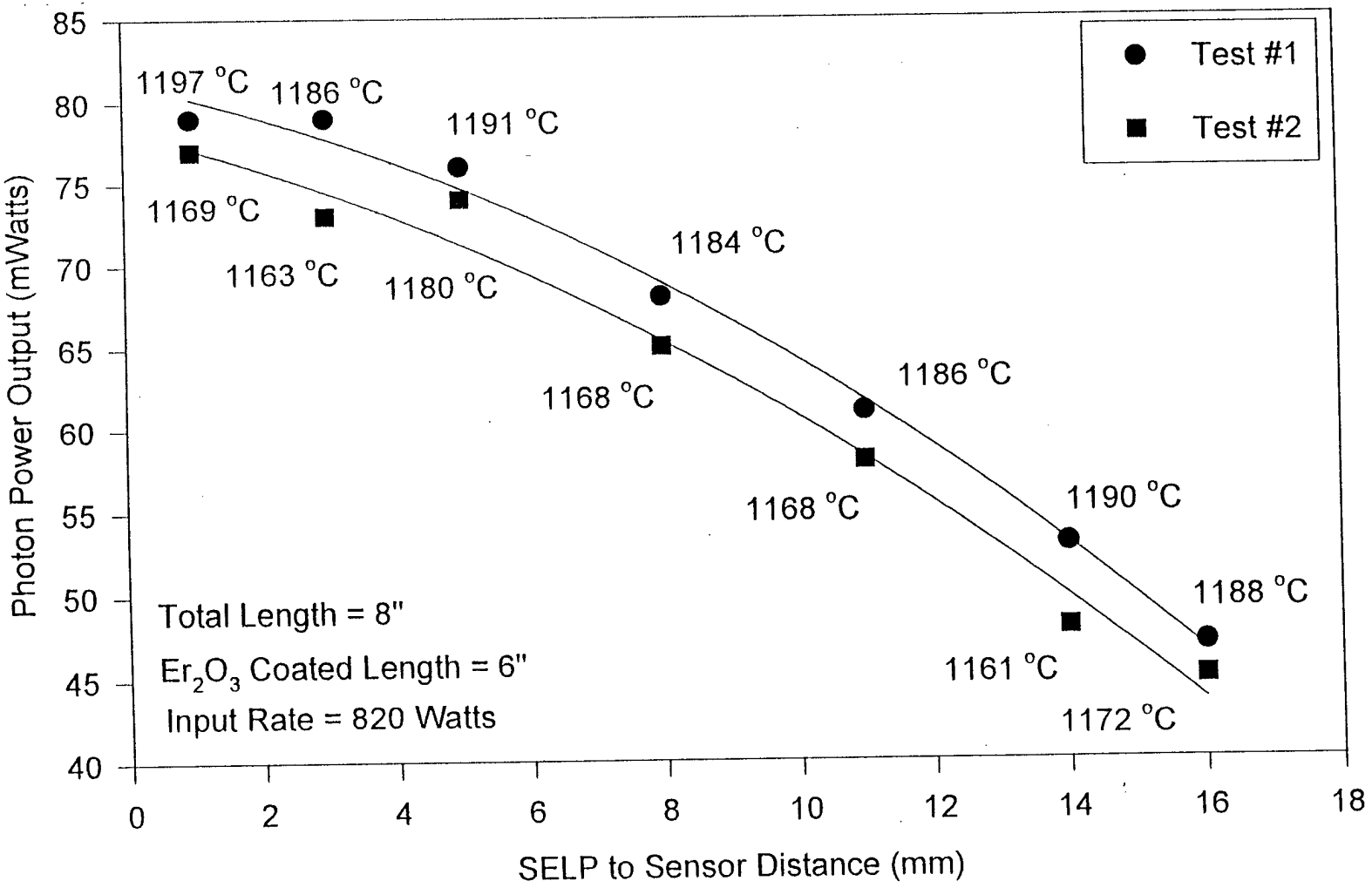

Figure 38. Photon Collection Efficiency at Different Distance from the SELP

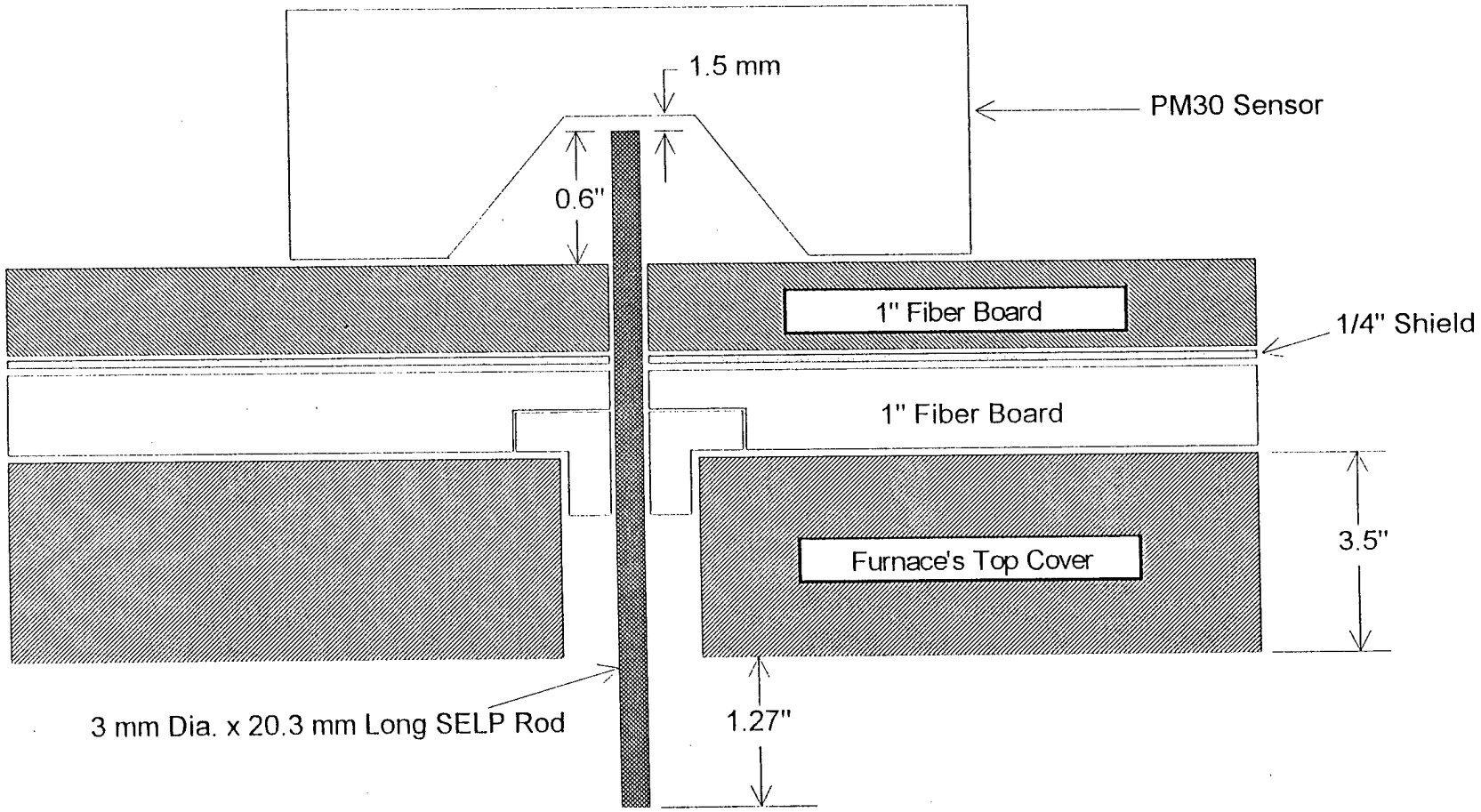

Figure 39. SELP Power Evaluation Test Setup Schematic

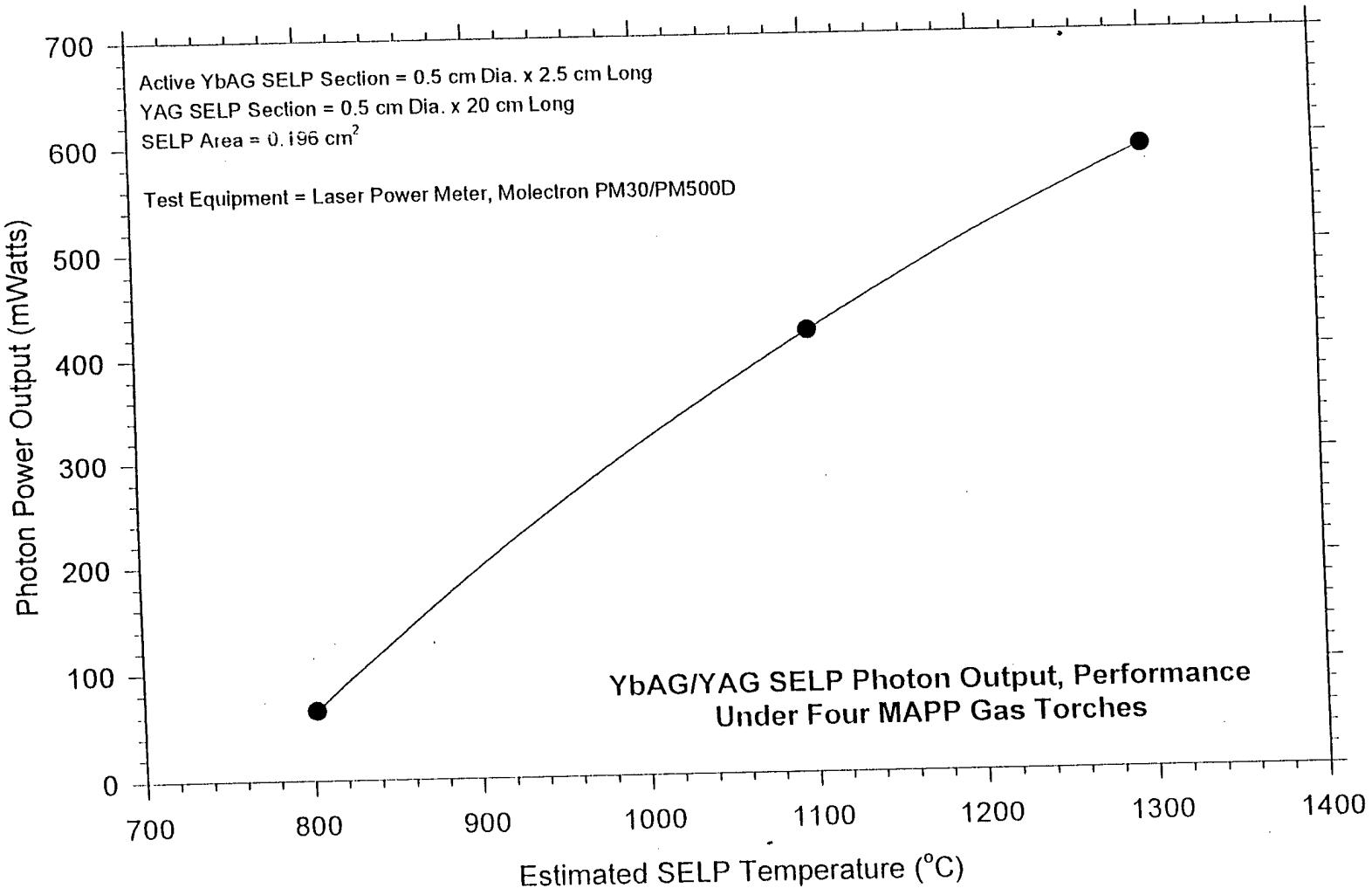

Figure 40. YbAG/YAG SELP Photon Emission with Combustion Heat Source

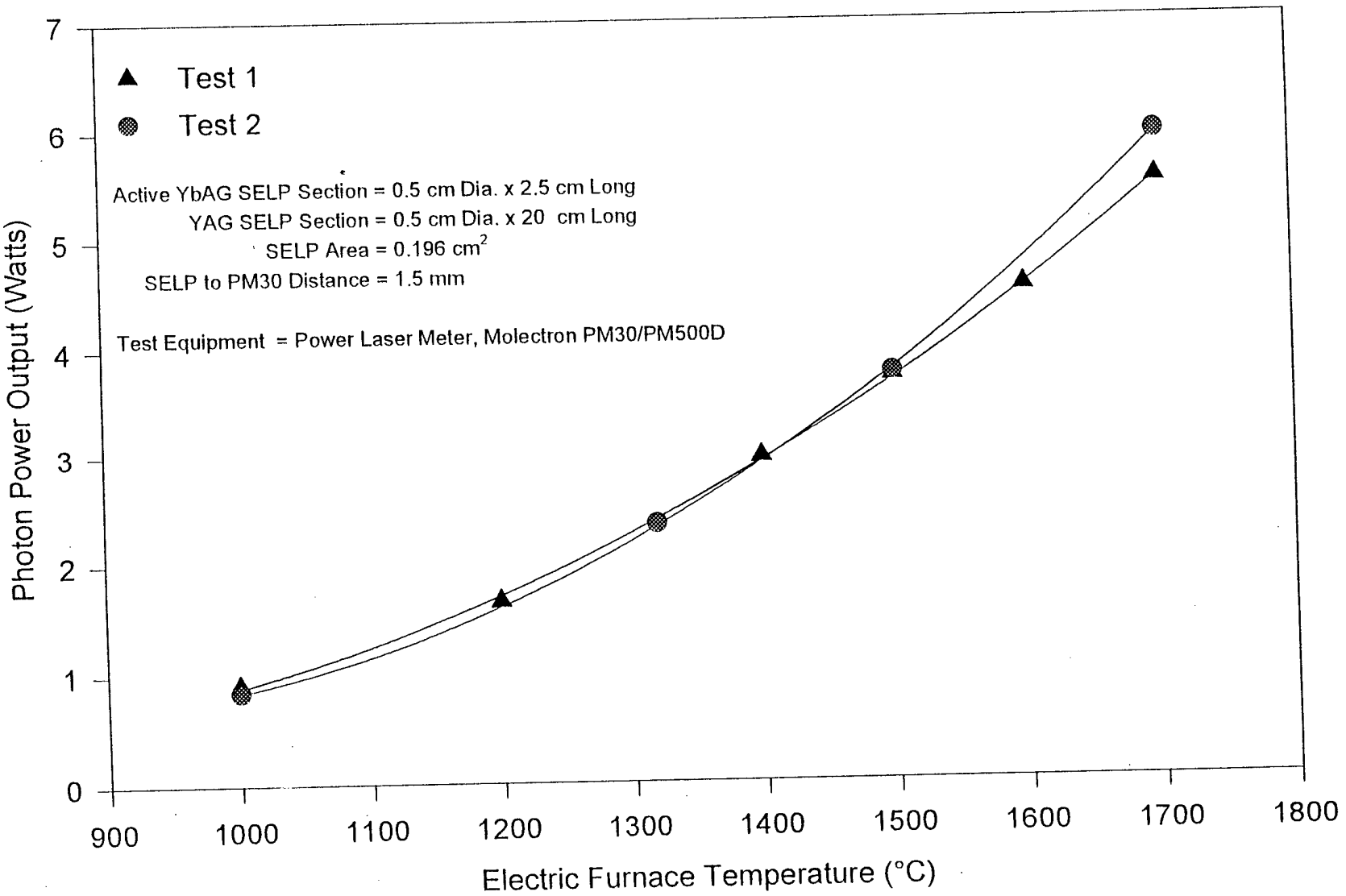

Figure 41. YbAG/YAG SELP Photon Power Test in Electric Furnace

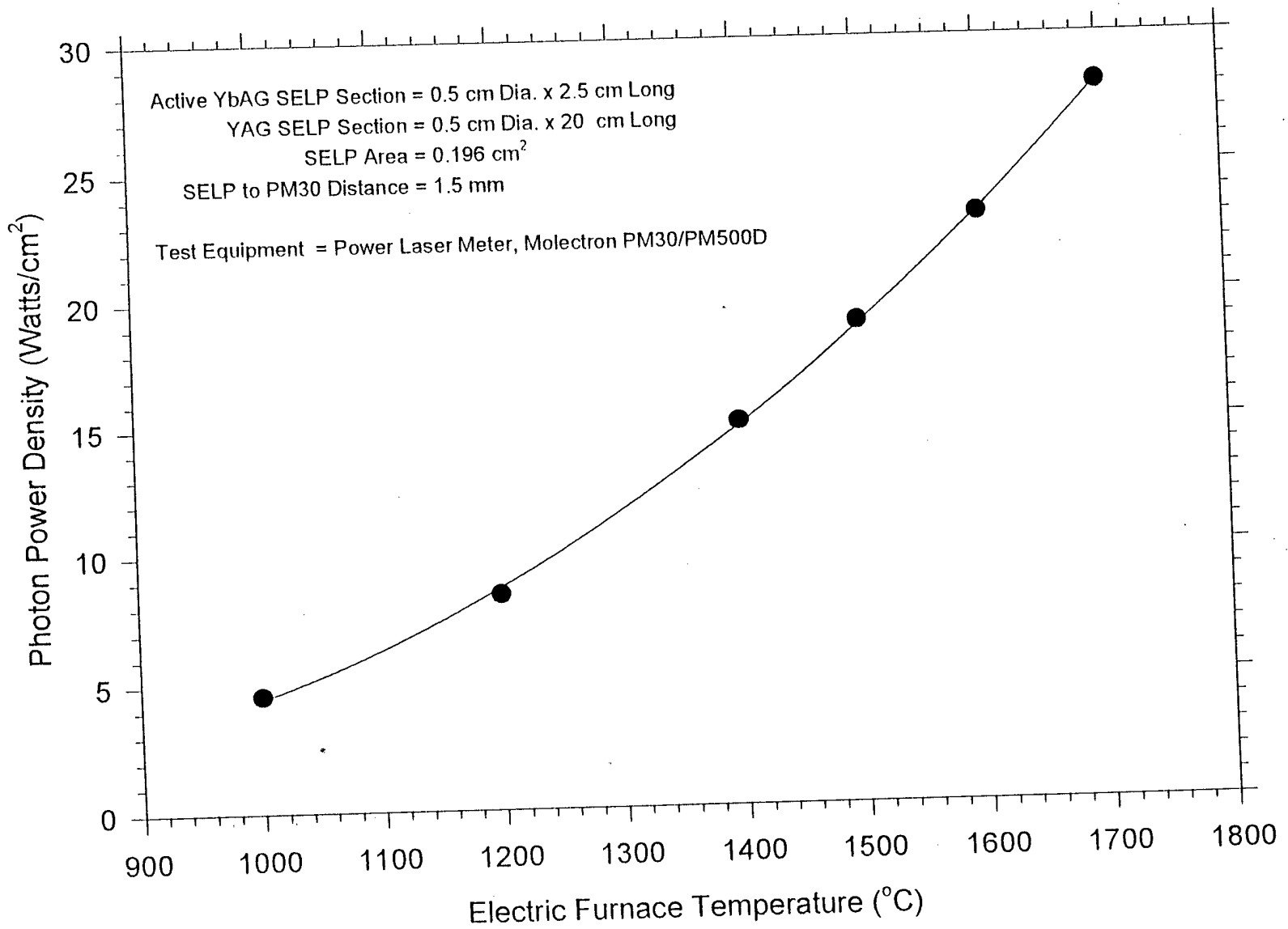

Figure 42. YbAG/YAG SELP Photon Power Density

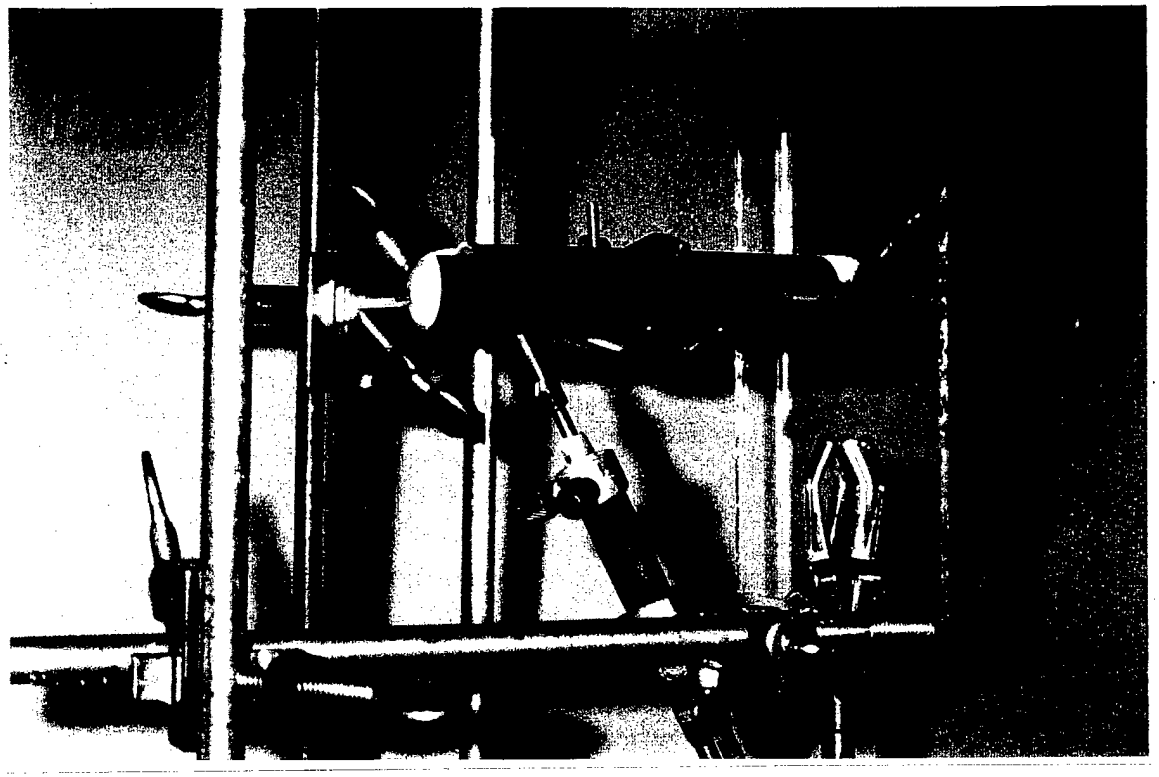

Figure 43. Light Source with ITO Filter

92:8 ITO reflects light at wavelengths longer than 1 μm
Added dielectric coating will extend cutoff to 890 nm

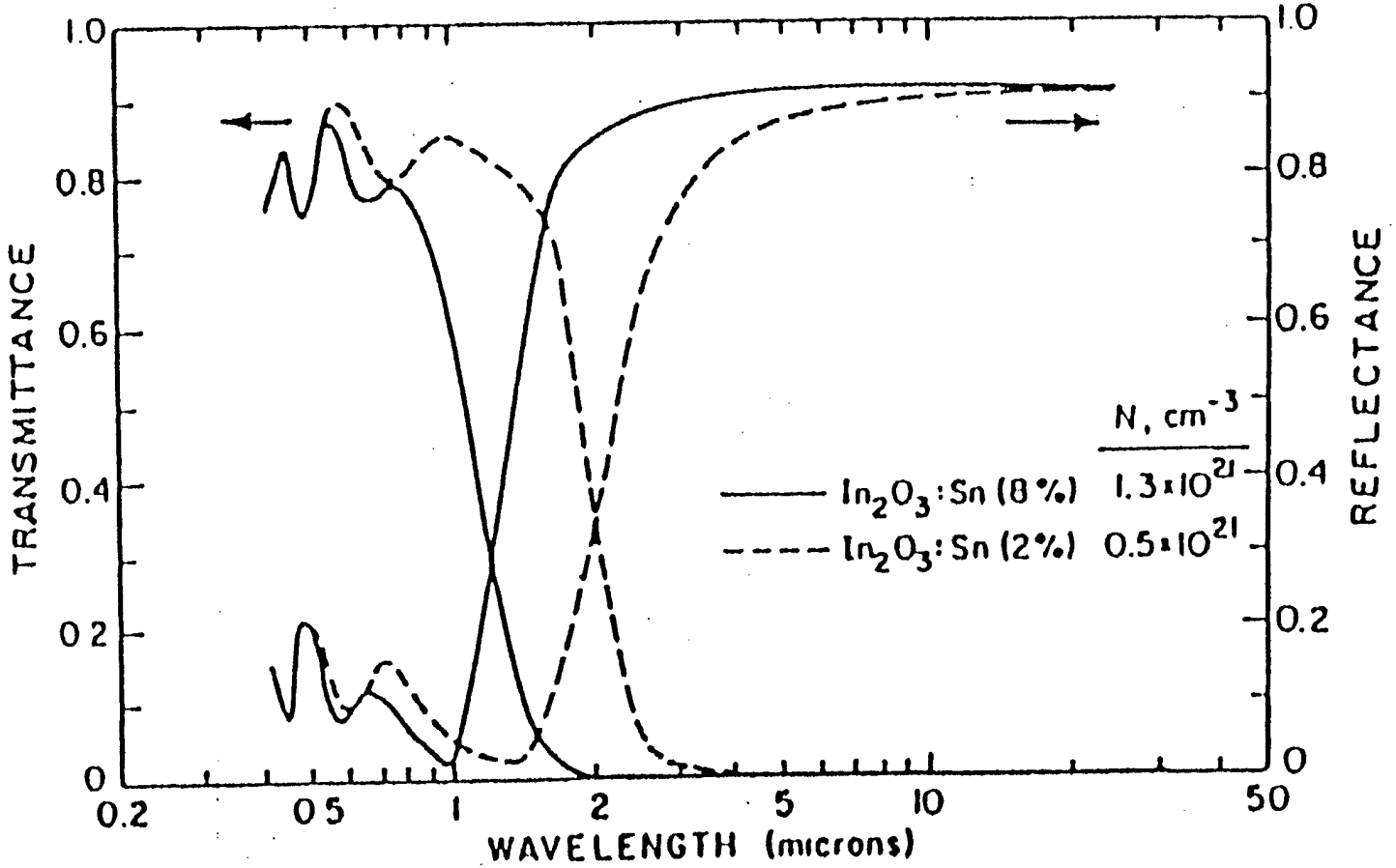

Figure 44. ITO Filter Characteristics

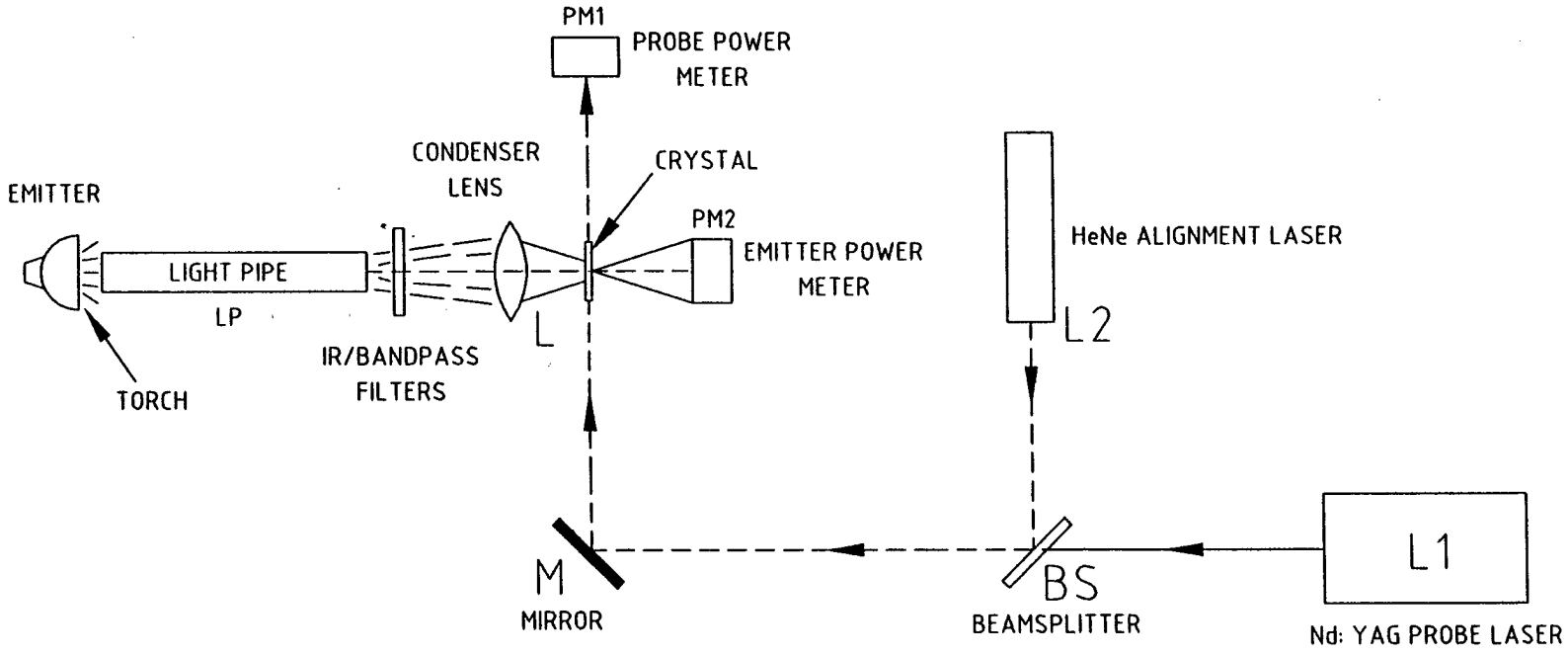

Figure 45. Schematic Laser Pumping Setup

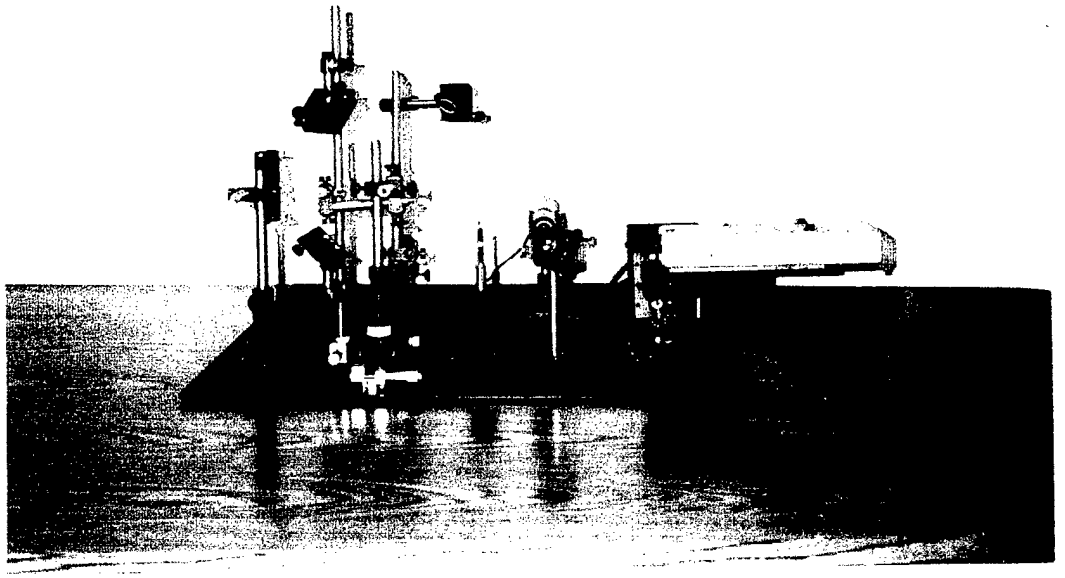

Figure 46. Laser Pumping Setup

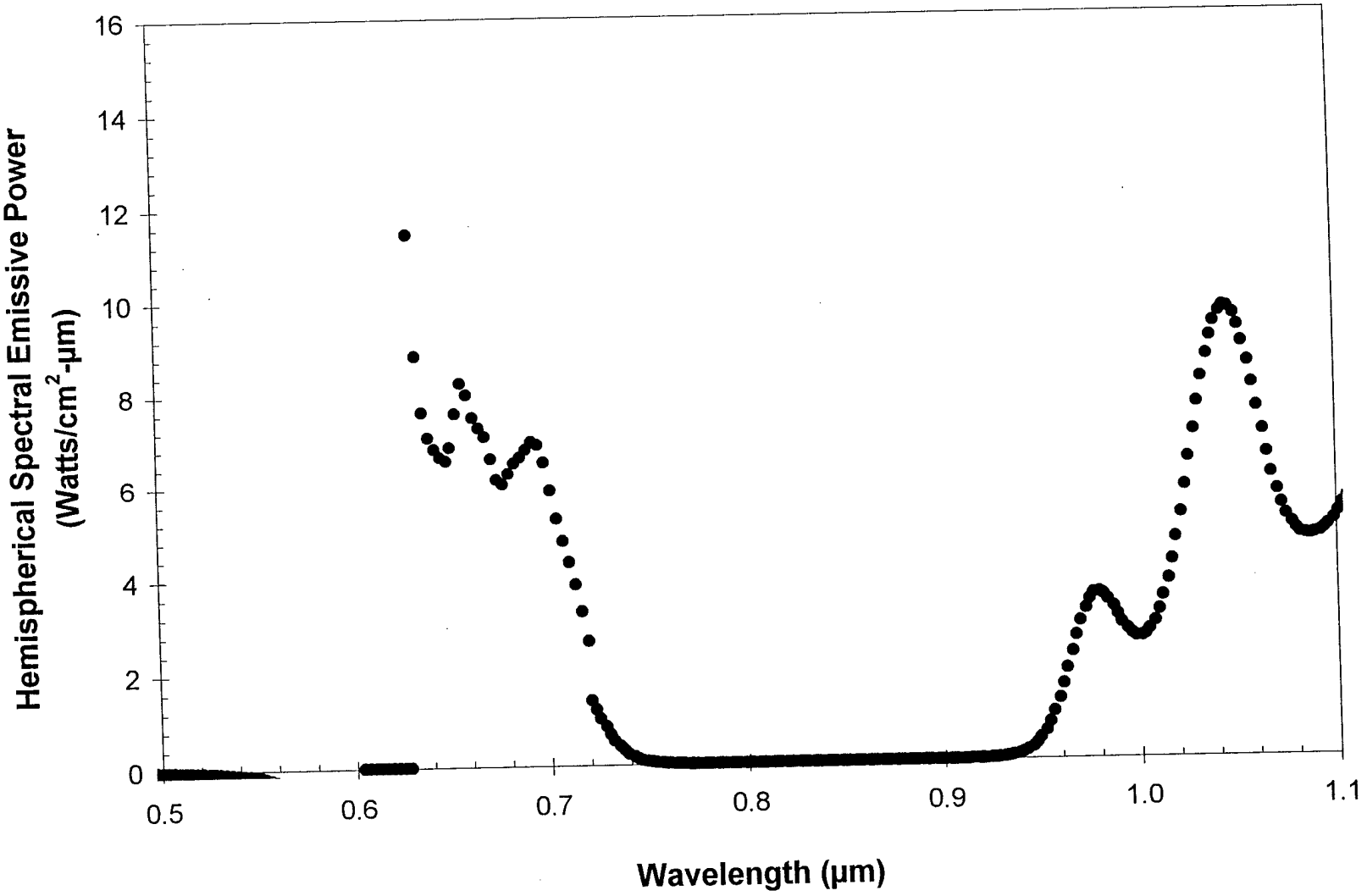

Figure 47. Nd: YAG Fluorescence at 980 nm and 1064 nm Filtered by Thullia Felt

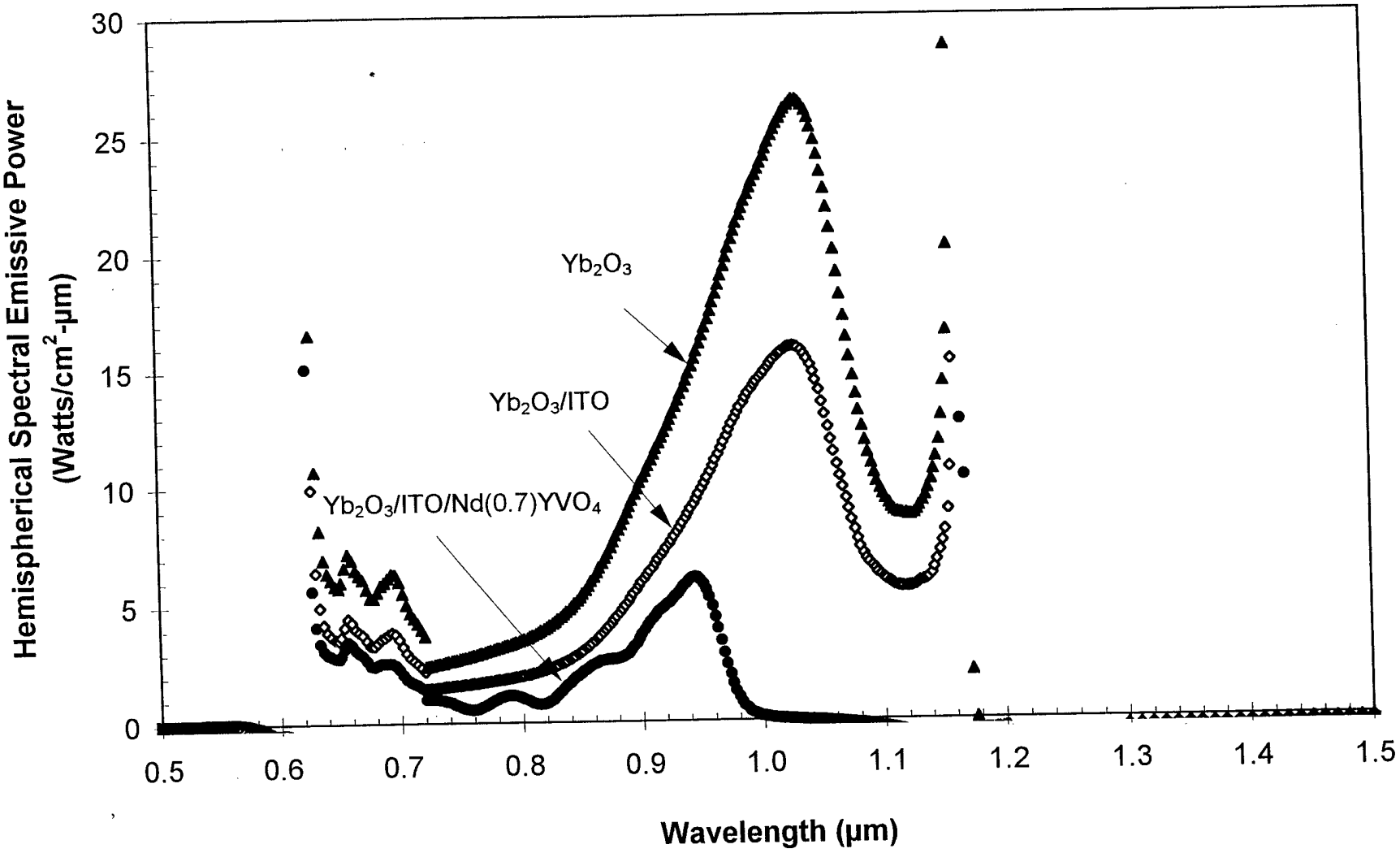

Figure 48. Spectra of Ytterbia Felt Through ITO and Nd (0.7%) YVO_4 Crystal

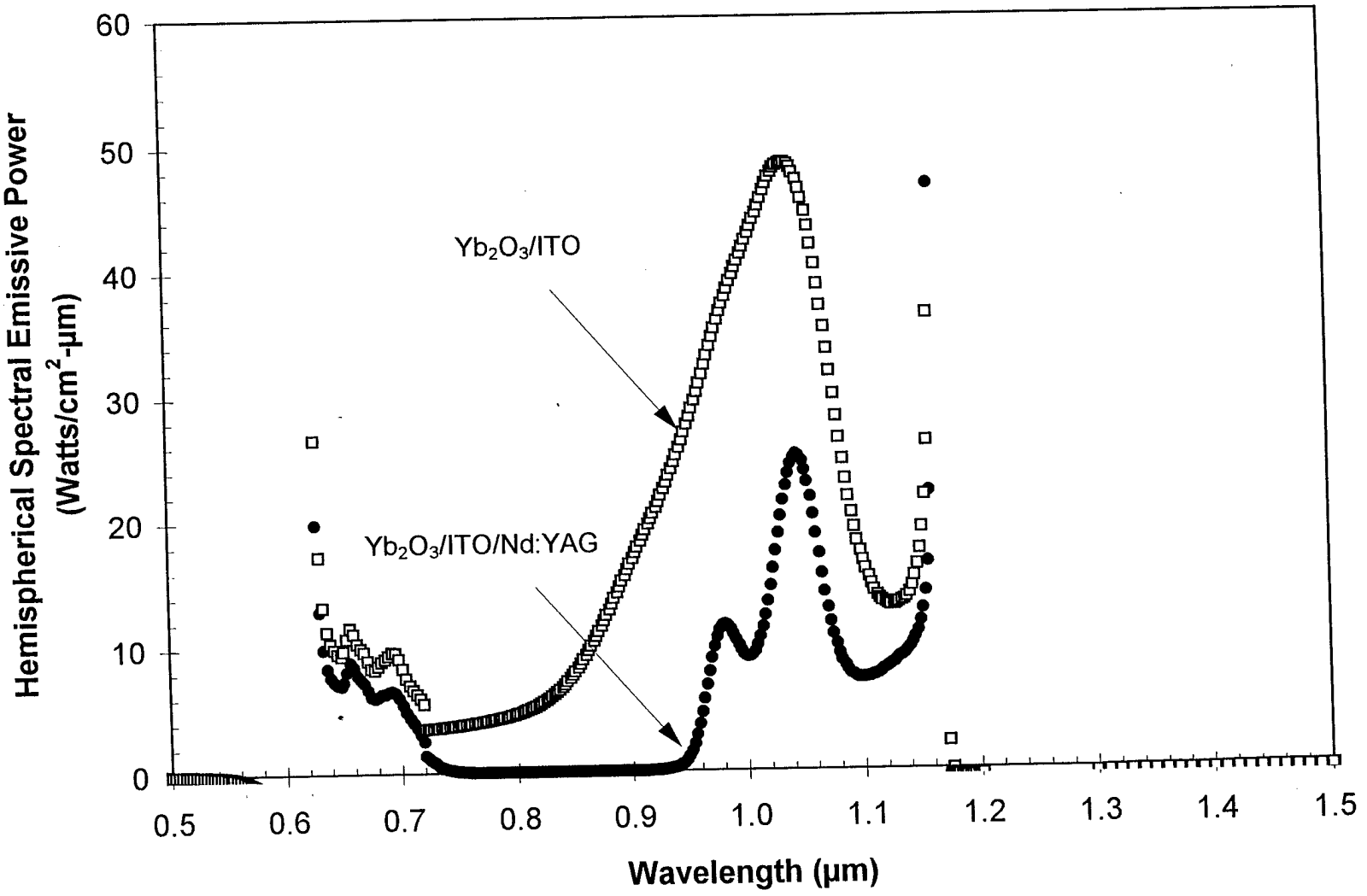

Figure 49. Spectra of Ytterbia Felt Through ITO and Nd:YAG Crystal

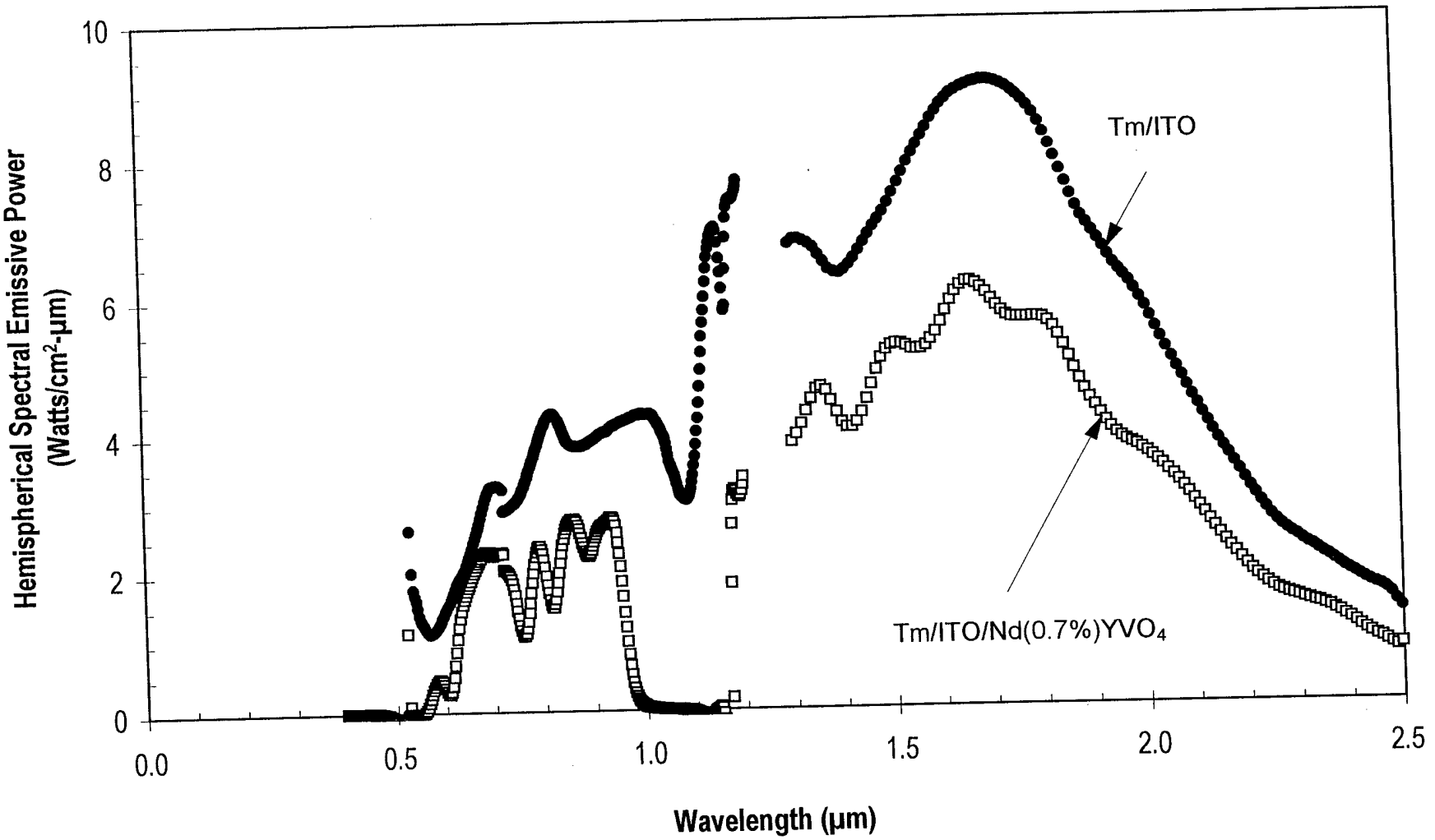

Figure 50. Spectra of Tm Felt Through ITO and Nd(0.7%)YVO_4

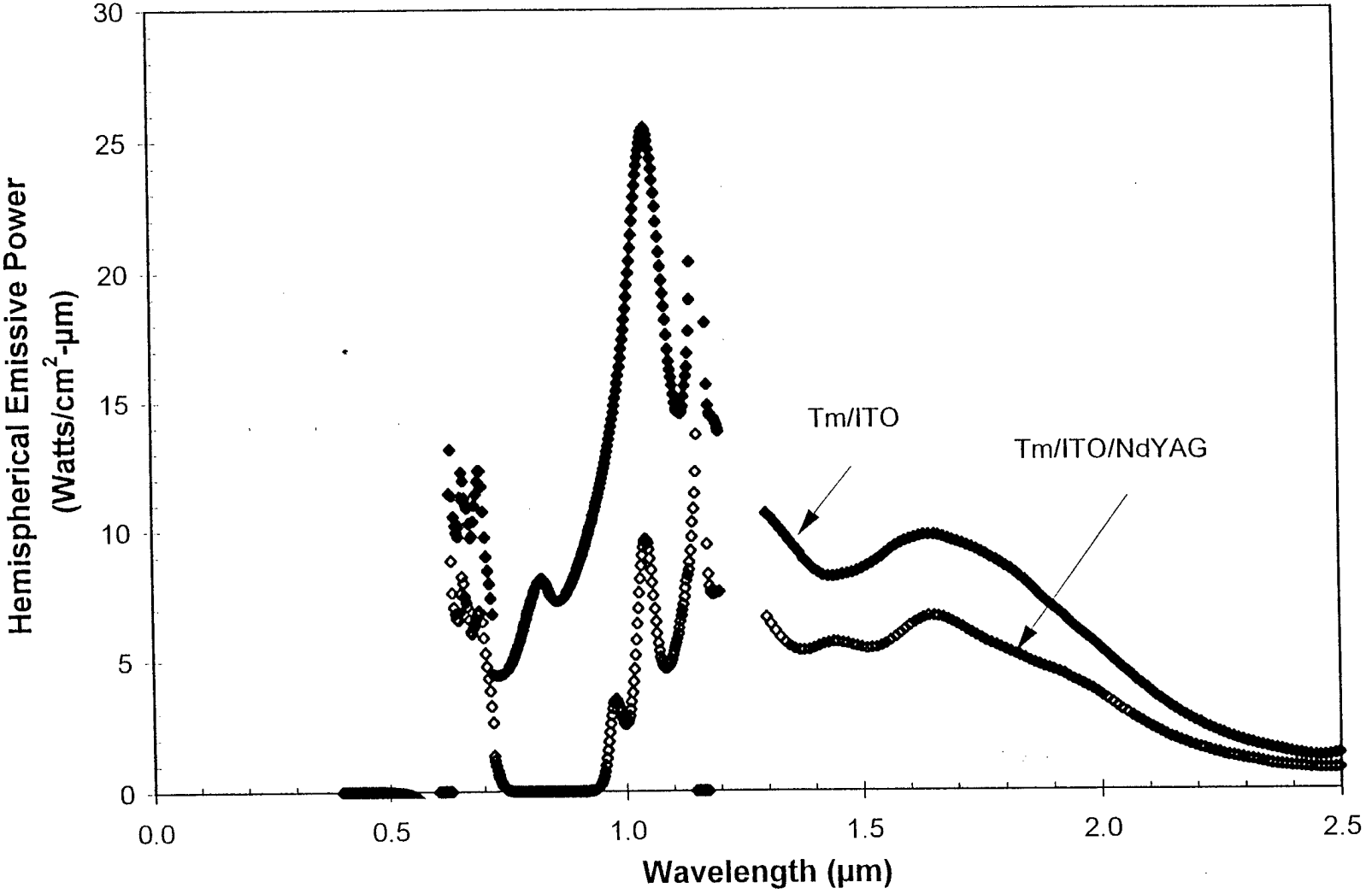

Figure 51. Spectra of Thullia Felt Through ITO and Nd:YAG

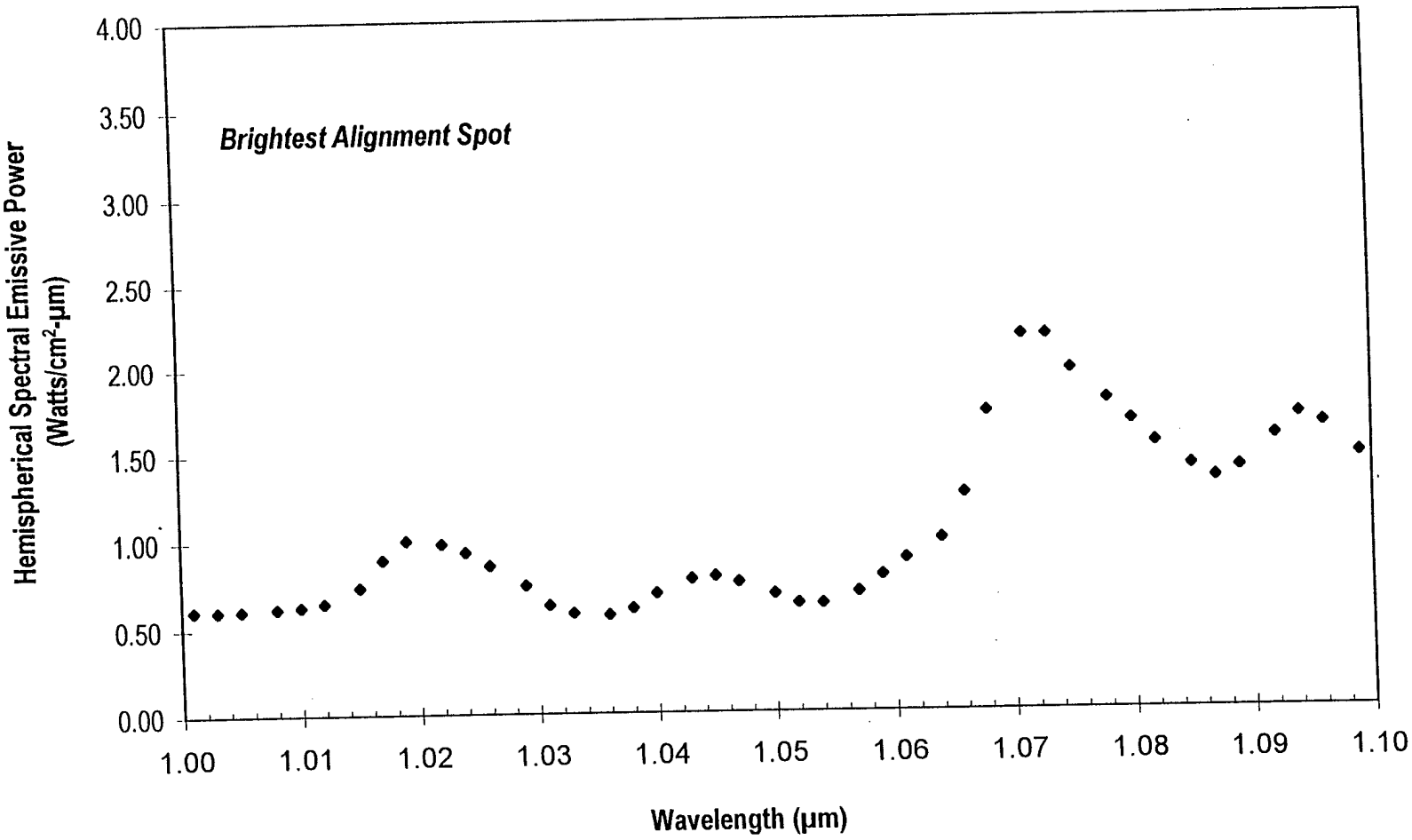

Figure 52. Enhanced Fluorescence Spectrum of Nd:YVO_4 when Exited by Tm Felt Emitter

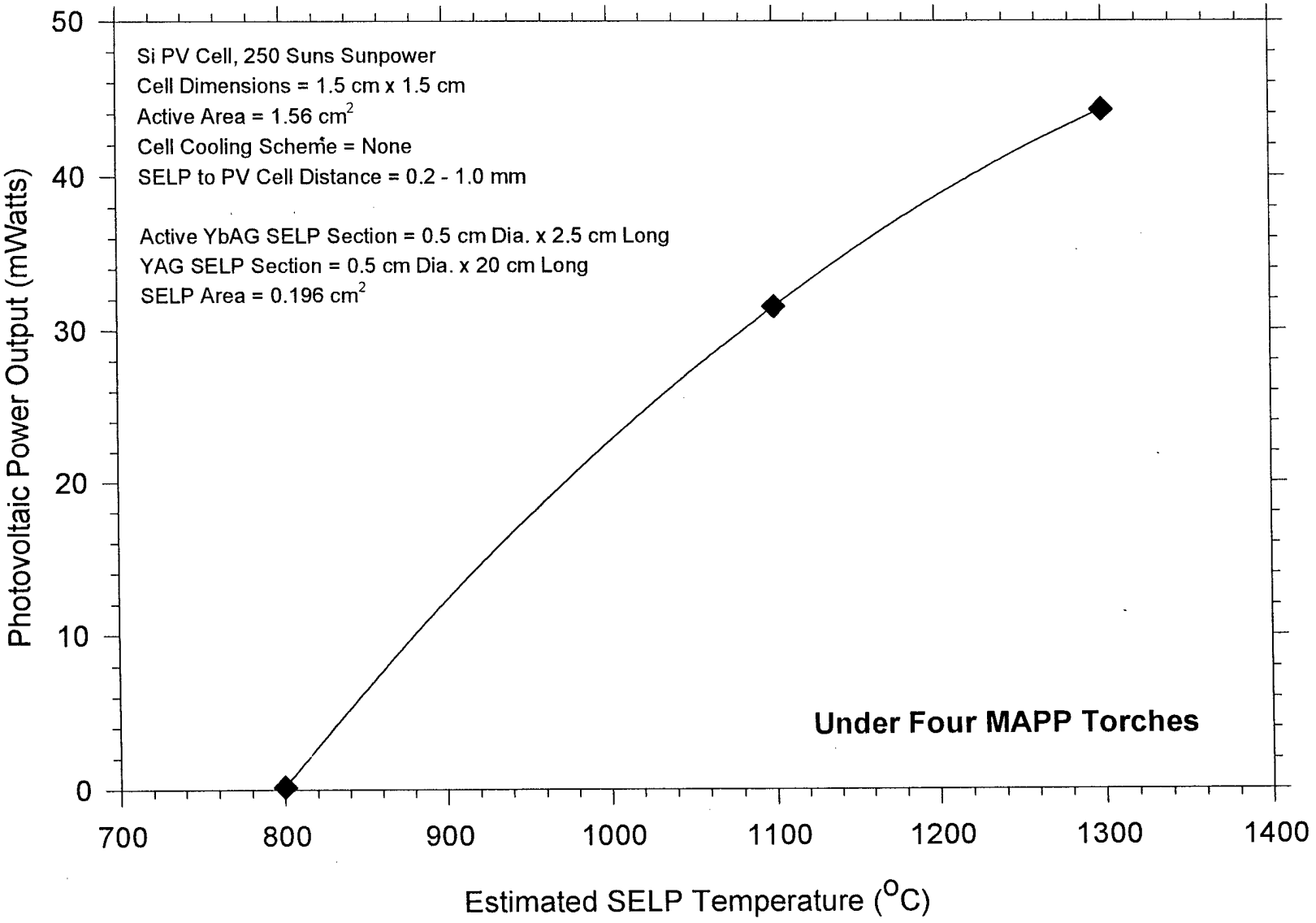

Figure 53. PV Power Output YbAG/YAG SELP Combustion Heat Source

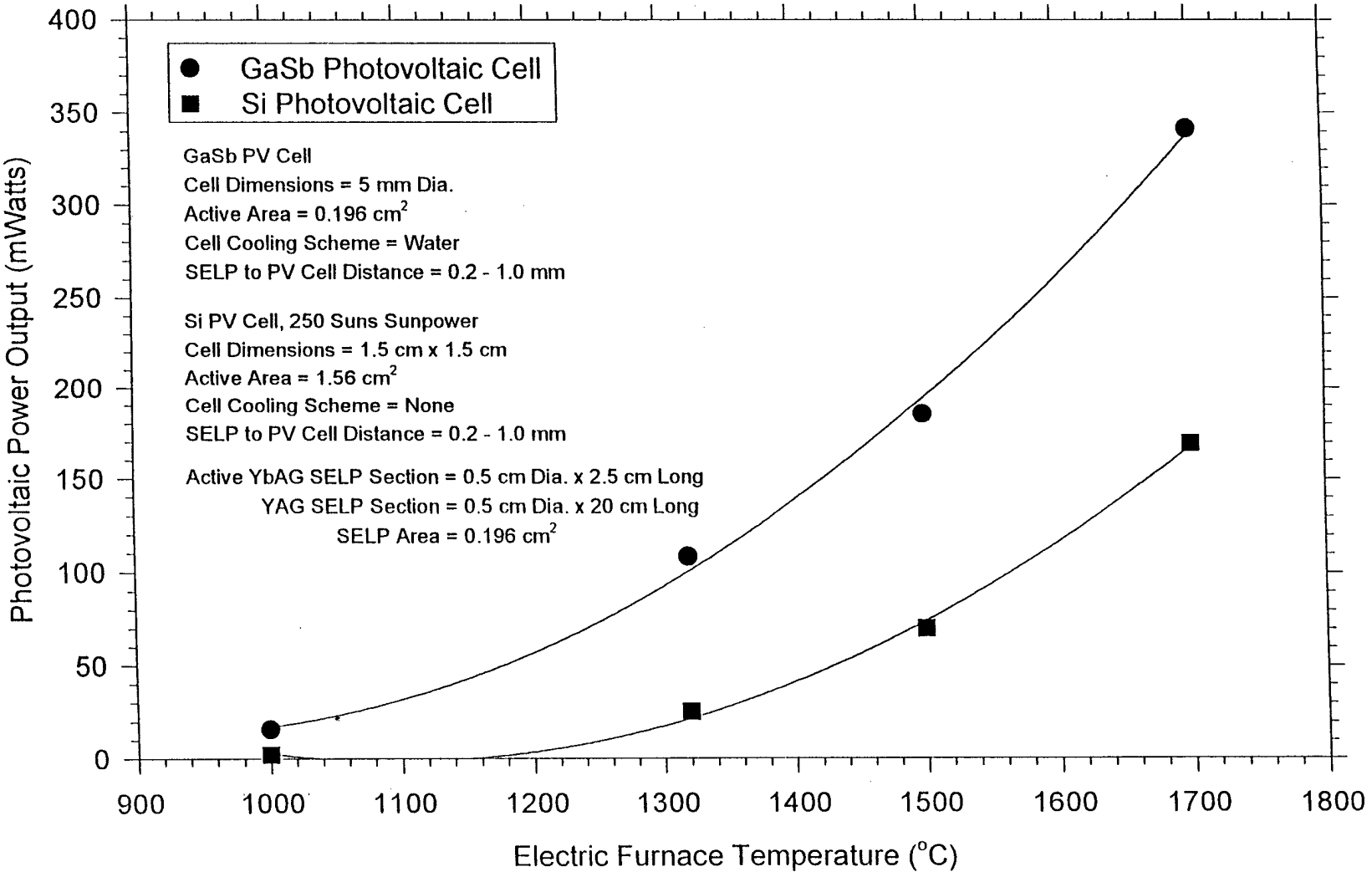

Figure 54. PV Power Test YbAG/YAG SELP Electric Furnace Setup

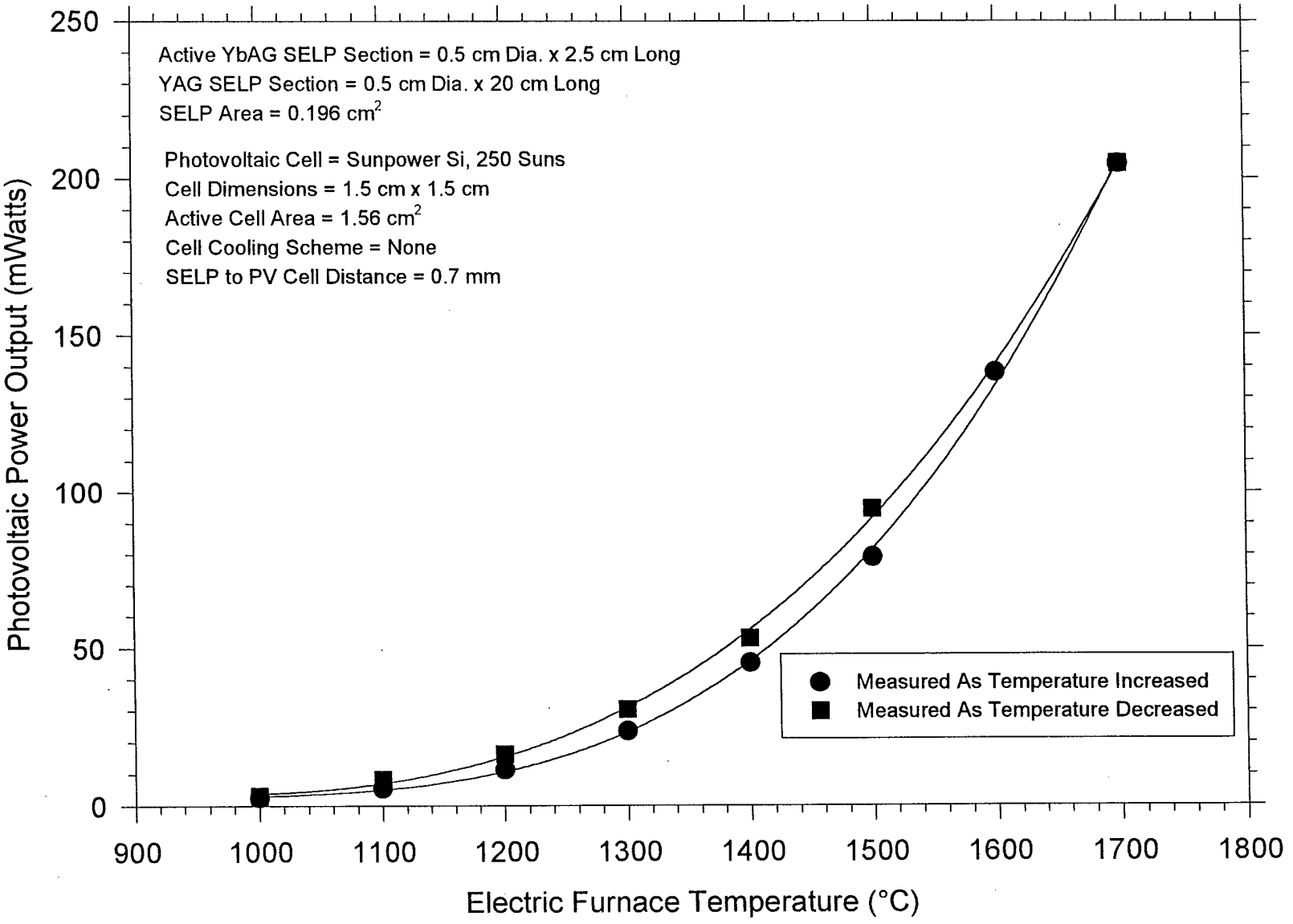

Figure 55. Si PV Power Consistency Test